DEVELOPMENT OF NANO/MICROMOTORS FOR POTENTIAL CANCER DIAGNOSIS AND THERAPY

by

Sezin Eren Demirbüken

B.S., in Biomedical Engineering, Yeditepe University, 2012

M.S., in Biomedical Engineering, Boğaziçi University, 2015

Submitted to the Institute of Biomedical Engineering

in partial fulfillment of the requirements

for the degree of

Doctor

of

Philosophy

Boğaziçi University

2023

DEVELOPMENT OF NANO/MICROMOTORS FOR POTENTIAL CANCER DIAGNOSIS AND THERAPY

APPROVED BY:

Prof. Dr. Bora Garipcan .....
(Thesis Advisor)

Prof. Dr. Filiz Kuralay .....
(Thesis Co-advisor)

Assoc. Prof. Dr. Esin Öztürk Işık .....

Assoc. Prof. Dr. Duygu Ege .....

Prof. Dr. Lokman Uzun .....

Assoc. Prof. Dr. Sedat Odabaş .....

DATE OF APPROVAL: 01.06.2023

ACKNOWLEDGMENTS

I would like to express my gratitude to my advisor Prof. Dr. Bora Garipcan for his individual guidance and support which help me to stay on track and improve my research.

I would like to present my deep gratitude to my Co-advisor Prof. Dr. Filiz Kuralay who have supported and encouraged me throughout my Ph.D. journey.

I would like to thank Prof. Dr. Ayşegül Uygun Öksüz and her student Dr. Gözde Karaca Yurdabak for sharing experiences related nano/micromotor synthesis.

I would like to thank my laboratory colleagues and peers, for their collaboration and constructive criticism, which enriched my research and broadened my perspective. Especially, I would like to thank Bengü Aktaş for being so supportive and makes this journey tolerable. In addition, I would like to thank specially Elif Öztürk, I couldn't finish synthesis and propulsion experiments without her support. In addition, I would like to thank Hilmi Kaan Kaya and Mustafa Ali Güngör for their support.

I would like to give special thanks to my husband and my family for their love, support, understanding especially during challenging times of this journey.

This Ph.D. work was supported by Boğaziçi University Research Fund (BAP) (Grant No:17061 and 6701 for metallic micromotor part) and The Scientific and Technological Research Council of Türkiye (TUBITAK) (Project No:116Z503 for PAPBA enriched nanomotor part). In addition, I would like to acknowledge to The Council of Higher Education 100/2000 Ph.D. scholarship program which allowing me to focus on my academic pursuits without financial burden.

ACADEMIC ETHICS AND INTEGRITY STATEMENT

I, Sezin Eren Demirbüken, hereby certify that I am aware of the Academic Ethics and Integrity Policy issued by the Council of Higher Education (YÖK) and I fully acknowledge all the consequences due to its violation by plagiarism or any other way.

Name :

Signature:

Date:

ABSTRACT

DEVELOPMENT OF NANO/MICROMOTORS FOR POTENTIAL CANCER DIAGNOSIS AND THERAPY

Recent developments in nano/micromotor based smart drug delivery and diagnosis systems have gained much attention due to their efficient capabilities and unique features. Smart drug delivery systems are preferred for reduced side effects, increased effectiveness, and controlled release in specific locations. Nano/micromotors enable motion control and propulsion, leading to reduced drug concentration, faster delivery, and enhanced penetration into inaccessible tissues. Hence, in the first part of the thesis, self-functionalized polymer poly(3-aminophenylboronic acid) (PAPBA) enriched nanomotors were developed by conjugating Paclitaxel (PTX) to PAPBA/platinum (Pt)-nickel (Ni)/ Pt according to demonstrate their efficacy in smart drug delivery with catalytic propulsion. Controlled drug delivery was achieved by inducing Near-Infrared irradiation (NIR) and altering the pH. Drug release and interaction of PAPBA-enriched nanomotors loaded with drugs were studied using MCF-7 breast cancer cells. In the second study of the thesis, two segmented, gold (Au), iron-nickel (Fe - Ni) as metallic micromotors were synthesized according to carry out controlled release of anti-cancer drug doxorubicin (DOX) to breast cancer cells and diagnosis of breast cancer with magnetic propulsion. Au segment surface of electrochemical fabricated micromotors were engineered to provide drug (DOX) loading and antibody (antiHER2) immobilization as capturing agent. Engineered Au segment surface made possible controlled drug release in acidic cancerous environment. Magnetic (Fe-Ni) segment ensured controlled drug delivery to MCF-7. Spheroids with nano/micromotor drug delivery systems offer valuable insights for optimizing their clinical use. These approaches highlight the potential of nano/micromotors as smart drug delivery methods over conventional systems.

Keywords: Nanomotor, micromotor, Drug Delivery, Drug release, Spheroid, Anti-HER2, PAPBA, Paclitaxel, Doxorubicin, MCF-7 Cells.

ÖZET

POTANSİYEL KANSER TEŞHİSİ VE TEDAVİSİ İÇİN NANO/MİKROMOTORLARIN GELİŞTİRİLMESİ

Son dönemde nano/mikromotor tabanlı akıllı ilaç taşıma ve teşhis sistemleri etkin özellikleri nedeniyle büyük ilgi görmektedir. Bu sistemler tercih edilerek yan etkilerin azaltılması, etkinlik artışı ve ilaçların belirli bölgelerde kontrol edilerek salımı sağlanır. Nano/mikromotorların hareket kontrolü ve hareket mekanizmaları, ilaç derişimi, teslim süresini kısalması ve ilaçların ulaşılması zor bölgelere daha iyi nüfuz etmesine olanak tanır. Bu nedenle, tez çalışmasının ilk bölümünde, kendiliğinden fonksiyonel polimer ile zenginleştirilmiş nanomotorlar, katalitik itki ile akıllı ilaç taşımak için poli(3-aminofenilboronik asit) (PAPBA)/platin (Pt)-nikel (Ni)/Pt olarak Paklitaksel (PTX) anti kanser ilacı yüklemek amacı ile geliştirilmiştir. Kontrollü ilaç salımı, yakın kızılötesi (NIR) ışınımı ve pH farkları indüklenerek başarılmıştır. İlaç salımıve ilaç yüklü nanomotorların etkileşimi MCF-7 meme kanseri hücreleri ile incelenmiştir. Tez çalışmasının ikinci bölümünde, manyetik hareket ile meme kanseri tanısı ve kontrollü ilaç salımını gerçekleştirmek için, iki segmentli altın (Au), demir-nikel (Fe - Ni) olarak metal mikromotorlar sentezlenmiştir. Elektrokimyasal olarak sentezlenen mikromotorların Au segment yüzeyi, ilaç (DOX) yüklemesi ve teşhis ajanı olarak antikor (antiHER2) immobilizasyonu sağlamak için modifiye edilmiştir. Modifiye edilen Au segment yüzeyi, asidik kanserli ortamda kontrollü ilaç salımını mümkün kılarak, manyetik (Fe-Ni) segment, MCF-7 hücrelerine manyetik hareket kabiliyeti ile kontrollü ilaç salımı sağlanmıştır. Ayrıca, mikromotor ilaç teslim sistemlerinin sferoidlerle çalışılarak geliştirilmesi, klinik kullanım için optimizasyon çalışmalarında öncü veriler sağlama potansiyeline sahiptir. Tüm bu yaklaşımlar, nano/mikromotorların akıllı ilaç teslim yöntemlerindeki potansiyel uygulamalarını göstermektedir.

Anahtar Sözcükler: Mikromotor, Nanomotor, İlaç Salımı, ilaç dağıtımı, Sferoid, AntiHER2, PAPBA, Paklitaksel, Doksorubisin, MCF-7 hücreler.

TABLE OF CONTENTS

LIST OF FIGURES

LIST OF SYMBOLS

°C	degree Celcius
eV	electrovolt
mg	milligram
mL	milliliter
mM	millimolar
mTorr	millitorr
micro	microgram
μL	microliter
μm	micrometer
Ω	ohm
rpm	round per minute
V	Volt

LIST OF ABBREVIATIONS

AINR	Asymmetric Intracellular Ion Nanoregulator
APBA	(3-aminophenylboronic acid)
ATP	Adenosine Triphosphate
Au	Gold
CDDP	cis-diamminedichloroplatinum
CRP	C-reactive protein
CD	Carbon Dots
DNA	Deoxyribonucleic Acid
DOX	Doxorubicin
DPV	Differential Pulse Voltammetry
EDX	Energy Dispersive X-ray
Fe	Iron
H_2O_2	Hydrogen peroxide
N/MM	Nano/micromotor
NP	Nano particle
NIR	Near Infrared
Ni	Nickel
MR	Magnetic Resonance
MRI	Magnetic Resonance Imaging
JMS	Janus Mesoporous Silica
PAPBA	poly(3-aminophenylboronic acid)
PSS	poly(sodium 4-styrenesulfonate)
Pt	Platinum
PTX	Paclitaxel
VSP	Virus Spike Protein
SPCE	Screen-Printed Carbon Electrode
SEM	Scanning Electron microscopy

1. INTRODUCTION

1.1 Motivation

Nanotechnology is a field that defined as the formation, manipulation, and utilization of materials, devices, and systems on a nanoscale level (1 to 100 nanometers) with the goal of manipulating and controlling materials at the atomic and molecular level. Richard Feynman's well known talk titled "There's Plenty of Room at the Bottom" is often considered the starting point for the field of nanotechnology. Since, he discussed the possibility of manipulating and controlling individual atoms and molecules, paving the way for development of nanotechnology. Although Feynman did not explicitly define the term "nanotechnology" in his talk, he described the concept of manipulating and controlling atomic and molecular scale of materials. He envisioned a future in which we could build machines that were incredibly small, but still capable of performing complex tasks in a lot of scientific area [1]. The nanotechnology as a term was first used by a Japanese scientist named Norio Taniguchi. At the time he introduced the term, he was a student at Tokyo Science University, and the concept of examining the properties of materials at an atomic or molecular level led to the emergence of significant research areas [2]. The foundations of this technology that has left its mark on today's world were laid by emphasizing the innovations and advantages that could arise from the production of different materials at the molecular level. As a result, this discipline, which is the science of manipulating matter at the atomic and molecular level, has become one of the technologies of our time as a result of the intensive efforts of researchers from various fields [3, 4]. Considering that a nanometer is 1 nm = 10^{-9} m and one millionth of a millimeter, it is clear that nanostructures (nanomaterials) can be visualized with the help of a microscope rather than the naked eye. What makes nanotechnology so interesting is that materials behave differently at the nanoscale than in the macro world [5–8]. Thanks to these properties, nanotechnology has found different uses in many fields. When the developments in the field of nanotechnology are combined with known technologies, great advantages are

provided. Some of the developments in nanotechnology have given way to different and ground breaking applications to replace known systems [9–12]. The use and acquisition of nanotechnology is a multidisciplinary field.

The guidance of the nanotechnology vision resulted particularly promising biomedical engineering applications and still has shown the influence on biotechnology and biomaterials. Drug delivery, tissue engineering, biosensors, imaging and nanomaterials could be designed in specific necessities with nanotechnological approaches. Engineered nanoparticles or nanomaterials have potential to increase targeting and the efficacy of the treatment and reduce the side effects of the treatments [13]. Over the past few decays, smart drug delivery systems have key roles for biomedical applications [14]. The use of nano/micromaterials has shown great potential in improving the efficacy and specificity of drug delivery, especially for the therapy of diseases that are difficult to target using conventional drug delivery methods [15]. Given that cancer remains one of the major global health challenges according to World Health Organization (WHO), with many existing therapies limited by poor tumor selectivity, low efficacy, and systemic toxicity. Nano/micromotors have been one of the feasible candidates used to surpass these drawbacks, and improve the therapeutic effect recently. Nano/micromotors are bioinspired structures [16] that possess ability to convert the energy into movement by various powering methods to implement assigned biomedical applications [17]. Besides drug delivery, there are also application examples such as biosensing [18, 19], microsurgery [20], cargo transports [21], and biomedical imaging [22]. Considering all this, nano/micromotors depict a promising method for targeted drug delivery to cancerous cells and offering enhanced control over drug release and transport.

It is known that, conventional methods of delivering drug are insufficient in preventing harmful effects on healthy tissues. In contrast active drug delivery systems which improve active transport offer a reduction in side effects, an increase in therapeutic effectiveness, and controlled release of drugs in specific location [23]. Compared to other drug carriers such as dendrimers [24], lysosomes, quantum dots [25], or gold nanoparticles [26]. Nano/micromotors have the advantage of motion control and the

propulsion mechanisms. These attributes allow for a reduction in drug concentration fluctuation, delivery time, and improved penetration of drugs into tissue, including hard-to-reach areas [27, 28]. Combination with nano/micromotors and surface engineering make them very promising candidate as an alternative smart drug carrier system. Propulsion mechanisms which could be magnetic, catalytic, light-driven or acoustic provide active transport of the drug in other words the acceleration of the drug transport could be provoked. Moreover, controlled drug released is actualized to targeted cells via surface engineering according to stimulation method, such as light, pH differences, thermal. In addition to smart drug delivery, the nano/micromotors are possible diagnostic apparatus by surface engineering with capturing agents.

In this thesis, smart drug delivery systems are developed with polymeric and metallic nano/micromotors with realization of active transport of anti-cancer drugs via propulsion. In addition, it is shown that, this nano/micromotors have potential to be used for not only therapeutic purposes but also diagnostic applications.

1.2 Objectives and Outline of the Thesis

In the first section of the thesis, polymeric poly(3-aminophenylboronic acid) (PAPBA)-enriched nanomotors were designed and synthesis were obtained to realize controlled drug (Paclitaxel) delivery to MCF-7 adenocarcinoma breast cancer cells. Surface modification was planned to load drug via feasible method and according to perform drug release by external stimulations, as acidic medium of MCF-7 and Near Infra-Red (NIR) light. The following section was dedicated to smart drug (Doxorubicin) delivery and diagnostic approach of metallic Au-FeNi micromotors. Controlled drug delivery was carried out by pH responsive method to MCF-7 cells. Herein, not only monolayer cell culture was used to execute anticancer drug delivery (Doxorubicin), but also tissue-like three-dimensional cell culture form of MCF-7 spheroids were used. Diagnostic approach was shown by antibody (Anti-HER2) immobilization. It is known that breast cancers were overexpressed HER2 receptors on the cell membrane. The interaction between antibody immobilized micromotors and MCF-7 cells were observed

under light microscope and captured videos. According to compare diagnostic purpose of antiHER2 immobilized micromotors, SH-SY5Y neuroblastoma cells were used, which has no overexpressed HER2 receptors on the membranes and the interaction were observed under light microscope and captured as video. Specific objectives of thesis include:

- Polymeric PAPBA-enriched nanomotors were designed and synthesized with electrodeposition and used for loading PTX and releasing in controlled way by external stimulations, pH and NIR-light.
- Catalytic propulsion adopted polymeric nanomotors were evaluated in terms of biocompatibility.
- Metallic Au:Fe-Ni micromotors were designed synthesized with electrodeposition according to perform smart drug delivery and ability to use as diagnostic approach.
- The design of micromotors provide magnetic propulsion, which made the active transport method biocompatible.

2. BACKGROUND

2.1 Nano/Micromotors

In daily life, motors are used according to obtain mechanical energy then into kinetic energy by transforming mostly electrical energy to power the operation of various other devices in mesoscales. In nature, biological motors have similar powering mechanisms are also possible to observe in nanoscales to create movement. In living organisms, there are some natural motors that help maintain cellular functions. Bacterial flagella, myosin, kinesin, actin, dynein, deoxyribonucleic acid (DNA) are the examples for biological motors which are commonly fueled by chemical energy generated by hydrolysis of adenosine triphosphate (ATP) molecules for linear or rotational movement [29–34]. Biological motors are inspiring scientists to develop artificial nano/micromotors that can mimic the working principles of biological motors that can convert energy in to movement by various powering methods. In 2002, Whitesides and his colleagues have published an article about autonomous movement of small (<1cm) hemicylindrical plates by propulsion of bubbles which are evoked by platinum-catalyzed decomposition of Hydrogen peroxide (H_2O_2) [35]. This study gave inspiration to the scientists to apply the similar powering mechanism to artificial nanomotors. The first studies related autonomous catalytic nanomotors especially focus on developing catalytic reactions that provide energy for movement. Thus, synthesized nanomotors can achieve autonomous and non-Brownian movement by catalytic reactions [36–38]. For instance, platinum/gold nanomotors use hydrogen peroxide (H_2O_2) as fuel commonly; the mechanism of powering nanomotors described as; Pt segment of the nanomotors oxidize H_2O_2, that provides travel of electrons through the nanomotors towards the Au segment where H_2O_2 is reduced and movement is occurred [36, 39]. These catalytic autonomous nanomotors mainly have self-electrophoretic or bubble propulsion mechanisms. Self-electrophoretic motion is originating from the electro-osmotic flow on the surface of nanomotor with self-induced electric field [40, 41]. On the other hand, bubble propulsion mechanism is movement by the impulse of bubble generated at catalytic

segment of nanomotors [36, 42].

In the literature, there are a lot of promising improvements related nano/ micromotors. At the beginning, scientists tried to accomplish motion control on nanomotors. The specific demands of various applications necessitate accurate management of the direction, speed, and intricate movement patterns of nanomotors, both in terms of their spatial and temporal guidance [10]. Early nanomotor studies, Sen and his colleagues designed nanomotors to control movement direction remotely. The nanomotors were synthesized in rod shapes and they are composed of gold, platinum and in addition nickel. Nickel parts provide remote-control of nanomotors by external magnetic field [43]. Different than macroscale, interstitial forces govern over inertia at nanoscale in fluid. Since the direction of propulsion occurs as random fluctuations [36]. Due to that reason, direction control gains important role for potential applications, such as drug delivery and cargo transport.

2.2 Propulsion Mechanisms of the Nano/Micromotors

The movement mechanisms of nano/micromotors are generally categorized as two categories: catalytic and non-catalytic motors. The first synthesized type, catalytic nanomotors, moves through the mechanism of chemical fuel degradation in the presence of a catalytic layer such as Pt [10, 38, 44, 45]. These chemical fuels are usually H_2O_2 and similar types, which studies have shown do not harm the human body at low concentrations (Figure 2.1). While high concentrations of H_2O_2 are hazardous to cells, low concentrations are known to be important for some physiological processes [46]. Based on this information, many nanomotors have been synthesized and applied that move with these fuels at low concentrations for different applications [47–50]. In addition, nanomotor applications that move in the gastric acid medium and water in the human body are also very significant [51, 52]. There are also catalytic motors that move based on enzymatic reactions [53–55]. By adding a magnetic layer (such as Nickel, Ni, and Iron, Fe) to nanomotors, controlled direction can be achieved with the help of a magnet [45]. In the other type of non-catalytic or fuel-free nanomotors, move-

ment occurs in the presence of an external effect. These structures can be moved in a magnetic field, electric field, acoustic field, ultrasonic, or light-controlled environment and thermal effect. These motors can also be in the form of wires, Janus particles, or spiral shapes [56–61].

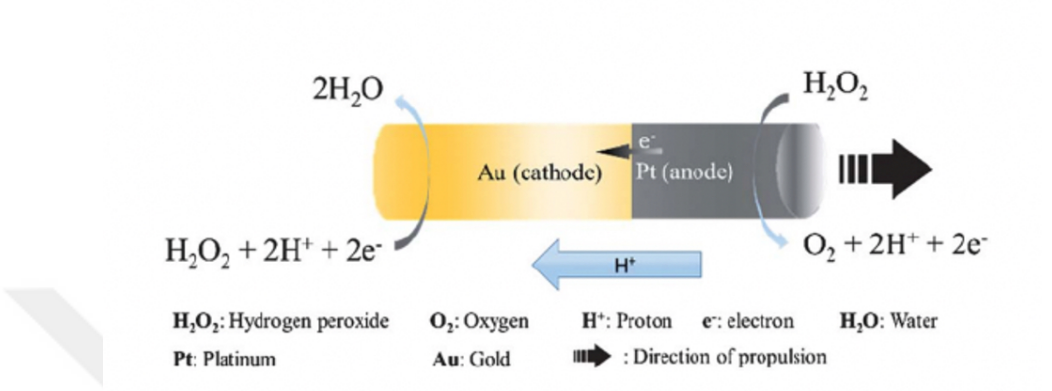

Figure 2.1 Catalytic wire shaped nanomotor and its working mechanism [52, 62].

The fuel-free nanomotors were developed to reduce the need for a chemical fuel environment that could potentially harm the cell, such as H_2O_2. Magnetic propulsion is one of the preferred movement mechanism since the magnetic field has biocompatible effect on the living organism. Besides, magnetic particles are viewed as a hopeful option since they provide diagnostic capabilities and have ability to produce *in vivo* imaging contrast in various imaging techniques, including nuclear magnetic resonance imaging (MRI), computer tomography, or magnetic particle imaging. In terms of nanomotors, although homogenous and static fields are employed for imaging purposes, strong magnetic field gradients are usually utilized to achieve directed motion of nanostructures. Nonetheless, it is difficult to attain significant gradients over considerable distances, which is necessary for applications within the body [63].

These mentioned propulsion mechanisms of nano/micromotors are summarized in Figure 2.2. It is possible to control, direct, accelerate, and decelerate nanomotors through catalytic effect, electric field, ultrasonic waves, magnetic fields, and light control.

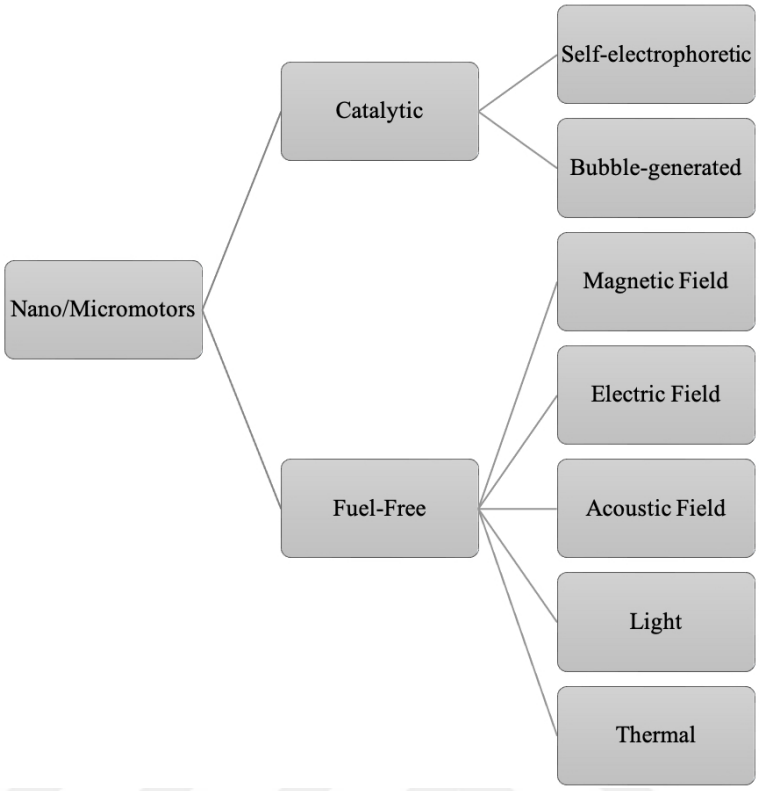

Figure 2.2 Classification of nano/micromotors according to propulsion mechanisms [64].

2.3 Synthesis Methods of the Nano/Micromotors

The synthesis stages of these motors involve nanotechnological approaches, which can be categorized into two types: Bottom-up Approach and Top-down Approach [64, 65]. In the Bottom-up Approach, nanomotors are designed at the atomic and molecular level, whereas in the Top-down Approach, they are designed at the macro or micro level. Figure 2.2 summarizes these approaches.

In the literature, template-assisted method is one of the common applications for nano/micromotor synthesis in terms of bottom-up approaches especially for rod, wire or tubular shaped structures. Electrodeposition of the nano/micromotors were governed with membranes. These membranes could be polycarbonate (PC) or Anodic Alumina Oxide (AAO) membranes depending on the type of nano/micromotors [50, 60]. The membranes are used as a template, and the membranes were coated with a conducted

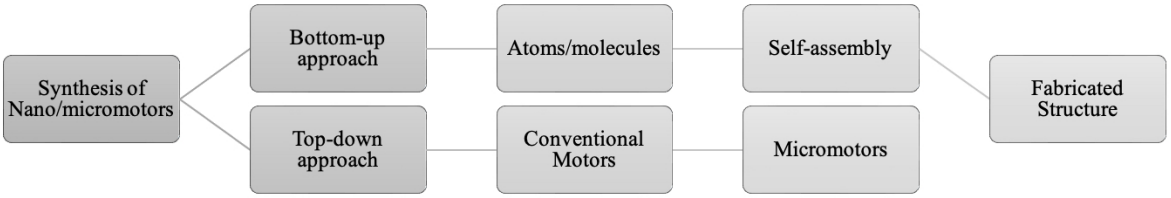

Figure 2.3 Synthesis approaches of nano/micromotors [64].

layer to work as an electrode, thus the membranes become ready to use deposition of demanded conducted material. After this process, membranes are solved to release electrodeposited nano/micromotors. Beside bottom-up approaches, lithography is one of the application methods to deal with micro and nanoscale materials. 3D direct laser writing technology is two-photon polymerization lithography and it can be a versatile implement generating for complex and qualified structures which possess nanometer precision and accuracy in three dimensions. By using this method, it is achievable to fabricate complex micro/nanostructures that are hard to produce with traditional procedures [66].

2.4 Biomedical Applications of Nano/Micromotors

Various biological motors in nature, such as kinesins, dyneins, sperms, and certain bacteria, have ability to convert energy, specifically adenosine triphosphate (ATP), into mechanical force. These motors exhibit autonomous motion and perform complex tasks efficiently. Drawing inspiration from these natural motors, researchers have developed artificial nano/micromotors, which are nano/micro devices or robots. By transforming different forms of energy, including chemical fuels and external field energies, into mechanical motion, synthetic nano/micromotors can propel themselves through various types of media. Due to their active propulsion, nano/micromotors can accomplish various tasks that passive devices cannot achieve [67]. As an example, they may exhibit superior cell/tissue penetration competence. As a result, these studies possess the potential to govern *in vitro* or *in vivo* applications more impactful, displaying encouraging prospects in biomedical areas like drug delivery, biosensing, cancer treatment, imaging, assisted fertilization, precision nano micro/surgery, and other related fields [62, 68].

2.4.1 Biosensing and Diagnosis Applications

Several research groups have described nano/micromotors that can capture and transport various loads based on donor-receptor interactions. These nano/micromotors have the potential to sense, diagnose, and isolate biomolecules and cells from biological samples. For instance, Molinero-Fernández *et. al* developed a sandwich immunoassay for C-reactive protein (CRP) determination using antibody-functionalized micromotors. The micromotors, composed of catalytically reduced graphene oxide (rGO)/Ni/PtNP, were functionalized with the capture antibody (anti-CRP) through covalent bonding. In the first step, the anti-CRP micromotors were mixed with the plasma sample, secondary antibody (HRP-tagged), surfactant, and fuel medium (H_2O_2) to execute the immunosandwich. After propulsion was deactivated, The magnetic properties of the micromotors caused them to be separated from the sample, possibly due to the intermediate magnetic layer of Ni. Finally, the electrochemical transducer was

used to introduce the micromotors for signal readout, which was mediated by the HRP-tagged secondary antibody via benzoquinone reduction [69].

The use of magnetic fields in traditional biosensing has been prevalent for many years, owing to their ability to simplify separation preconcentration steps. Additionally, magnetic fields can serve a safe energy supply for propelling nano/micromotors, even *in vivo* [18]. To synthesize magnetic fluorescent hybrid micromotors, Zhang *et. al* utilized Fe3O4 magnetic NPs and fluorescent carbon dots (CDs) to modify *Ganoderma lucidum* spores. The hydrothermal process caused CD modification, resulting in the surface of the spore hybrid micromotor primarily consisting of oligosaccharides. Due to this modification, the spore hybrid micromotors exhibit a strong attraction towards the repetitive oligopeptides present on the *Clostridium difficile (C. diff)* toxin. This interaction had ability to quench the fluorescence of the propelled micromotors, creating a motion-based fluorescence biosensor [70]. The biosensor field has been greatly impacted from the SARS-CoV-2 pandemic, resulting in the engineering of fast, accurate, and cost-effective methodologies for scanning the virus. Pumera *et. al* created a magnetic nanomotor for electrochemical detection of the virus spike protein (VSP) for biomarker purpose. They functionalized commercial magnetic nanoparticles with anti-VSP antibodies that could be propelled using a rotating magnetic field to implement on-the-fly biorecognition of VSP. For electrochemical detection, a secondary antibody tagged with Ag-Au nanorods was utilized to determine VSP, HER on a commercial electrochemical platform [71]. These studies show that the engineered and developed nano/micromotors are promising potential for biosensing and diagnosis applications.

2.4.2 Imaging Applications

Nanomotors offer several advantages in imaging applications. One of the main benefits is improved resolution. By moving through complex environments and getting closer to the imaging target, nanomotors can capture high-resolution images that would not be possible with traditional imaging techniques. Moreover, nanomotors exhibit a heightened sensitivity to detect and react to even minor fluctuations in their

surroundings. This makes them valuable tools for imaging applications where high sensitivity is critical. Nanomotors also offer enhanced maneuverability, allowing them to navigate through tight spaces and complex environments. This makes them ideal for imaging applications in biological systems, where traditional imaging techniques may not be able to reach. Finally, nanomotors can be designed to be non-invasive, reducing the risk of damage or interference with the imaging target. Overall, the usage of nanomotors for imaging applications possess the potential to enhance our understanding of biological systems and enable the upgrading of more effective diagnostic and therapeutic methods [72]. For instance, the limited ability of imaging agents to penetrate solid tumor tissue and cells is a significant challenge in cancer diagnosis. To address this issue, researchers have developed a near infrared radiation (NIR) light-driven Janus mesoporous silica nanomotor (JMS nanomotor) that can foster magnetic resonance (MR) imaging *in vivo*. The process of creating JMS nanomotors involves depositing gold on the half-sphere surface of mesoporous silica nanoparticles doped with gadolinium. When exposed to NIR irradiation, the nanomotors move efficiently through biological media by thermophoresis. The in vitro experiments indicate that the nanomotors can actively target, adhere to, and mechanically puncture tumor cells, leading to enhanced cellular uptake and MR imaging. The JMS nanomotors have shown improved accumulation and penetration in solid tumor models *in vivo* when exposed to NIR laser, resulting in significantly enhanced MR imaging contrast in most of the tumor tissue. These JMS nanomotors offer new insights into precise cancer diagnosis and MR imaging, which can be used for real-time tracking of nanomotors *in vivo* [73].

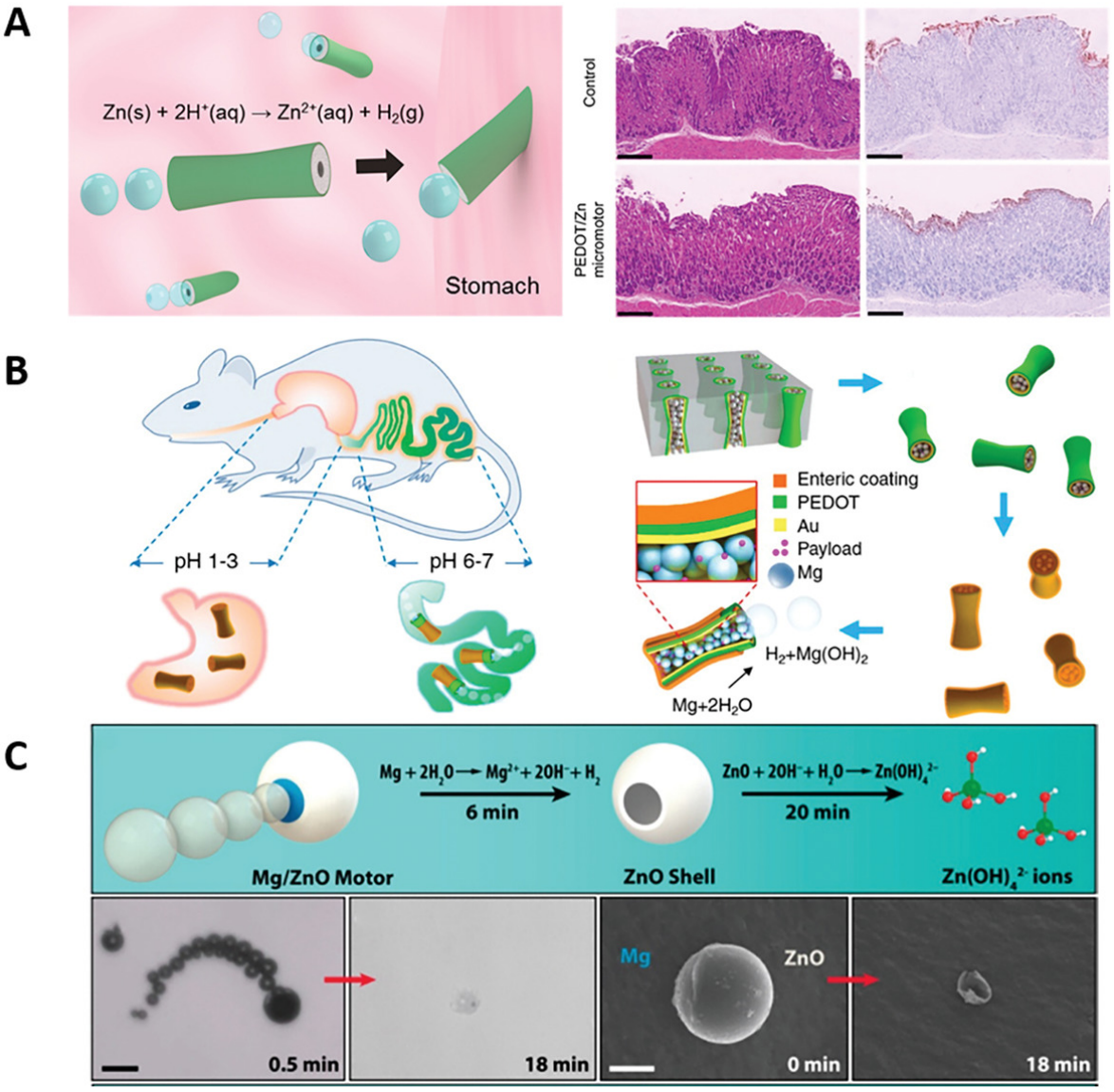

Figure 2.4 Biocompatible nano/micromotor examples of biomedical application [68].

2.4.3 Drug Delivery Applications

In recent decades, nanotechnology has offered numerous additional advantages in drug delivery, such as heightened effectiveness and accuracy in contrast to conventional therapies. Various recent drug delivery methods have been developed, like polymeric nanoparticles, liposomes, micelles, nanofibers, nanocrystals, nanoemulsions, solid lipid nanoparticles, and dendrimers, which have demonstrated promising findings in addressing unmet biomedical medical needs for various diseases. Nanoparticles are another significant tool in nanomedicine, offering many benefits such as improved pharmacokinetics. The physical characteristics of nanoparticles, such as their shape, size, and surface chemistry, are crucial factors that influence various pharmacokinetic parameters. These include adsorption, cellular uptake, biodistribution patterns, and clearance mechanisms. Nanotechnology offers numerous advantages over conventional drug delivery systems. First, preparation of biomaterials and drug carriers at the nanoscale level has high potential for the diagnosis and therapy of diseases through advanced targeted drug delivery and immunotherapy methods. Second, it gives opportunities to design applications with proteins, genes, and several cellular structures. Lastly, nanotechnology enables the enhancement of the natural physiological functions of the human body by using molecular machine systems and nanomotors at the chromosomal level, which can aid in both diagnosis and treatment [6]. Due to that reason, the autonomous propulsion of nano/micromotors through the transformation of various energy sources into mechanical motion is their most significant property. The propulsion feature of nano/micromotors has piqued the interest of scientists in the field of drug delivery, as it enables access throughout the entire human body and allows for new procedures at the cellular level, as well as localized diagnosis and treatment with enhanced precision and efficiency [74] micro/nanomotor synthesis and propulsion may utilize via various materials, geometries, surfaces, fabrication methods, and mechanisms [75].

The application of smart drug delivery systems in cancer therapy, particularly for solid tumors, has garnered significant attention due to its potential to enhance the efficacy of the treatment. Nanotechnology-based drug delivery systems have shown promise in this regard, as they present some advantages, like improved drug solubility

and stability, targeted drug delivery, and sustained drug release. The use of smart drug delivery methods for solid tumors can improve drug concentration level in the cancerous tissue while reducing exposure of healthy tissues to the drug. This can lead to better therapeutic outcomes, and minimize the incidence and severity of side effects [76, 77]. In the past ten years, the advancement of nanomotors has highlighted for their various biomedical applications, and one of these applications is targeted drug delivery. Due to their small size and exceptional mobility, nanomotors are capable of actively targeting the diseased area and performing specific functions in a non-invasive manner, which is expected to be beneficial in future clinical applications [78]. The design of nano/micromotors is significant to control propulsion, drug transport, and drug loading and controlled drug release, overall targeted drug delivery. Herein, the structure and surface modification of nanomotors are crucial factors in achieving controlled drug release for targeted therapy. Nanomotors with tailored structures can be designed to encapsulate drugs and deliver them to specific locations in the body. Surface modification of nanomotors can enhance their stability, improve biocompatibility, and enable specific targeting of cells or tissues. Functionalization of the surface can also enable controlled drug release, by using stimuli-responsive materials that respond to specific triggers, such as changes in pH [50, 60], acoustic field [79], or light [80]. The importance of nanomotor structure and surface modification lies in their ability to enable controlled drug release for targeted therapy. This approach can help to reduce the side effects due to the systemic drug administration and improve the efficacy of treatment. Besides controlled release mechanism, the design and the surface structure of the nano/micromotors should be taken into account according to engineer for not only drug loading mechanism, but also propulsion method, ability to engineer biocompatibility and maintain drug stability and drug penetration rate. For instance, magnetic propulsion systems are one of the preferable powering mechanism due to fuel-free biocompatible application. Due to that reason, nano/micromotor structures should contain paramagnetic materials as Co, Ni, and Fe in a way that does not affect biocompatibility [81]. Overall, the development of nanomotors with tailored structures and surface modifications holds great promise for the advancement of controlled drug delivery, and has the potential to revolutionize the field of targeted therapy.

Paclitaxel and doxorubicin are two commonly used drugs in controlled drug release studies due to their effectiveness in treating a variety of cancers and their favorable physicochemical properties for controlled release. Paclitaxel is a potent anti-cancer drug that acts by inhibiting cell division. It has a low water solubility, which makes it suitable for encapsulation in nano-carriers for controlled release. Paclitaxel also has a prolonged half-life, which allows for sustained release over an extended period. Moreover, paclitaxel has shown promising results in treatment of wide type of cancers, including breast, ovarian, and lung cancer [82]. Doxorubicin is another widely used anti-cancer drug that is effective against a variety of solid tumors and hematological malignancies. It has a high solubility in water, making it a suitable candidate for encapsulation in nano-carriers for controlled release. Doxorubicin also has a favorable pharmacokinetic profile and a long half-life, which makes it a suitable candidate for sustained release. In summary, paclitaxel and doxorubicin are preferred in controlled drug release studies due to their effectiveness against a variety of cancers, their favorable physicochemical properties for encapsulation and sustained release, and their well-established pharmacokinetic profiles [83].

Paclitaxel works by disrupting the normal process of cell division, which is essential for cancer cells to grow and proliferate. The mechanism of action of paclitaxel involves its ability to stabilize microtubules, which are long, thin, protein fibers that form the structural framework of cells and play an important role in cell division. During cell division, microtubules help to separate the duplicated chromosomes and pull them to opposite ends of the dividing cell, allowing the cell to divide into two daughter cells. Paclitaxel prevents microtubules from breaking down, which causes them to accumulate and become abnormally stable. This disrupts the normal process of cell division, leading to the formation of abnormal structures within the dividing cells and preventing the cells from completing the division process. As a result, the cancer cells are unable to grow and divide, and they eventually die. In addition to its effect on microtubules, paclitaxel can also induce apoptosis, or programmed cell death, in cancer cells. Apoptosis is a natural incident which cells eliminate damaged or abnormal cells, and it plays a vital role in the body's defense mechanism opposed to cancer. Overall, the mechanism of action of paclitaxel is complex and involves multiple

pathways. While it can be effective in killing cancer cells, it can also cause side effects due to its toxicity to healthy cells, which can limit its usefulness in some cases [82, 84]. Doxorubicin is a chemotherapy drug that works by damaging the DNA of cancer cells, thereby preventing them from dividing and growing. It is classified as drugs called anthracyclines, which are widely preferred for the therapy of various types of cancer. When doxorubicin enters the cancer cell, it binds to the DNA molecule and causes breaks in the strands of DNA. This leads to the formation of abnormal DNA structures, which prevent the cell from properly replicating its DNA during cell division. As a result, the cancer cell is unable to divide and grow, ultimately leading to its death. In addition to damaging DNA, doxorubicin can also generate toxic oxygen molecules known as free radicals, which further contribute to cancer cell death. Furthermore, doxorubicin can interfere with the function of enzymes involved in DNA synthesis and repair, further impairing the ability of cancer cells to survive and proliferate. Overall, the mechanism of action of doxorubicin is complex and involves multiple pathways. While it can be effective in killing cancer cells, it can also cause side effects due to its toxicity to healthy cells, which can limit its usefulness in some cases [83].

In the literature there has been many drug delivery applications with paclitaxel and doxorubicin which were designed with nano/micromotors. For instance, paclitaxel loaded nanomotors were used for smart drug delivery which triggered by near-infrared laser and pH change in first part of this thesis studies which will be explained in detail in the third section of the thesis [50]. Chen *et. al* have created wire-shaped magnetoelectric nanorobots as a proof-of-concept for an integrated device capable of wireless movement and on-site therapeutic release triggered by a single external power source as a magnetic field. Magnetic fields are a popular choice for wireless execution of nano/micromotors due to their precision and versatility in controlling magnetic structures, as well as their high biocompatibility. Magnetoelectric materials exhibit changes in electric polarization in response to magnetic stimulation, and it has been shown that these changes can induce redistribution of surface charges, triggering chemical and/or biochemical processes. By integrating magnetoelectric materials into nanorobotic platforms, the motor can be precisely propelled towards a targeted location using external magnetic fields and also perform on-demand magnetoelectrically assisted paclitaxel to

cells. [85]. Feng *et.al* investigated a new nanomotor system composed of poly lactic-co-glycolic acid drug-loaded magnetic Janus particles that were created with electrohydrodynamic co-jetting. The aim of this research was to improve the efficacy for treatment of the cancer while reducing the hazardous effects of paclitaxel to healthy tissues. The Janus particles were preferred because of their structural and functional versatility, and the nanomotors consisted of three parts. The first part contained paclitaxel to kill the cancer cells, the second part contained rhodamine B for monitoring, and the third part contained Fe_3O_4 for targeting the nanoparticles to the cells. The Janus particles were directed towards the cells and monitored with a magnetic field. Upon internalization into the cells, the particles released paclitaxel, resulting in significant lethality to the cancer cells without harming normal cells [86]. Doxorubicin is much more common preferred anti-cancer drug than some other anti-cancer drugs and one of the reasons is intrinsic fluorescence property which can make it useful for imaging and tracking purposes in cancer research [87]. A nanomotor system for DOX-delivery has been reported by Wilson's group using self-assembled bowl-like stomatocytes composed of poly(ethylene glycol)-b-poly(styrene) (PEG-b-PS) functionalized with platinum nanoparticles, Pt-NPs. The amorphous PS block is necessary for the vesicles to acquire the bowl-like structure. The nanomotors were able to move at a speed of about 40 $\mu m s^{-1}$ at 37 °C in a 4.98 mM (0.2%) H_2O_2 solution and cellular uptake was actualized by HeLa cells. Payload release was achieved through two methods, one of which involved the introduction of a redox-responsive disulphide bond between the polymer blocks [88]. A second mechanism involves incorporating a biodegradable component into the stomatocytes' structure. To achieve this, the PEG-b-PS copolymer was blended with up to 75% of a biocompatible and biodegradable copolymer based on poly (ϵ - caprolactone), known as PEG - b - PCL [88]. Another example, Au/Ni/Au/porous Au ultrasound-propelled nanowire motors were prepared by Wang's group through template-directed electrodeposition. The nanowires had a length of 1.7 μm and a diameter ranging from 230 to 280 nm. These nanowires achieved a speed of around 60 $\mu m s^{-1}$ when exposed to ultrasound (2.01 MHz, 6 V). Wang's group loaded DOX onto the nanowires through two different methods: non-covalent or covalent bonding. In the first method, DOX was loaded onto the nanowires via electrostatic interactions after coating them with a polyelectrolyte such as poly(sodium 4-styrenesulfonate) (PSS) or poly(acrylic acid)

(PAA). In the second method, DOX was covalently bonded to the nanowires' methyl thioglycolate (MTG) thiol coating through a hydrazine linker. The loading capacity of DOX was 13.4, 12.6, and 8.6 μg/mL for PSS, PAA, and MTG, respectively, which was sufficient for valid therapy [80]. In addition, the second part of this thesis also includes DOX drug delivery micromotors which is pH sensitive drug release mechanisms. It will be explained in details in the 4th section of the thesis.

The development of smart drug delivery systems for cancer studies that can precisely target specific cells or tissues has the potential to revolutionize the field of biotechnology. However, in order to accurately predict the behavior of *in vivo*, it is essential to analyze the system in physiologically relevant *in vitro* models. It is known that 2D *in vitro* models provide preliminary substantial results to carry the drug delivery studies to the next steps. In addition, 3D *in vitro* models such as spheroids present better mimicking the cellular organization and microenvironment of tissues *in vivo* [89]. Especially drug penetration and drug toxicity can be assessed more accurately owing to densely packed nature of spheroids. In order to analyze the effects of nanomotors used in drug studies, spheroids produce promising results before *in vivo* studies [90, 91]. It should be emphasized that, nano/micromotors which are engineered for smart drug delivery also should be evaluated not only for the drug delivery, but also the propulsion towards the cells and penetration chance within the cells. The barrier that is created by spheroids could limit the penetration of the nano/micromotor drug delivery systems and provide more realistic test environment of their ability to target specific cells or tissues. Overall, the use of spheroids in combination with nano/micromotor drug delivery systems can provide valuable insights into their effectiveness and guide their optimization for clinical use. In the light of this information, scientist have begun to study nanomotors with smart delivery systems with 3D cell culture as well as 2D cell culture. For example, Sanchez *et. al* utilized a $mSiO_2$ nanomotors that was powered by urease and a bladder cancer antibody modified $mSiO_2$ nanomotors were used for active targeting of bladder cancer cells in 3D tumor spheroids. By modifying the nanomotor's surface with the specific antibody, the possibility of the antibody contacting the antigen were improved, thereby penetration of the nanomotors into the spheroid was upgraded. The nanomotor's targeting and motion capabilities, combined with its ability to im-

prove internalization efficiency, resulted in almost 14 times higher internalization in 3D tumor spheroids compared to passive particles without antibodies. Moreover, the targeted nanomotor showed stronger inhibitory effects on spheroid proliferation compared to the unmodified one, suggesting that the antibody-modified nanomotor could be a highly effective tool for targeting bladder cancer treatment [92]. The development of an asymmetric intracellular ion nanoregulator (AINR) is another example that utilizes autonomous movement powered by H_2O_2 and intracellular dual-ion regulation to enhance tumor treatment efficacy. For the self-assembly of a nanocarrier for CDDP delivery, building units such as tanic acid (TA) and poloxamer 188 (F68) were selected. An asymmetric nanoarchitecture (AINR) was formed by in situ deposition of Ag nanoparticles (NPs) on one side of the CDDP-loaded polymer. The AINR autonomously moves in tumor tissues fueled by H_2O_2, leading to the production of a large number of oxygen (O_2) bubbles by catalytically decomposing H_2O_2 into O_2. This local concentration gradient of O_2 bubbles facilitated drug penetration deeper into the tumor. The AINR was rapidly internalized by tumor cells through endocytosis. AINR cascade promoted the accumulation of Pt-DNA adducts, with Ag NPs down-regulating intracellular Cl- through the formation of AgCl precipitation, promoting dechlorination of cisplatin, and increasing the Pt-DNA adducts formation. Herein, TA, which is a natural polyphenol, acted as a yielding chelating agent to reduce intracellular Fe2+ and increase the maintenance of Pt-DNA adducts by inhibiting Fe^{+2} dependent DNA repair enzymes. Cisplatin induced the production of H_2O_2 through specific activation of tumor overexpressed NADPH oxidases, which accelerated the down-regulation of intracellular Cl- and realized a self-augmented CDDP chemotherapy. Overall, the AINR induced robust cisplatin-based tumor chemotherapy by overcoming the cascade chemotherapeutic barriers [93].

2.4.4 Cargo Transport and Nanosurgery Applications

As a possible substitute for conventional passive delivery methods, nano/micromotors can actively and swiftly transport drug payloads, gather medical diagnostic analytes, and carry out microsurgery on cells. Moreover, guided nano/micromotors

can offer targeted controllable movement towards specific tissues or cells, allowing for precise cargo delivery, transportation, and isolation. Nano/micromotors are presently under extensive exploration as an active and controllable delivery system for transporting biomedical payloads. Besides the drugs, genes, proteins even cells can be transported via nano/micromotors [94].

Accurate and targeted cutting is crucial for the success of a surgical procedure. Nevertheless, performing minimally invasive surgery using traditional scalpels and scissors can pose significant difficulties. As a result, there has been significant interest in magnetic microdrillers and rolled-up nanojets due to their ability to penetrate with the aid of an external magnetic field or fuel. This makes them effective instruments for precise and localized incisions [95]. In the literature, it was observed that asymmetric InGaAs/GaAs/(Cr)Pt microjets with sharp tips could spiral in a corkscrew-like motion when exposed to H_2O_2. This unique movement allowed them to drill into fixed HeLa cells. Nonetheless, the use of toxic fuels like H_2O_2 or hydrazine limited their *in vivo* application. To address this issue, the same research group explored the use of remotely controlled Ti/Cr/Fe microtubes for drilling operations. The microdrillers were manipulated and controlled under an external magnetic field, eliminating the effect of toxic fuels. The microdrillers had sharp tips produced by depositing an iron layer on the Ti/Cr layers in a trapezoid pattern before a tilted roll-up process. By increasing the frequency of the rotational magnetic field, the microdrillers could reorient from horizontal to vertical rotation, propel within porcine liver tissue, and start the drilling operation. The diameter of the micro-holes drilled closely matched that of the microdrillers, and different surgical needs could be met by fabricating microdrillers of various diameters by adjusting the material thickness and stress [96]. It was shown that ultrasound can trigger the motion of micro bullets, which have potential as nanosurgery tools. The micromachine was loaded with perfluorocarbon, and when subjected to ultrasound, the vaporization of the perfluorocarbon generated a powerful thrust. This caused the micro bullet to move at an ultrafast speed of 6.3 m/s, allowing it to deeply penetrate lamb kidney tissues [97].

3. SYNTHESIS OF POLYMERIC NANOMOTORS AND INTERACTIONS WITH MCF-7 CELLS FOR DRUG DELIVERY

Nano/micro motors (NMMs) are artificial motors that mimic natural motors and have gained much attention due to their impressive capabilities and unique features. They have been successfully employed in various fields such as (bio)sensing, cargo transportation, cell isolation and trapping, nanosurgery, gene therapy, and drug delivery. In this part of the thesis, self-functionalized robots by conjugating Paclitaxel (PTX) to a poly(3-aminophenylboronic acid) outer layer, a platinum (Pt)-nickel (Ni) segment, and a Pt catalytic inner layer were developed to demonstrate their efficacy in smart drug delivery. The robots exhibited good and smooth autonomous movement with velocities of 44± 9 μm/s and 34 ± 4 μm/s after 6 and 12 h of drug incubation. The fabrication of these motors was accomplished through electrochemical protocols, and the drug loading was carried out by the interaction of the antitumor agent with the outer polymeric layer. The targeted drug delivery was achieved by inducing Near-Infrared irradiation (NIR) to control the movement of the robots towards human breast cancer cells (MCF-7). Moreover, the pH dependency of the system was demonstrated at acidic pH values. The study also showed that the NIR irradiation increased the drug release efficiency through the polymeric robots. The biocompatibility of the motors was investigated using 3-(4,5-dimethylthiazol-2-yl)-2,5-diphenyltetrazolium bromide tetrazolium reduction (MTT) assays, indicating their practical applications in real-world scenarios.

3.1 Experimental Procedures

3.1.1 Instrumentations and Reagents

Electrochemistry-based experiments were acquired at a CHI 720E (CH Instruments Inc., USA) and Autolab-PGSTAT 204 (Metrohm, The Netherlands) electro-

chemical analyzers. AUTOLAB-PGSTAT 204 system was supported with the NOVA 2.1 software. Scanning electron microscopy (SEM) images were obtained with FEI Quanta FEG 250 Model (FEI, USA). Optical microscopic images, videos and fluorescence studies were performed with a Nikon Instrument Inc. Optic LV100ND (Nikon, Japan) coupled with a Andor Zyla VSC-02912 camera. 3-(4,5-dimethylthiazol-2-yl)-2,5-diphenyltetrazolium bromide tetrazolium reduction (MTT) assay was carried out with microplate reader (Biorad,iMARK, USA). Absorbance values were analyzed via UV-Vis spectrophotometer NanoDrop (Thermo Fisher Scientific, USA). Zeta potential analysis were carried out with Zetasizer Nano ZSP (Malvern, UK).

3-aminophenylboronic acid (APBA), sodium sulfate, Triton X-100, methylene chloride, ethyl alcohol ($\leq$ 99.9%) and paclitaxel (PTX) ($\leq$97%) were purchased from Sigma-Aldrich. Polycarbonate (PC) membranes with 2 μm diameters were obtained from Whatman (The Cyclopore polycarbonate membranes, Catalog No 7060-2511, Whatman, Maidstone, UK). Platinum (Pt) plating solution was purchased from Technic Inc. (Platinum RTP, Technic Inc., Anaheim, CA, USA). All other reagents were from Sigma-Aldrich.

3.1.2 Synthesis of Polymeric Tubular Nanomotors

Template-assisted electrodeposition method was used to synthesize PAPBA nanomotors via polycarbonate membranes (2 μm holes in diameter). During electrodeposition of the nanomotors, polycarbonate membrane with conical shaped pores should serve as working electrode, due to that reason, one side of the PC membrane was sputtered with Au film possessed 80 nm thickness [45]. Sputtering was conducted under these parameters at room temperature: 6 cm target-substrate distance, 50-Watt radio frequency power, 2x10^{-2} Torr pressure under Argon flow [98]. After that, teflon cell was used to place Au sputtered PC membrane for electrodeposition. A Pt wire and, Ag/AgCl electrodes were used as the counter and reference electrodes. Poly(3-aminophenylboronic acid) layer was first electrodeposited then the rest of the metallic layers were deposited as Pt/Pt-Ni/Pt, respectively. PAPBA layer was created from

3-aminophenylboronic acid (APBA) monomer using at about a charge of 0.5 C in aqueous acidic solution containing 80 mM APBA, 0.3 M Na_2SO_4 and 0.125 M HCl. Then Pt was electrodeposited at -0.5 V for 50 s. Pt-Ni alloy layer electrodeposition was carried out at -1.0 V for 300 s. Synthesis of nanomotors was completed with the inner catalytic Pt layer deposition at -0.5 V for 180 s (Figure 3.1) [45]. Subsequently, membrane and conductive Au thin film was separated mechanically in 3-4 μm alumina slurry delicately. After separation of Au film, PC membrane was immersed in methylene chloride for 20 min. Immersed PC membrane fragment were washed 3 times with methylene chloride, 3 times ethanol, and 3 times distilled water via centrifugation (6000 rpm, 5 min) to collect the synthesized nanomotors (Figure 3.1). Vortex step was applied in every washing step for 30 s for dissolving of the membrane completely.

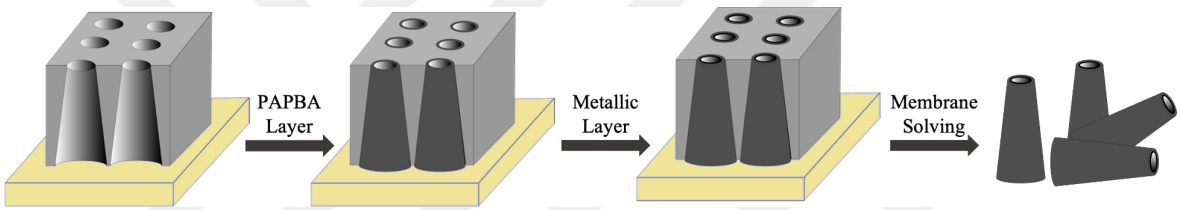

Figure 3.1 Electrodeposition synthesis steps of polymeric PAPBA-enriched nanomotors with template-assisted method.

3.1.3 Electrochemical Characterization of Polymeric Nanomotors

Cyclic voltammetry studies with the nanomotors modified screen-printed carbon electrodes (SPCEs) (DropSens DS 110, Spain) were carried out between -0.4 V and +0.8 V at a scan rate of 100 mV/s. Electrochemical impedance studies with the nanomotors modified SPCEs between the frequency range of 0.1 Hz and 1000 Hz at +0.2 V. The solution was 0.1 M KCl containing 5 mM $Fe(CN)_6^{3-/4-}$ probe in the experiments. Modification was carried out by dropping the nanomotor dispersion prepared in ethyl alcohol for 15 min.

For the control of the release of drug from the polymeric nanomotors, differential pulse voltammetry (DPV) was used. The working electrode was pencil graphite

electrode in the experiments. The reference electrode used was Ag/AgCl (BASi, USA), and the counter electrode was a Pt wire (BASi, USA).

3.1.4 Chemotherapeutic Drug Loading onto Polymeric Nanomotors

Drug loading onto the polymeric nanomotors was carried out with anticancer drug PTX. According to optimize drug loading incubation time, PAPBA nanomotors were incubated in 600 μM PTX solution at pH 9.0 conditions provided by 50 mM phosphate buffer. After that, drug-loaded nanomotors were washed with 50 mM pH 9 phosphate buffer. Florescence intensities were taken after immersion durations (for 2, 4, 6, and 12 h). In addition, velocity of the nanomotors was investigated depending on the drug loading incubation time to compare differences in nanomotor propulsion velocity. Velocity studies were run smoothly under 1% H_2O_2 and 5% Triton-X 100 surfactant. The fuel concentration was up to 10%.

According to analyze the change of surface potential after drug loading procedure, the zeta potential of the nanomotors surfaces were measured by Zeta Potential in ultrapure water at 25 °C Zetasizer Nano ZSP (Malvern, UK). The unmodified nanomotors were compared with nanomotors which were incubated with PTX for 2h and 6h for drug loading. Drug loading was carried out for zeta potential analysis with 600 μM pH 9.0 phosphate buffered PTX solution.

Drug entrapment efficiency was investigated in order to evaluate drug loading capability of the motors. First, drug loading profile was extracted via UV/Vis spectrophotometer (NanoDrop, Thermo Fisher Scientific, USA). PTX stock solution was prepared as 5 mg/mL in absolute ethanol. A batch of nanomotors were immersed into 100 μg/mL diluted PTX solution with pH 9.0 phosphate buffer for 6 h. After incubation, supernatant of the drug loading solution was collected via centrifugation at 6000 rpm for 3 min. Absorbance values of serial diluted 100 μg/mL to 3.13 μg/mL PTX drug solutions were measured, respectively. Additionally, absorbance value of collected drug loading supernatant was measured to obtain drug loading profile. According to

absorbance values, linear regression of trendline equation was determined. The equation was used to calculate unloaded drug amount in the supernatant, which helped to determine loaded amount from the drug loading solution. Drug entrapment efficiency was calculated as follows [92]:

$$Drug\ Entrapment\ Efficiency\ (\%) = \frac{Mass\ of\ Drug\ Loaded}{Total\ Drug\ Mass} \times 100 \qquad (3.1)$$

3.1.5 Chemotherapeutic Drug Release Studies from Polymeric Nanomotors

Controlled drug release experiments were carried out with NIR light and pH difference stimulation. As NIR, 808 nm light was applied to drug-loaded PAPBA nanomotors to stimulate drug release to MCF-7 cells under fluorescence microscope. Propulsion directions of the nanomotors were taken under control by magnetic guidance (external magnet) according to contact MCF-7 cells. Fluorescence intensities were began to take right after the connection between nanomotors and cells. The measurements were recorded at 0, 5,10, 20, 25, and 30 min durations, respectively. The effect of pH on drug release was investigated at pH 6.5 and pH 9.0 as the control group. Fluorescence intensity measurements were recorded at 0, 5, 15, 20, 25, and 30 min. In addition, drug release was evaluated via electrochemical and UV-Vis spectroscopy. The experimental procedure for the preparation of the MCF-7 cells to interact with nanomotors under microscope is summarized in Figure 3.2. The motors were added to cell seeded coverslips with 1% H_2O_2 medium during video capturing. External magnet was used to control the direction of the nanomotors during propulsion.

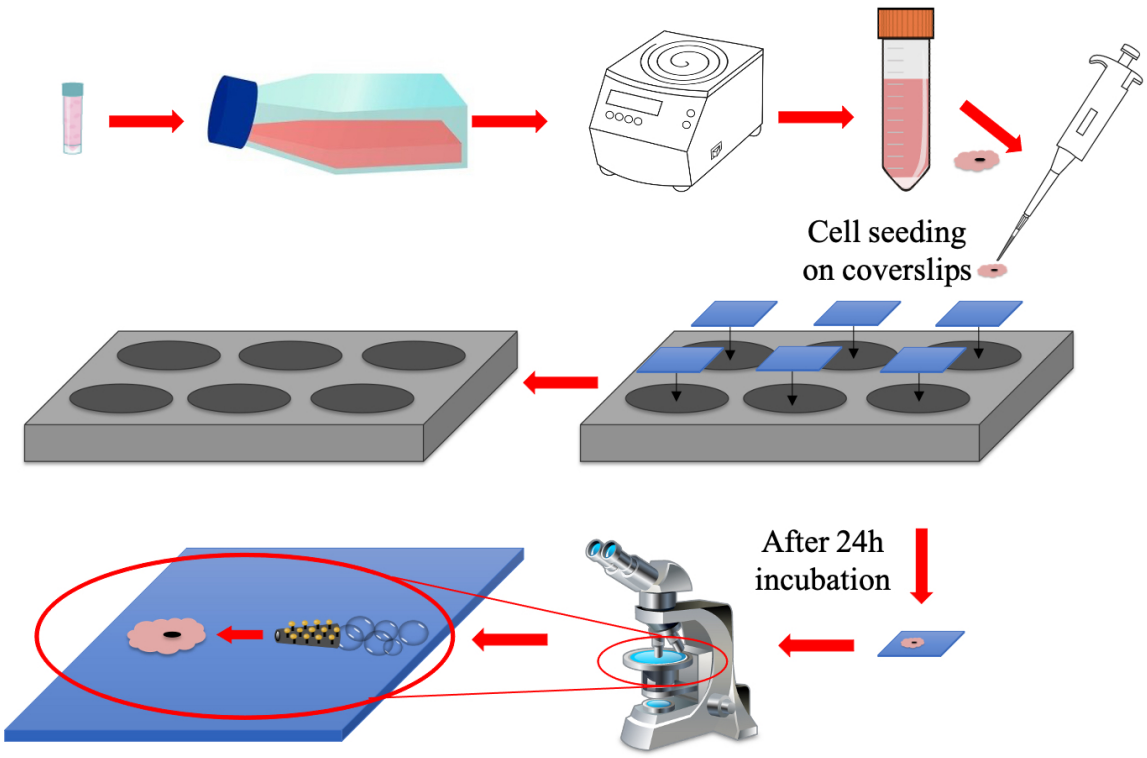

Figure 3.2 Experimental steps of the preparation of MCF-7 cells for interaction with PAPBA nanomotors under microscope: Coverslips were placed in 6-well plates. Cells were seeded on the coverslips before interaction. Nanomotors and cells were interacted after 24 h of incubation.

3.1.6 Cell Viability, and Drug Release Analysis with MTT Assay

In order to assess the cytotoxic effect, 3-(4,5-dimethylthiazol-2-yl)-2,5-diphenyl-tetrazolium bromide (MTT) assay (Glentam, UK) was performed. MTT assay was used for not only evaluate cytotoxicity of the PAPBA nanomotors, but also understand the cytotoxic effect of the controlled PTX release on MCF-7 cells. For this reason, MTT assay as cytotoxicity test was performed using adenocarcinoma continuous cell line (MCF-7, ATCC CRL-1658TM, USA), according to the EN ISO 10993-5 standard with modification. The ATCC-formulated Dulbecco′s Modified Eagle′s Medium F-12 (DMEM F-12) (BioSera, France), containing 10% fetal bovine serum (BioSera, France) and Penicillin/Streptomycin at 100 U/mL (BioSera, France) was used as a complete culture medium. 2X104 cells in each well were pre-cultivated for 24 h in a 96 well-plate, after the cultivation process, the medium was subsequently replaced with serial diluted samples, which were blank and PTX loaded nanomotors and incubated for 24

h. As a control, cells were cultivated in a complete medium and considered as 100% viability. The changes in cell morphology were observed with an optical microscope. The absorbance was measured by Micro Plate Reader (Biorad iMark). All tests were performed in triplicates.

3.1.7 Interaction Studies of PAPBA Nanomotors and MCF-7 Cells

MCF-7 human adenocarcinoma breast cancer cell line was used in order to investigate interaction between PAPBA nanomotors and MCF-7 cells. Targeted drug delivery was performed via catalytic propulsion mechanism. Controlled drug release was triggered via NIR irradiation and also performed via acidic medium of MCF-7 cells after delivery of drug. Cells were cultured in complete medium with DMEM F12 in T25 flask. Cells were removed via trypsin EDTA (Multicell, USA) after reaching confluence then cells were seeded on sterile cover glasses which could fit in well belongs to 6 well-plates. Then interaction between drug loaded nanomotors and cells were observed under light microscope.

3.2 Results

3.2.1 Characterization and Optimization of Catalytic Propulsion Conditions of the Polymeric Nanomotors

Synthesized PAPBA nanomotors were characterized to confirm the achievement of formation in terms of morphology, size and chemical composition at first. Synthesized PAPBA nanomotors were observed under light microscope (Figure 3.3a) and polymerization curve of PAPBA from APBA was seen in Figure 3.3b. Then, SEM images and EDX results were collected to investigate the structure and the polymeric and metallic layers analysis (Figure 3.4). SEM images demonstrated that the conic shaped tubular structures were electrodeposited successfully. The uniformity of the synthesized motors is presented in Figure 3.4a by giving the SEM image of them during their

removal step from the membrane. SEM image of the resulting nanomotor is given from its narrower side opening with a diameter of 1.693 μm in Figure 3.4b. The length of the tubular structures was approximately between 9 and 10 μm (Figure 3.4c). Moreover, EDX results showed that the polymeric and metallic layers were plated successfully (Figure 3.4d). According to this analysis, carbon (C), oxygen (O), nitrogen (N), boron (B), platinum (Pt) and nickel (Ni) contents of the nanomotors were obtained. The structure was mainly comprised of C and Pt as given in EDX spectrum (Figure 3.4e). It is also noted that the N content existed with a high standard deviation.

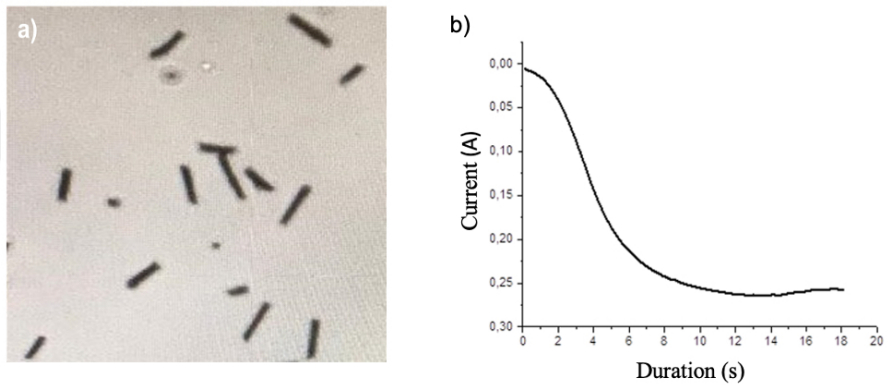

Figure 3.3 Synthesized PAPBA nanomotors observed under light microscope with 100X magnification, b) APBA electrochemical polymerization curve to PAPBA.

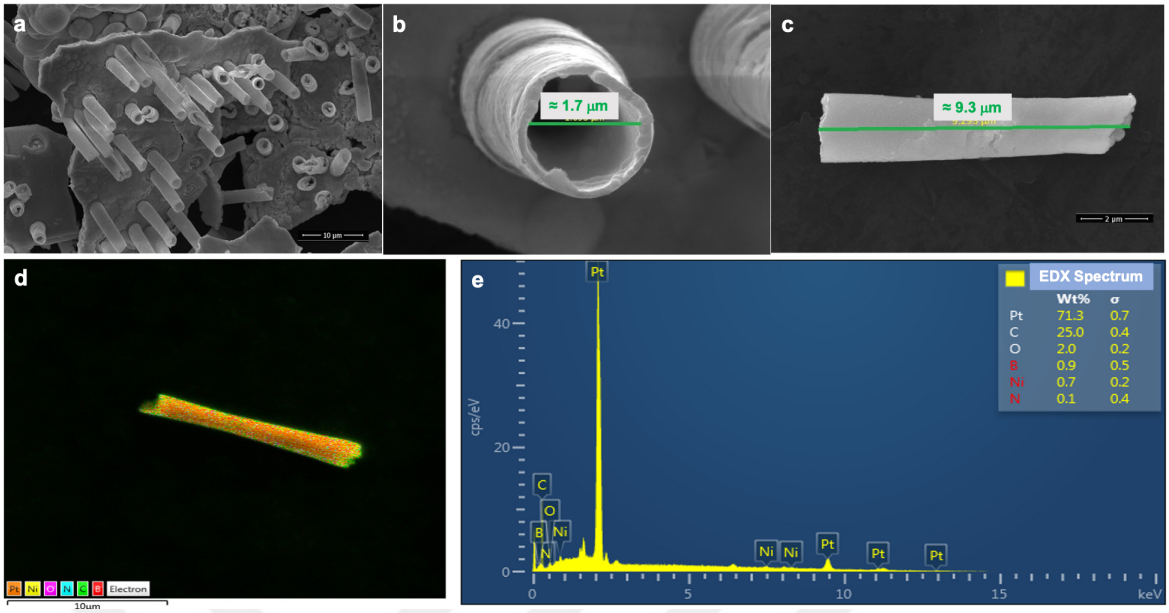

Figure 3.4 SEM images of synthesized nanomotors: a) during their removal step from the membrane, b) narrower opening, c) tubular structure, d) EDX mapping of the nanomotors, e) EDX spectrum.

Following these studies, electrochemical characterization was performed with the polymeric/metallic structures. In Figure 3.5a, CV responses of the PAPBA nanomotors modified SPCE and the unmodified surface were compared in 0.1 M KCl solution that contained containing 5 mM $Fe(CN)_6^{3-/4-}$ to show their surface characteristics. The anodic and cathodic peak currents due to the oxidation/reduction of the redox probe was higher at the modified electrode since the electrode surface area was improved and the electron transfer rate was better. In addition, peak-to-peak separation was lower at the modified electrode owing to the better electron transfer rate. In Figure3.5b compares the electrochemical impedance studies at the polymeric/metallic nanomotors modified electrode and unmodified electrode. Obtained loops were the criterion for the charge transfer resistance (Rct) that occurred at the electrode interface. Rct value was smaller at the modified electrode ($1500 \pm 10\ \Omega$) than the value at the unmodified electrode ($4950 \pm 5\ \Omega$) (n = 3).

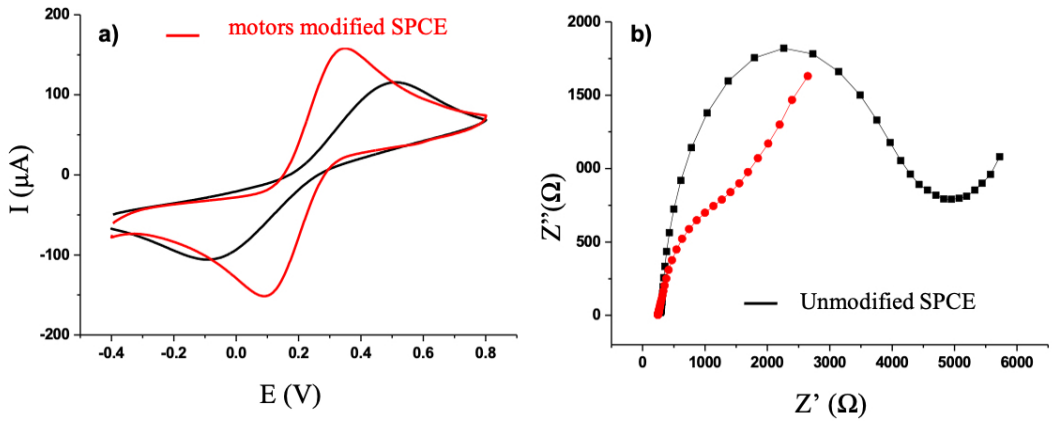

Figure 3.5 a) CV responses at the PAPBA nanomotors modified electrode and unmodified electrode, b) electrochemical impedance spectroscopy responses at the PAPBA nanomotors modified electrode and unmodified electrode.

To present the movement of the nanomotors, their routes were tracked under low and higher fuel concentrations. When using only 1% of H_2O_2, the nanomotors were smoothly moved approximately at a velocity of 127 $\pm$ 6 μm/s. Faster nanomotors moved 293 $\pm$ 3 μm/s using 10% of H_2O_2. Moreover, magnetic control of the immobile motor is shown in figure 3.6 The PTX loaded PAPBA nanomotor were guided by external magnet during catalytic propulsion through the MCF-7 cell.

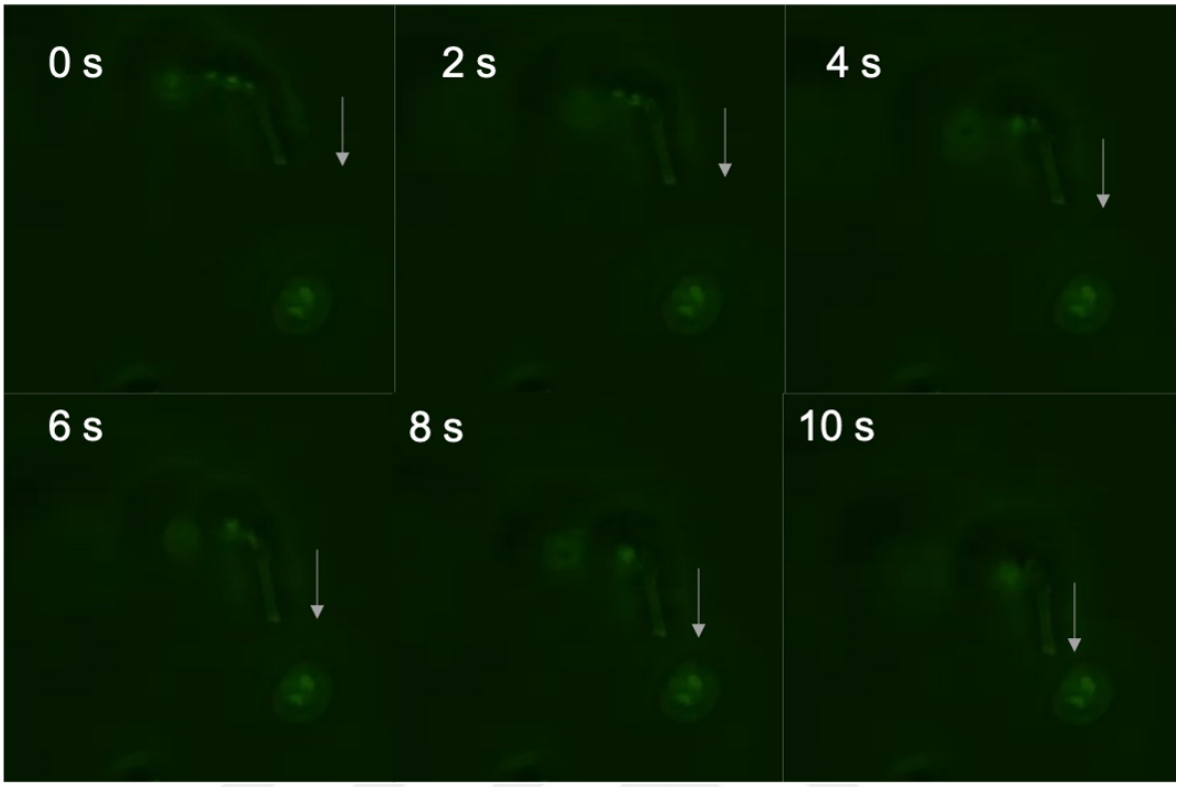

Figure 3.6 Visualized Video by splitting into frames every 2 seconds to show the guided movement of the catalytic motor by external magnet through MCF-7 cell under 1% H_2O_2 condition. (The images were captured under fluorescence microscope with 100 x magnification.).

3.2.2 Chemotherapeutic Drug Loading and Drug Release Studies of Polymeric Nanomotors

Drug loading and release studies of PAPBA nanomotors were completed using chemotherapeutic drug PTX. Phenylboronic acid-enriched surfaces have been used in biomedical applications owing to their pH dependency or boronate affinity by forming conjugates drug molecules [99, 100]. Figure 3.7a after 6 h interaction between PTX and PAPBA nanomotors under pH 9.0 medium. This image shows that PTX loading can be observed easily under microscope with fluorescence attachment. Based on this result, drug loading studies were continued to investigate the effect of the drug incubation duration on PAPBA nanomotors in terms of fluorescence intensity. The correlated change in fluorescence intensity was observed according to increase of incubation durations in Figure 3.7b. The measured fluorescent intensities were 271 ± 25, 849 ± 21,

1758 ± 24, 1972 ± 21, and 2064 ± 23 according to incubation durations, respectively. In addition, 24 h incubation duration was also studied; however, the corresponding fluorescence intensity value did not differ from 12 h duration time. Due to that reason, the study was carried out at 12 h incubation duration time. The effect of incubation time on the velocity of nanomotors was also investigated in medium with 1% H_2O_2 fuel. Decreased velocity of the nanomotor values were found to vary as the increased in incubation duration as expected (Figure 3.7c).

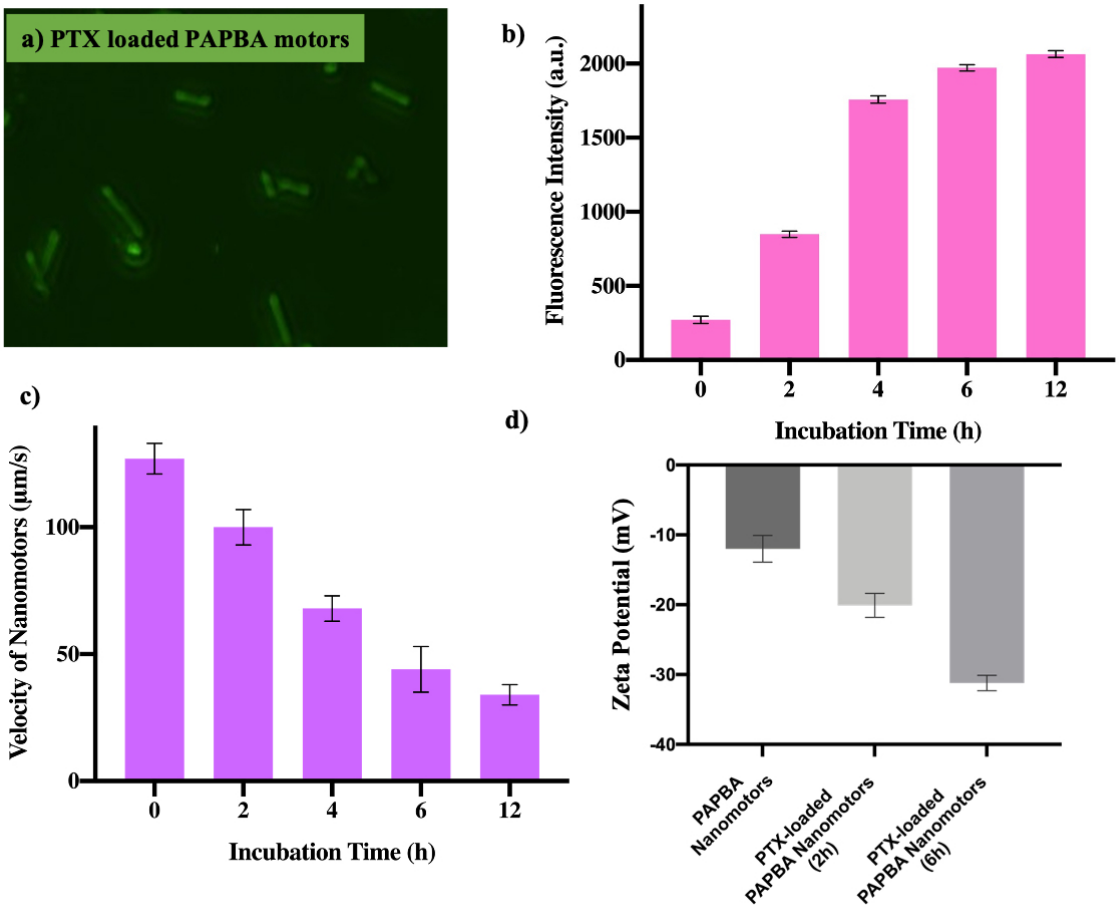

Figure 3.7 a) Fluorescence microscope image of PTX-conjugated PAPBA-enriched nanomotors (6 h incubation), b) Fluorescence intensities of PTX loaded PAPBA enriched nanomotors at different drug incubation times (n = 6), c) Velocity values of PTX loaded PAPBA enriched-nanomotors at different drug incubation times (n = 6), d) Zeta potential values (n = 3) (Conditions for drug loading: 600 μM pH 9.0 phosphate buffered PTX solution. Error bars indicate standard deviations.).

In order to examine the charge of the nanomotor surfaces before and after PTX conjugation, zeta potential analysis was performed in ultrapure water at 25°C. The

average zeta potential value of the PAPBA-based nanomotor was found to be -12.0 ± 1.9 mV (n=3). The average zeta potential value of the PTX conjugated PAPBA-based nanomotor was found to be -31.2 ± 1.1 mV (n=3). The drug incubation time was 6 h in these experiments. PTX loading onto the nanomotors resulted in the reduced zeta potential (Figure 3.7d).

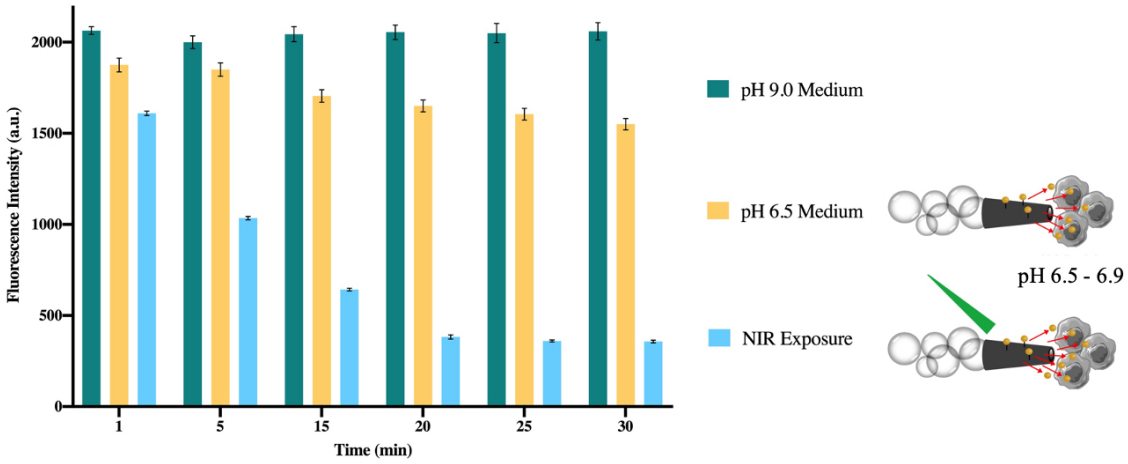

Figure 3.8 Changes in fluorescence intensities of the motors depending on the NIR application durations (blue bars), fluorescence intensities of the PAPBA nanomotors in pH 9 as control (dark green bars), and fluorescence intensities of the PAPBA nanomotors in pH 6.5 as control (yellow bars): comparison for NIR exposure, pH 6.5, and pH 9.0 (n = 6).

For controlled drug release studies, NIR (808 nm) laser was applied to the PAPBA nanomotors which were incubated for 12 h with PTX, and the changes in the fluorescence intensities of PTX loaded nanomotors were recorded over varying durations of NIR application. The fluorescence intensity of the PTX-loaded PAPBA nanomotors was approximately 2100 a.u. (n=6) For a 12 h drug-loaded PAPBA nanomotors, the fluorescence intensity decreased in as much as 1 min. For instance, as a result of the measurements taken 10 min after the laser was removed from the environment, the nanomotor fluorescence intensity was measured as approximately 636 a.u (n=6). These changes in fluorescence intensities upon NIR application is shown in Figure 3.9 (blue bars). The intensities diminished up to 20 min of NIR application and after this duration, they remained almost constant (Figure 3.8). Distribution graph for the changes in fluorescence intensities of motors based on NIR durations is given in Figure 3.9.

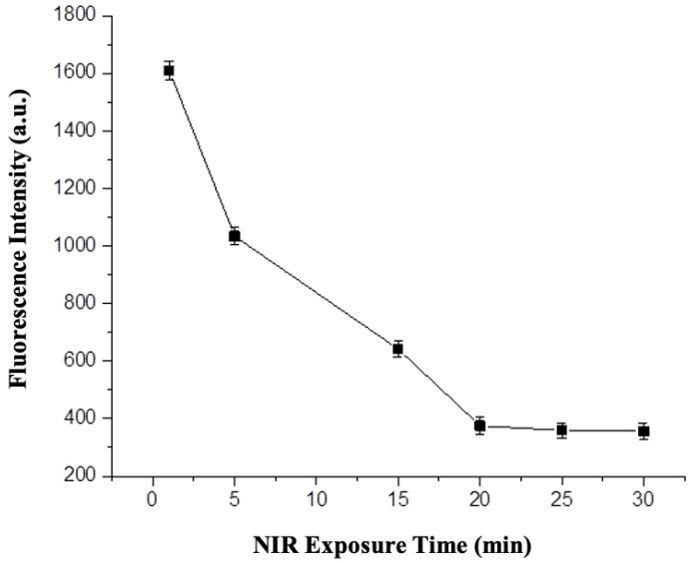

Figure 3.9 Distribution graph for the changes in fluorescence intensities of motors based on NIR exposure time durations (n=6).

During controlled drug release studies, in order to be a control group and to compare with the performance of the NIR-induced system, drug release studies were also carried out depending on the pH change. pH 9.0 was determined as control group and no significant change in fluorescence intensity of nanomotors was observed at this pH (Figure 3.8, dark green bars). Fluorescence intensities of PAPBA enriched nanomotors in pH 6.5 is illustrated in the same figure (yellow bars). As seen from this graph, there is a release response at pH 6.5 according to the increasing release time. However, it was not efficient as NIR radiation application. It is also seen that in longer durations, the release response at pH 6.5 will be more effective. These results presented the NIR triggered delivery of PTX in a rapid and efficient manner.

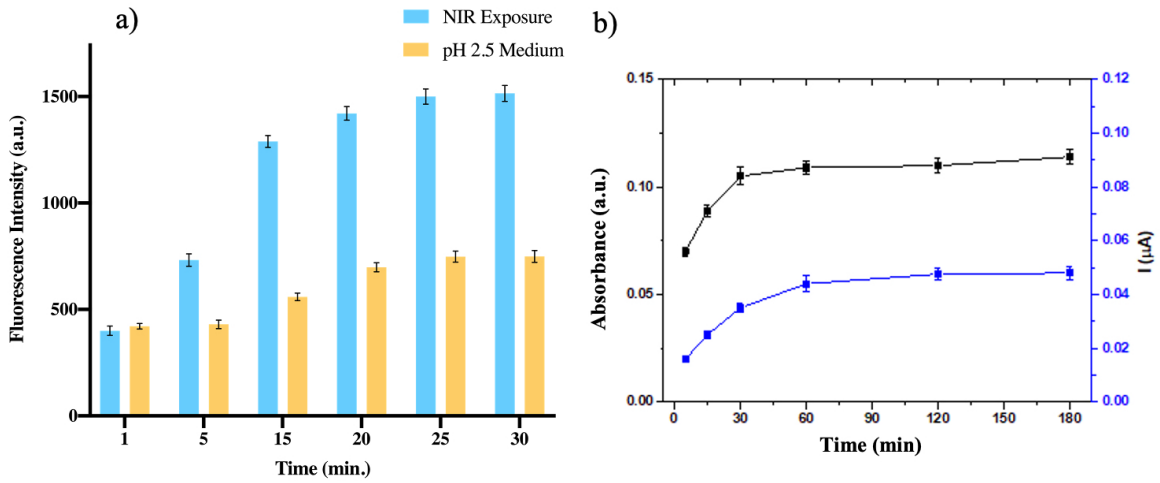

Figure 3.10 a) Comparison of drug release of PAPBA nanomotors for NIR exposure and pH 2.5 (n=6), b) Release profiles for PAPBA-based motors at pH 2.5 by using differential pulse voltammetry and UV-vis spectroscopy (n=3).

Another control for understanding the pH sensitive manner of the PAPBA-enriched motors, the fluorescence intensities of nanomotors were tested in more acidic medium such as pH 2.5. At this value, the trend in release response was more dominant compared to pH 6.5 release response. In addition, the responses of controlled release at pH 2.5 were compared with NIR-induced drug release and NIR response showed more release profile than pH 2.5 medium (Figure 3.10a).

Additionally, the behavior of PTX released from PAPBA catalytic nanomotors was investigated by electrochemical and UV-vis methods. Thus, the presence of drugs (whether they are released or not) was checked with 2 different methods, apart from fluorescence and nanomotor velocity-dependent behaviors. Electrochemical behavior of PTX was investigated at a disposable pencil graphite working electrode using 2 mL of buffer solution. In electrochemical experiments, first of all, since the release studies of this drug in pH 6.5 and pH 9 media is well known from above studies, the release of the drug was controlled depending on the pH change. There was no obvious release response from the nanomotors at pH 9.0. However, by keeping then at an acidic medium such as pH 2.5, the controlled release response was more explicit. This situation was then used to control the presence of the drug. It is reported in the literature that the oxidation

signal of paclitaxel in carbon-based electrodes is approximately +1.3 V (vs. Ag/AgCl) by using differential pulse voltammetry [101]. The release curves created in the light of this information are presented together in Figure 3.10b. In addition, these behaviors were examined on the basis of UV-vis spectroscopy and the results were included in Figure 3.11b. The UV-vis spectra were obtained at about 280 nm [102]. According to these curves, after approximately 60 min, the response of PTX released started to stabilize at the differential pulse voltammetry results, while in UV-vis experiments the response started to stabilize after 30 min.

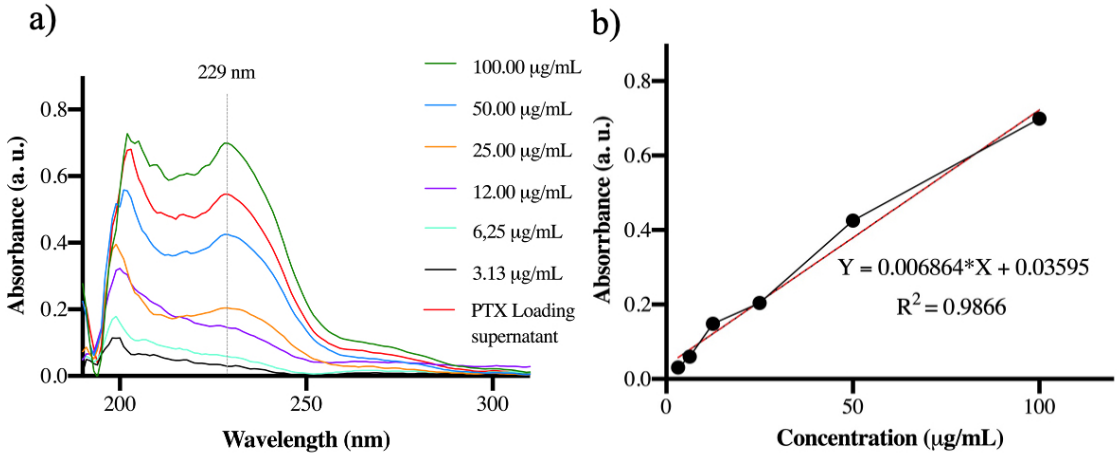

Figure 3.11 a) Drug loading profile of PTX, b) Regression line of the concentration vs. absorbance.

Before drug release experiments with MCF-7 cells, drug loading profile was determined with UV/Visible spectrophotometer in terms of wavelength/absorbance. PTX concentrations (3.13 to 100 μg/mL) and supernatant of drug loading solution gave peak at 229 nm which was correlated with the literature (Figure 3.11a). These absorbance values at the PTX peak gave regression line for concentration per absorbance. This line depicted linear trend and gave an equation according to Beer-Lambert Law to calculate unknown concentration of drug loading supernatant [103, 104]. According to the calculation from equation, the concentration of the supernatant was calculated as 74.3 μg/mL (Figure 3.11b). That means 25.7% of the 100 μg/mL of PTX was loaded to the motors, in other words the entrapment efficiency is 25.7%.

3.2.3 MTT Analysis for Polymeric Nanomotors and Drug Loaded Nanomotors

Drug release experiments were also continued with *in vitro* analysis. MTT analysis was used not only to test the cytotoxicity of the nanomotors themselves but also to evaluate the effect of released anticancer drug from nanomotors on MCF-7 cells [92]. Based on this concept, it is possible to evaluate drug release on basis of cytotoxicity for anticancer drug studies [105, 106]. MTT assay is one of the effective cytotoxicity methods that provides opportunity for quantification results basis on cell viability which showed absorbance values under 570 nm of formazan crystals of viable cells. Herein, in order to determine the required amount of drug that should be loaded to the nanomotors, the half maximal inhibitory concentration (IC 50) of the PTX for 20000 MCF-7 cells was calculated according to MTT assay results of PTX itself. The IC50 value was calculated as 23.74 μg/mL according to the MTT results (Figure 3.123). Based on 25.70% drug entrapment efficiency and 23.74 μg/mL IC 50 value, drug loading was performed at 25 μg/mL nanomotor concentration with the amount of drug loaded corresponding to the IC 50 value, and cells were incubated for 24 h with drug-loaded nanomotors. Then, MTT analysis was performed with PAPBA-based nanomotors.

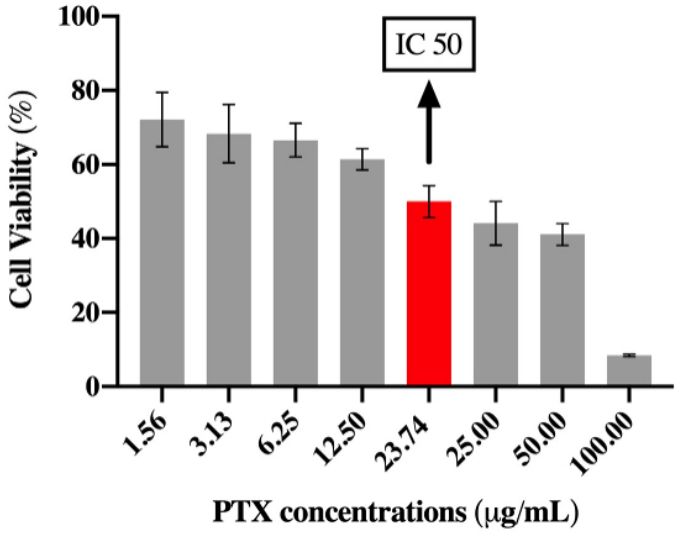

Figure 3.12 IC 50 value calculated for PTX for 2X10^4 MCF-7 cells by MTT analysis (n=3).

In the Figure 3.13, the cytotoxic effect of nanomotors, drug-loaded nanomo-

tors and controlled drug released PAPBA nanomotors were compared in terms of cell viability. According to MTT results, the decrease in cell viability percentages due to controlled drug release was clearly demonstrated. The drug release demonstrated by 25 μg/mL PAPBA-based nanomotors loaded with PTX remained below the IC 50 value.

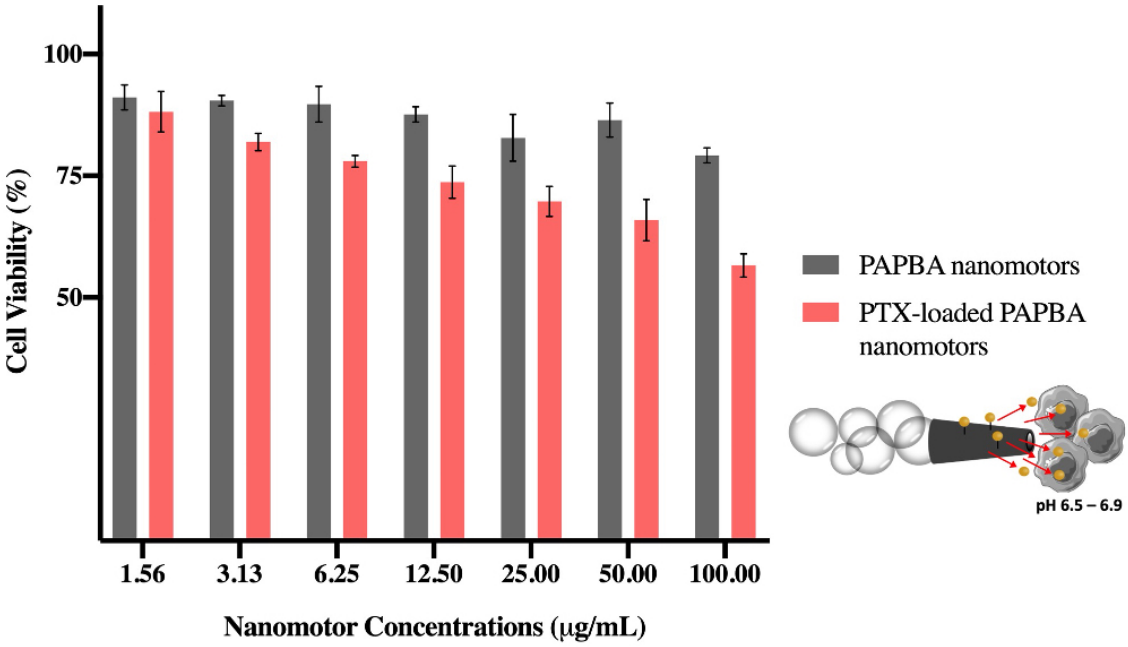

Figure 3.13 Bar graph for the incubation of PAPBA nanomotors and PTX loaded PAPBA nanomotors for 24 h with cells and their MTT analyses.

3.3 Discussion

In this section, PAPBA-enriched nanomotors were synthesized successfully according to characterizations. The study was illustrated in Figure 3.14. SEM images show that tubular structures were synthesized uniformly. In addition, EDX analysis showed the chemical composition was achieved. The structure was mainly comprised of C and Pt as given in EDX spectrum. It is also noted that the N content existed with a high standard deviation (Figure 3.4). Electrochemical characterization CV response showed that the anodic and cathodic peak currents due to the oxidation/reduction of the redox probe was higher at the modified electrode since the electrode surface area

was improved and the electron transfer rate was better (Figure 3.5). Electrochemical impedance studies also presented the faster electron transfer at the nanomotors modified electrode which consisted of electroactive polymer and metallic layers [107]. Therefore, modified electrode with electroactive polymeric and metallic layers-based motors showed improved electrochemical features over unmodified electrode.

Paclitaxel (PTX) is one of the common anti-cancer drug for breast cancer therapy [102]. Drug loading and release studies were carried out on PTX using PAPBA nanomotors. The surfaces enriched with phenylboronic acid have been utilized in biomedical applications due to their pH dependency and boronate affinity which facilitate the formation of drug molecule conjugates [99, 100]. Based on this approach, PTX loading was carried out and in Figure 3.7a can be observed under fluorescent microsope. The correlated change of fluorescence intensity values were observed according to incubation durations. Also the decreased in velocity values under 1% H_2O_2 medium according to increased incubation duration time as expected (Figure 3.7c). This effect is a common result in nano/micromotor studies with cargo loading [45, 108]. In fact, implications of the change in fluorescence intensity and the velocity versus incubation durations can be used as the indicators of drug incubation steps [108]. The propulsion of the PAPBA nanomotor towards cell is shown in Figure 3.6. In addition to this, PTX loading onto the nanomotors resulted in the reduced zeta potential. The surface charge appeared to be more negative due to the alternating changes depending on the surface functional groups. These results demonstrated the successful modification of the drug on the polymeric nanomotors. It is known that the stability of nanoparticles is affected via the alterations in the local dielectric property of the environment [109–111].

During controlled drug release studies, NIR (808 nm) was applied to the PTX loaded PAPBA nanomotors and pH effect was analyzed the effect on drug release with pH 6.5 medium and as a control pH 9 medium. For instance, as a result of the measurements, the nanomotor fluorescence intensities showed dramatic decrease by time (Figure 3.8). This effect is in parallel with the literature [80]. The main emphasis in drug release studies was the realization of NIR-induced release in drug-loaded nanomotors successfully. In addition, drug release was controlled without NIR

application at pH 9.0 medium owing to the loading process was also achieved at this pH value. pH-dependent release behavior of the PAPBA enriched nanomotors was carried out since the pH value has been between 6.5-6.9 around cancerous tissue [112, 113]. Therefore, these experiments conducted in pH 6.5 for PAPBA nanomotors directed to the cell and interacting with the external environment of the cell were added to emphasize the real-life applications of the proposed drug delivery system. With these comparisons, the effective and advantageous use of NIR was demonstrated.

According to investigation of the behavior of PTX released from PAPBA catalytic nanomotors by electrochemical and UV-vis methods, there was an increased response up to these durations. NIR approach was also used in these experiments and it was found that at the end of 5 minutes, the drug release behavior of PTX in the NIR-induced environment was approximately 1.5 times higher over both techniques without NIR exposure.

Entrapment efficiency of PTX was calculated as 25.7%. It should be noted that washing process after drug loading process and hydrophobicity of the drug itself could also affect the drug loading efficiency [105, 114].

The MTT assay was employed to examine the cytotoxicity of both the nanomotors and the released anticancer drug on MCF-7 cells. This approach enables the evaluation of drug release through cytotoxicity measurements in anticancer drug studies [92, 106, 115]. The drug release demonstrated by 25 μg/mL PAPBA-based nanomotors loaded with PTX remained below the IC50 value. This proves that controlled drug release has occurred and shows that PAPBA nanomotors are promising canditate as drug carriers. Also this MTT results give opportunity to compare the source of cytotoxicity of non-drug loaded nanomotors themselves or released drug from nanomotors. When the effect of non-drug loaded nanomotors on cell viability is examined according to the results, their biocompatibility has been proven too [116–118]. In addition, as it was mentioned before in drug release experiments at pH 6.5, the fluorescence change were slightly increased and it was concluded that the release, which would depend on the pH change, might provide an effect for longer periods. Herein, the drug release result

obtained after incubation with MCF-7 cells (which have acidic environment around 6.5 to 6.9) after 24 h was in longer period than the experiments at pH 6.5 condition as we predicted [112].

4. SYNHESIS OF METALLIC MICROMOTORS AND INTERACTIONS WITH MCF-7 CELLS FOR DIAGNOSIS AND DRUG DELIVERY

This chapter discusses the potential of micromotors as active drug delivery systems for cancer treatment. Conventional drug delivery methods can be ineffective and cause harm to healthy tissues, while smart drug delivery systems offer reduced side effects, increased effectiveness, and controlled release of drugs in specific locations. Nano/micromotors have the advantage of motion control and propulsion mechanisms, which allows for reduced drug concentration fluctuation, delivery time, and improved penetration of drugs into hard-to-reach areas. The surface modification of nano/micromotors plays a critical role in the controlled drug release mechanism and drug loading. The development of smart drug delivery systems for cancer treatment has the potential to revolutionize the field of biotechnology. According to these objectives, two segmented, gold (Au), iron-nickel (Fe - Ni) as metallic micromotors were synthesized according to carry out controlled release of anti-cancer drug doxorubicin (DOX) to breast cancer cells and diagnosis of breast cancer with magnetic propulsion. Au segment surface of electrochemical fabricated micromotors were engineered to provide drug (DOX) loading and antibody (antiHER2) immobilization as capturing agent. Engineered Au segment surface made possible controlled drug release in acidic cancerous environment. Magnetic (Fe-Ni) segment ensured biocompatible controlled drug delivery to MCF-7 with magnetic propulsion. In addition, the use of spheroids in combination with nano/micromotor drug delivery systems can provide valuable insights into their effectiveness and guide their optimization for clinical use. All these approaches demonstrate that nano/micromotors present promising application to achieve smart drug delivery methods instead of conventional drug delivery.

4.1 Experimental Procedures

4.1.1 Instrumentations and Reagents

Electrochemical deposition of the micromotors and their electrochemical characterizations were governed by using Autolab-PGSTAT 204 (Metrohm, The Netherlands) which was supported with NOVA 2.1 software. EIS studies were carrried out with the help of FRA32M module which is integrated into this electrochemical system. Optical microscopy studies were realized by using Zeiss Axiovert A1 inverted microscope (Germany) and fluorescence studies were conducted with a Leica, DM, IL (Germany). SEM images and EDX data were obtained by using Thermo Scientific Quattro S (USA). Zeta potential data were collected from Zetasizer Nano ZSP (Malvern, UK). Microplate reader (Biorad, iMark, USA) was used for the 3-(4,5-dimethylthiazol-2-yl)-2,5-diphenyltetrazolium bromide tetrazolium reduction (MTT) and Alamar Blue assay. Absorbance values were obtained from UV-Vis spectrophotometer NanoDrop (Thermo Fisher Scientific, USA).

Iron(II)sulfate ($FeSO_4$), nickel(II)sulfate ($NiSO_4$), trisodium citrate ($Na_3C_6H_5O_7$), ethyl alcohol ($\leq$99.9%), boric acid (H_3BO_3) and Triton X-100 were from Sigma-Aldrich. A commercial gold plating solution (Orotemp, Italgalvano spa, Technic Group) was used to deposit the Au layer. Dox ($\leq$97%) was purchased from Glentham Science, USA. Alumina membrane template containing 200 nm diameter cylindrical pores (catalogue no.6809-6022; Whatman, Maidstone, UK) were used for micromotor fabrication. The other chemicals used in the experiments were purchased from Sigma-Aldrich.

4.1.2 Synthesis of Magnetic Rod-Shape Metallic Micromotors

Template-assisted electrodeposition method was chosen to synthesize Au:Fe-Ni micromotors via AAO membranes (0.2 μm holes in diameter). During electrodeposition of the micromotors, AAO membrane should serve as working electrode, since, one side of the AAO membrane was sputtered with Ag film. In order to coat conductive Ag

layer, sputtering was realized under Argon flow (Plazmatek, Turkey). The Ag sputtered alumina membranes were then placed into teflon cell and the deposition solutions were poured into the cell. First, Au segment was deposited. This step was followed by the codeposition of Fe-Ni metallic segment. During Au electrodeposition, commercial gold plating solution was used at -0.05 A by using a charge of 60 C. Fe-Ni were codeposited from laboratory made Fe-Ni plating solution which was containing 0.1 M $FeSO_4$, 0.3 M $NiSO_4$, 0.06 M $Na_3C_6H_5O_7$, and 0.5 M H_3BO_3 at -1.3 V [119] by using a charge of 30 C. After these deposition steps, dissolving procedure was done as follows: the alumina slurry was used to remove the Ag thin layer mechanically from the membrane. Then alumina membrane was immersed in 3 M sodium hydroxide (NaOH) solution for 30 min. This step was followed by the 3 times NaOH washings and 3 times distilled water washings via centrifugation at 6000 rpm for 5 min [119]. As a result, magnetic motors were released from the alumina membrane and collected (Figure 4.1).

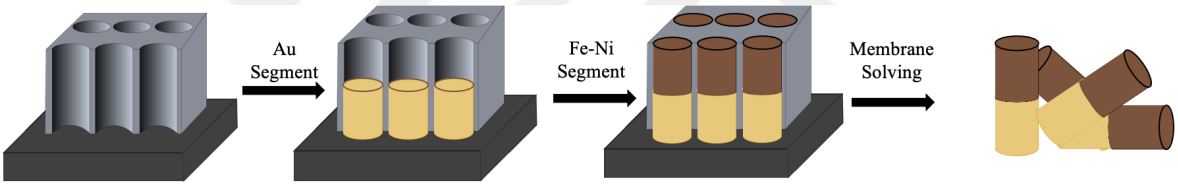

Figure 4.1 Au:Fe-Ni micromotor synthesis steps with template - assisted method by electrodeposition.

4.1.3 Anti-Cancer Drug Loading onto Metallic Micromotors

Drug loading onto the metallic micromotors was carried out with anticancer drug DOX. The surface of the motors were functionalized with immersion in 1 mL poly(sodium 4-styrenesulfonate) (PSS) solution (2 mg/mL in 8 mM NaCl) for 3 h [60, 120]. The metallic micromotors were washed after immersion with distilled water 3 times. Then, the anti-cancer drug DOX solution was incubated with the micromotors 24h at 4°C and washed three times with distilled water. After that, the nanomotors were observed under light microscope with fluorescent attachment to visualize the DOX on nanomotors at 480nm. The velocity studies were governed under light microscope, propulsion of the micromotor were provided by external magnet and captured as video.

The velocity values were determining by using Imaje J tracking extension after video capturing.

According to analyze the change of surface potential after drug loading procedure, the potential of the micromotor surfaces were measured by Zeta Potential in ultrapure water at 25°C Zetasizer Nano ZSP (Malvern). The unmodified micromotors were compared with DOX loaded micromotors. Drug loading was carried out for 24h incubation with 500μg/mL DOX solution after PSS incubation for 3h at 4°C.

Drug entrapment efficiency was calculated in order to reveal drug loading capability of the nanomotors. First, drug loading profile was determined via UV/Vis spectrophotometer (NanoDrop, Thermo Fisher Scientific, USA). Nanomotors were immersed into 100μg/mL diluted DOX solution overnight. After incubation, supernatant of the drug loading solution was collected by centrifugation at 6000 rpm for 3 min. Absorbance values of serial diluted 100 μg/mL to 3.13 μg/mL DOX drug solutions were measured, respectively. Moreover, absorbance value of collected drug loading supernatant was measured to extract drug loading profile. According to absorbance values, linear regression of trendline equation was determined. The equation was used to calculate unloaded drug amount in the supernatant, which helped to determine loaded amount from the drug loading solution. Drug entrapment efficiency was calculated according to equation 3.1.

4.1.4 Chemotherapeutic Drug Release Studies of Metallic Micromotors

Controlled drug release experiments were realized by pH difference stimulation. The effect of pH on drug release was investigated at pH 6.5 and pH 9.0 as the control group. The measurements were taken at 0, 12h, and 24h durations via UV-Vis spectroscopy, respectively. Moreover, drug release from drug loaded micromotors was analyzed by testing cell viability due to cytotoxicity on cells as a result of the acidic environment of MCF-7 cells [112]. Moreover, the released or uptake of DOX by cells was visualized under light microscope with fluorescent attachment. The DOX-loaded

micromotors were incubated with 5X103 MCF-7 cells for 24h. After that, cells were fixed with 4% formaldehyde solution prepared with PBS. The fixation solution was added and removed after 10 minutes. According to stain nucleus, diluted 1:1000 DAPI solution was added to fixed cells and after 3 minutes, the staining solution was removed and the cells were washed with PBS. Thus, the DOX uptake of cells from micromotors and their nuclei was observed under microscope (DM IL Leica) as red and blue with fluorescent attachment at 358nm filter (blue) [121].

In addition, the cellular uptake was analyzed by UV-Vis spectroscopy. The DOX-loaded micromotors were prepared as a suspension with cell culture medium. Then DOX-loaded micromotors were incubated with cells for 24h. According to control the drug release in cell medium, the absorbance value of medium supernatant was measured. Then cell medium was removed from the wells and lysis buffer (0.1 TritonX-100 and 0.01M NaOH solution) [122] was added to rapture cells and the absorbance values was measured.

4.1.5 Antibody Immobilization on Metallic Micromotors

It is known that; breast cancer cell membranes have overexpressed HER2 receptor than healthy breast cells and other cancer cells [123]. Due to that reason, the synthesized micromotors were investigated for their movement and cell interaction, in addition to their drug delivery purpose, by immobilization of antiHER2 antibody on their surfaces for targeting approach of MCF-7 cells. First of all, the micromotors were immersed in 0.01M DTDPA for 24h to create -COOH groups on the micromotor surface [124]. Then micromotors were washed with distilled water at the end of the duration. After that, to immobilize antiHER2 antibodies, the -COOH functional groups on the Au segment was activated using carbodiimide activation method. The motors were incubated in 1-ethyl-3-(3-dimethylaminopropyl) carbodiimide N-hydroxysuccinimide (NHS/EDC) (10mM/20mM) solution for 15 minutes, and then washed 3 times with PBS solution. Afterwards, 5 μg/mL of antiHER2 antibodies prepared in PBS solution were incubated for 1h. Thus, a covalent bond was formed between the carboxyl

group created on the surface with DTDPA and terminal amino groups of the antiHER2 antibodies [125, 126].

4.1.6 Cell Viability, and Drug Release Analysis Experiments with Monolayer Cell Culture

In order to evaluate the cytotoxic effect, 3-(4,5-dimethylthiazol-2-yl)-2,5-diphenyltetrazolium bromide (MTT) assay (Glentam, UK) was performed. MTT assay was used to evaluate cytotoxicity of the metallic nanomotors and understand the cytotoxic effect of the controlled DOX release on MCF-7 cells. MTT assay, as cytotoxicity test was performed using adenocarcinoma continuous cell line (MCF-7, ATCC CRL-1658TM, USA), according to the EN ISO 10993-5 [127] standard with modification. The ATCC-formulated Dulbecco′s Modified Eagle′s Medium F-12 (DMEM F-12) (Capricorn, Germany), containing 10% fetal bovine serum (BioSera, France) and 1% Penicillin/Streptomycin (Capricorn, Germany) was used as a complete culture medium. 2 x 10^4 cells in each well were pre-cultivated for 24 h in a 96 well-plate, after the cultivation process, the medium was subsequently replaced with serial diluted samples, which were blank and DOX loaded nanomotors and incubated for 24 h. As a control, cells were cultivated in a complete medium and considered as 100% viability. Then MTT solution was prepared as 10% with complete cell medium. Then cells were incubated for 4 hours with MTT solution. Supernatant removed, then DMSO were added to the wells to solve the formazan crystals before absorbance reading. The absorbance was measured by Microplate Reader (Biorad, iMARK, USA). All tests were performed in triplicates.

4.1.7 2D and 3D Cell Culture Studies

MCF-7 human adenocarcinoma breast cancer cell line was used in order to investigate interaction between Au:Fe-Ni micromotors and MCF-7 cells. Targeted drug delivery was conducted via magnetic propulsion mechanism with external magnet (≈

4700 Gauss). Controlled drug release was performed via acidic environment of MCF-7 cells after delivery of drug. Cells were cultured in complete medium with DMEM F12 in T25 flask. Cells were removed via trypsin EDTA (Multicell, USA) after reaching confluence then cells were seeded on sterile coverslips which could fit in well belongs to 6 well-plate and this procedure was also summarized in (Figure 3.2). Moreover, the seeded 5 x 10^3 MCF-7 cells on cover classes were used to show the diagnostic approach as interaction between antiHER2 immobilized nanomotors and MCF-7 cells. SH-SY5Y neuroblastoma cell line was also used as a control group to compare the interaction between MCF-7 and antiHER2 immobilized micromotors. The magnetic propulsion through the cells were captured as video. The micromotors were added to the cell seeded cover glasses before the video capturing under light microscope (Carl Zeiss Axiovert A1 Inverted microscope, Germany).

SH-SY5Y cells were cultured with complete DMEM F12 medium as MCF-7 cells in T25 flasks. After confluence of the cells, they were trypsinized and seeded 5 x 10^3 on sterile cover glasses which placed in 6 well-plates.

Then the magnetic propulsion of the DOX-loaded and antiHER2 immobilized micromotors towards the cells and interaction between nanomotors and the cells were observed, after 24h cultivation. The micromotors were added onto cell seeded coverslides which placed under microscope and the propulsion provided by external magnet ($\approx$ 4700 Gauss). During propulsion, their videos were captured under light microscope camera (Zeiss, Axiovert A1 inverted microscope).

According to create 3D structured cell culture, MCF-7 cell line was used with hanging drop method. The optimum cell number was determined considering that the microscope image and and video would be taken (Figure 4.2c-e). Cells were trypsinized after reaching confluence from monolayers with the same procedure in section 2.7 and cell suspensions were prepared at 3000 cells per drop (30μL), the drops were placed onto lids of non-treated dishes. Herein, the difference from the monolayer cell culture, the cell medium was prepared with 0.24 (w/v)% methylcellulose which provide dense and regular structure [128]. In addition, 15mL sterile PBS was added to petri

dishes to prevent extra evaporation from cell suspension drops. The cell suspension drops were hanged and incubated for 3 days. After that, the spheroids were harvested and transferred to non-treated petri dishes to eliminate proliferation, in other words, to eliminate change in structure. The spheroids were incubated for 7 days before performing cell culture experiments. Spheroids were transferred to the non-treated U-bottom 96 well plates according to govern experiments. For the magnetic propulsion through the spheroid experiments, spheroids were transferred to the cover slip and, micromotors were added to the medium for observation of magnetic propulsion of micromotors through spheroids before video capturing. The structure of spheroids was characterized with F-actin/DAPI (Thermo Fisher) staining. F-actin provided to visualize actin filaments of the cells within the spheroids and DAPI stained the nuclei of the cells within the spheroids under light microscope with fluorescent attachment. The spheroids were fixed by 4% formaldehyde solution for 30 minutes. Then, the spheroids were washed by PBS. After that, images were captured with fluorescent attachment at 488nm (green) for f-actin cytoskeleton and 358nm (blue) filter for DAPI nuclei of cells under microscope (DM IL, Leica) [129].

According to analyze drug release on spheroids, the cytotoxic effect of DOX was evaluated via Alamar Blue cell viability assay due to its uniform permeability into spheroids [128, 131]. Spheroids were incubated with 10% (v/v) Alamar solution cell medium for 24h as control and the absorbance of the incubation solution was read by microplate reader. Then the same spheroids were incubated with DOX loaded nanomotors for 24h as monolayer cell culture studies mentioned above (section 4.1.6). After removing DOX loaded micromotors suspension, the spheroids were incubated with 10% Alamar blue / cell medium for 24h, then the absorbance of the supernatant was read by microplate reader (Biorad, iMark) (n=3).

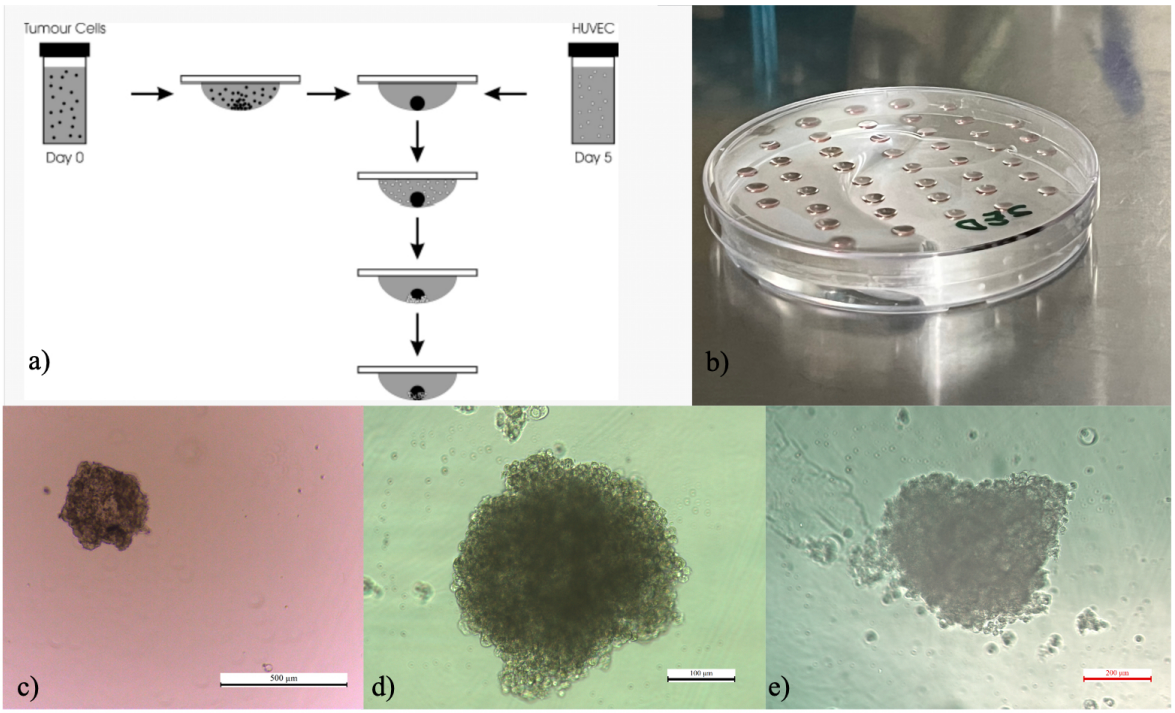

Figure 4.2 a) Hanging drop cell culture method [130], b) hanged cell suspension drops (30 L) on petri lid, c) spheroid with 1000 cells (scale bar = 500μm), d) spheroid with 3000 cells (scale bar = 100μm),e) spheroid with 5000 cells scale bar = 200μm).

4.2 Results

4.2.1 Characterization Studies of Synthesized Metallic Nanomotors

Synthesized Au:Fe-Ni nanomotors were characterized to confirm the achievement of formation in terms of morphology, size and chemical composition at first. Scanning electron microscopy (SEM) images demonstrated that the rod-shaped structures were electrodeposited successfully (Figure 4.3). The uniformity of the synthesized motors is presented in Figure 4.3 by giving the SEM image of them after removal step from the membrane. SEM image of the resulting micromotor is given from its Au segment is around 2.640 μm and Fe-Ni segment is around 1.547 μm in Figure 4.3. The length of the rod-shaped structures was approximately around 4 μm (Figure 2a, b). Moreover, EDX results showed that the metallic segments were plated successfully (Figure 4.3). According to this analysis, gold (Au), iron (Fe) and nickel (Ni) contents

of the nanomotors were obtained. Au, Fe, and Ni were demonstrated as yellow, blue and green in EDX color mapping, respectively.

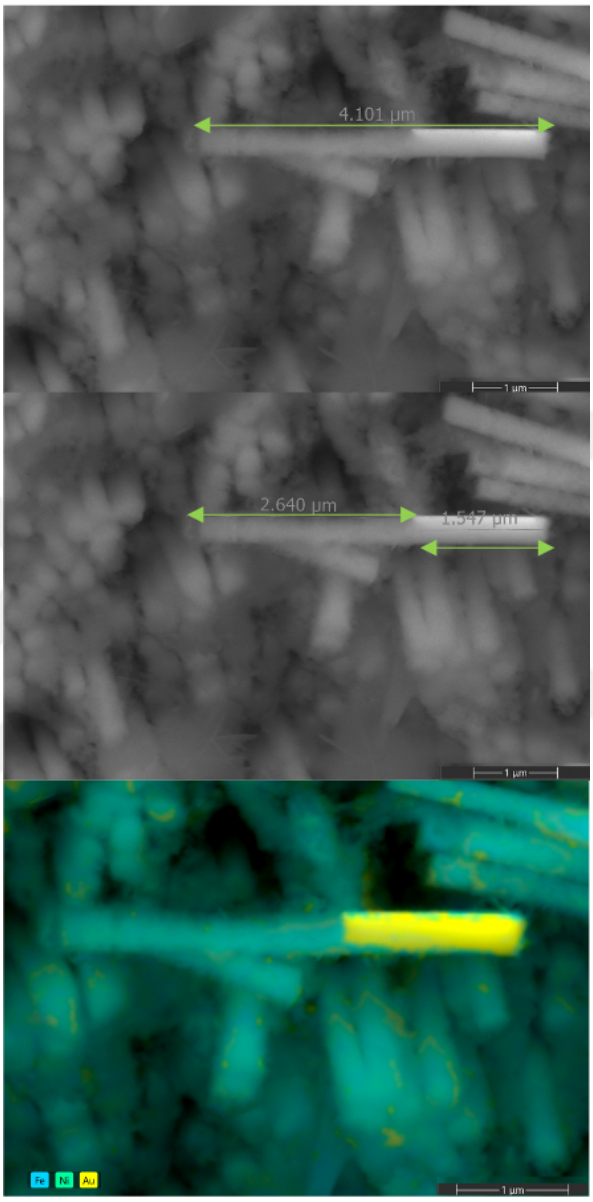

Figure 4.3 SEM images of synthesized micromotors and EDX color mapping of the micromotors, The length measurements of the micromotors and the Au and Fe-Ni segments, EDX color mapping of the nanomotors results of the Au, Fe, and Ni were demonstrated as yellow, blue and green in EDX color mapping, respectively.

4.2.2 Chemotherapeutic Drug Loading and AntiHER2 Immobilization Studies of Au:Fe-Ni Micromotors

Doxorubicin (DOX) is one of the common anti-cancer drug for breast cancer therapy. Drug loading and release studies of metallic motors were completed by using chemoterapeutic drug DOX. First of all, micromotors were modified with PSS as mentioned in experimental section. Then DOX and PSS modified micromotors were incubated for 24h. After 24h incubation, washed drug loaded micromotors were observed under microscope with fluorescence attachment owing to self-fluorescent feature of DOX (Figure 4.4a). The velocity of the micromotors also were evaluated after drug loading process and drug loaded micromotors had decreased 51.2 ± 5.2 to 41.3 ± 10.9 $\mu m/$s velocity in comparison to blank micromotors (Figure 4.4c). In addition, before cell culture experiment, drug loading profile was determined and the result also show that DOX was successfully loaded on the micromotors (Figure 4.5.)

According to prepare micromotors for diagnostic approach, the gold segment of micromotors were modified with firstly DTDPA, then anti-HER2 was immobilized via EDC/NHS crosslinker. According to show antibody immobilized micromotors under microscope with fluorescent attachment, immunostaining was conducted with fluorescence tagged seconder antibody (Figure 4.4b). Velocity of the Anti-Her2 immobilized micromotors were also analyzed as were DOX-loaded micromotors and the decreased velocity result were obtained as expected (Figure 4.4c).

Surface charge of the micromotor surfaces before and after DOX loading and antiHER2 immobilization, zeta potential analysis was carried out in ultrapure water at 25 °C. Zeta potential of unmodified surface Au:Fe-Ni micromotors measured as -19.43 ± 0.23 mV. After DOX loading, the Zeta potential value was measured as -22.67 ± 0.92. In addition, zeta potential of antiHER2 immobilized Au:Fe-Ni micromotors was measured as -4.50 ± 1.77 (Figure 4.4d).

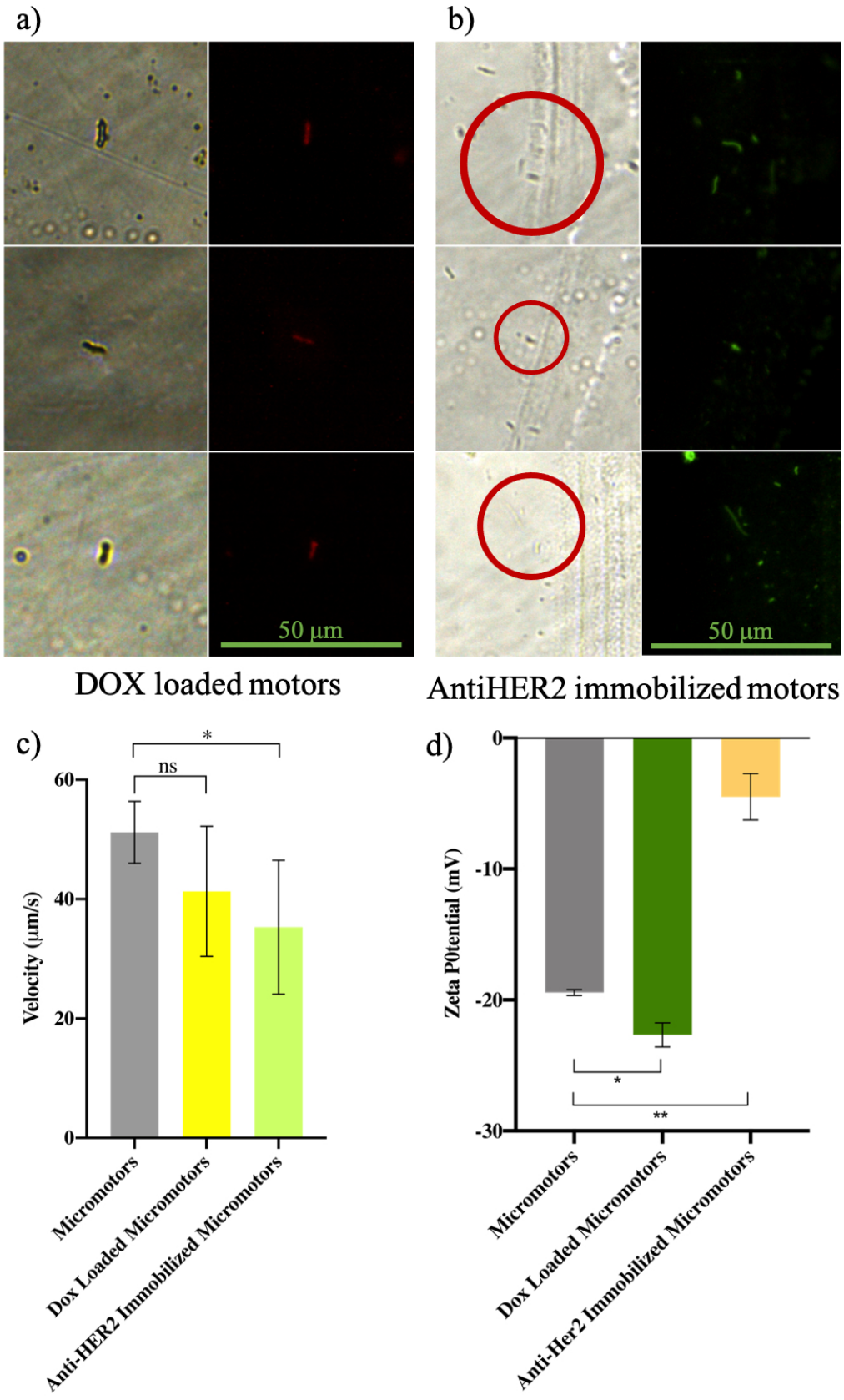

Figure 4.4 a) Fluorescent images of DOX loaded motors (Scale bar = 50 m)b) immunocytostained AntiHER2 immobilized motors (Scale bar = 50 m), c) Velocity values of unmodified, DOX loaded and antiHER2 immobilized motors (n=3), d) Zeta potential values of unmodified, DOX loaded and antiHER2 immobilized motors (n=3) (Conditions for drug loading: 500 μg/mL DOX solution. Error bars indicate standard deviations.).

4.2.3 Chemotherapeutic Drug Release Studies

Controlled pH responsive DOX release from micromotors was analyzed with several methods. First of all, pH 6.5 and pH 9 media were used to test the pH effect on DOX release from micromotors (Figure 4.5). The test duration was determined based on the duration of cell experiments with DOX loaded micromotors. DOX released was measured by UV-Vis spectroscopy due to the fluorescent property of DOX. It was observed that, changes in the absorbances values of DOX were recorded in increased manner in pH 6.5 as 0.082 ± 0.004, 0.143 ± 0.002, and 0.397 ± 0.030 a.u., respectively. It could be clearly observed that pH 9 medium buffer had no significant effect as control group on drug release which values are 0.002 ± 0.0006, 0.004 ± 0.0010, and 0.005 ± 0.0010, respectively.

According to show quantitative analysis of cellular uptake, the absorbance values were measured after 24h incubation with DOX loaded micromotors. First, the absorbance values of complete cell culture medium supernatant with DOX loaded micromotors was measured as 0.019 ± 0.002 a.u. After that, the medium which was measured with UV-Vis Spectroscopy, then lysis buffer was added to the wells to rupture the cells. The absorbance values of the supernatant of ruptured cells with lysis buffer was measured as 0.099 ± 0.002 a.u. After 24h incubation, the cellular uptake has higher absorbance value than DOX loaded micromotor suspension within cell culture medium, the measures are 0.099 ± 002 and 0.019 ± 0.002, respectively. (Figure 4.54b). This analysis also shows that, drug release around the cells were performed realized and cellular uptake of the released drug was occurred.

The controlled drug release was tested on MCF-7 cells. Drug loaded micromotors were incubated with cells which were added to the cells within the cell culture medium. Cellular uptake was observed under microscope after 24h incubation. Before observation, cells were fixed and the nuclei of cells were stained with DAPI (Figure 4.5c).

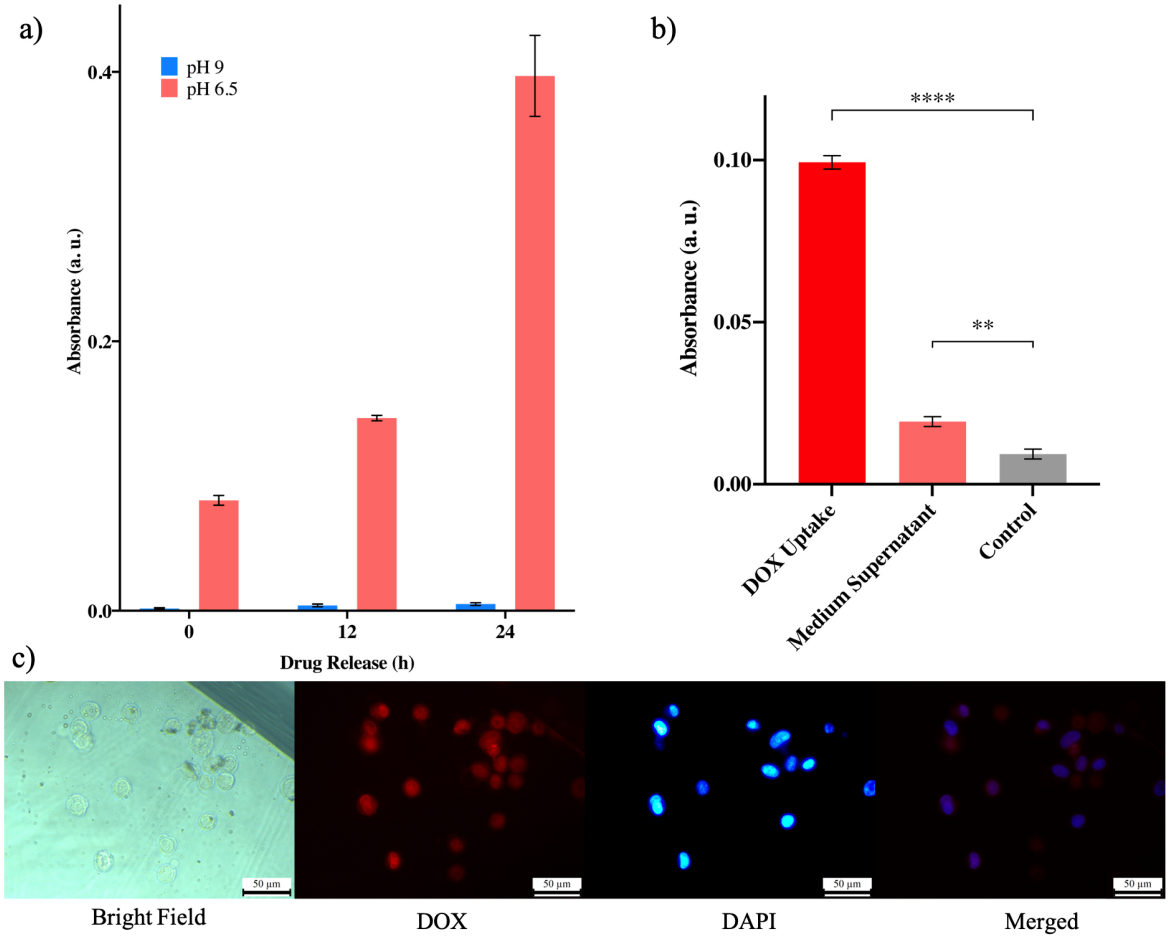

Figure 4.5 a) Changes in absorbance values of the pH 6.5 and pH 9 media in terms of drug release, b) Cellular uptake absorbance values comparison with medium supernatant after 24h cell and DOX-loaded micromotors incubation, c) cellular uptake fluorescent images of MCF-7 cells with DAPI staining. (Conditions for drug loading: 500 μg/mL DOX solution. Error bars indicate standard deviations.).

4.2.4 2D and 3D *in vitro* Studies

According to evaluate the cytotoxicity of the micromotors themselves and the effect of the DOX released from MCF-7 cells, MTT analysis was used. Before MTT analysis, drug loading profile was extracted with UV-Vis Spectroscopy. Absorbances of DOX concentrations (3.13μg/mL to 100μg/mL) and supernatant of DOX loading solution was measured. The absorbance wavelength of the DOX observed at 480nm, which was correlated with the literature (Figure 4.6a) [132]. The regression line for concentration per absorbance was obtained from absorbance values at DOX peak. This

line exhibited a linear trend and provided an equation, based on the Beer-Lambert Law, for determining the unknown concentration of drug loading supernatant (Figure 4.6b). According to result, entrapment efficiency was calculated as 30.72%. It should be mentioned that the efficiency of drug loading may be influenced by washing procedure.

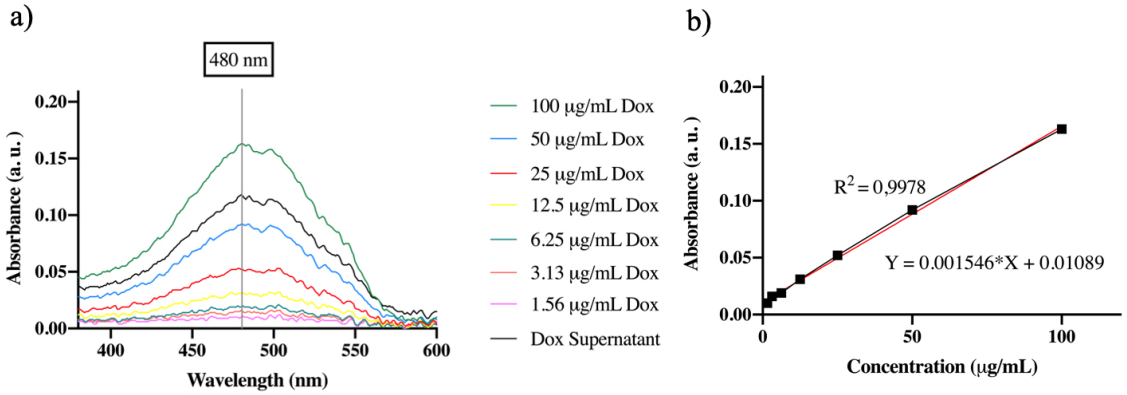

Figure 4.6 a) Drug loading profile of DOX, b) Regression line of the concentration vs. absorbance of DOX.

The MTT analysis served dual purpose of testing both cytotoxicity of the micromotors and the impact of the anticancer drug was released from micromotors on MCF-7 cells. This approach enables the evaluation of drug release by correlating it with cytotoxicity, which is useful technique for studying anticancer drugs [106, 115]. Since MTT assay is a highly effective method for measuring cytotoxicity that permits quantification of result based on cell viability, as indicated by the absorbance values under 570 nm of the formazan crystals formed by cells. To determine the optimal amount of drug to load onto micromotors, the half maximal inhibitory concentration (IC 50) of DOX was calculated for a sample of 2 x 10^4 MCF-7 cells based on the MTT results obtained for the drug. The IC 50 value was determined to be 12.37 μg/mL (Figure 4.7). Given drug entrapment efficiency of 30.72% and IC 50 value of 12.37 μg/mL, drug loading was conducted at a concentration of 25 μg/mL for micromotors, corresponding to the IC50 value. The cells were treated with DOX loaded micromotors and incubated for 24h before conducting MTT analysis.

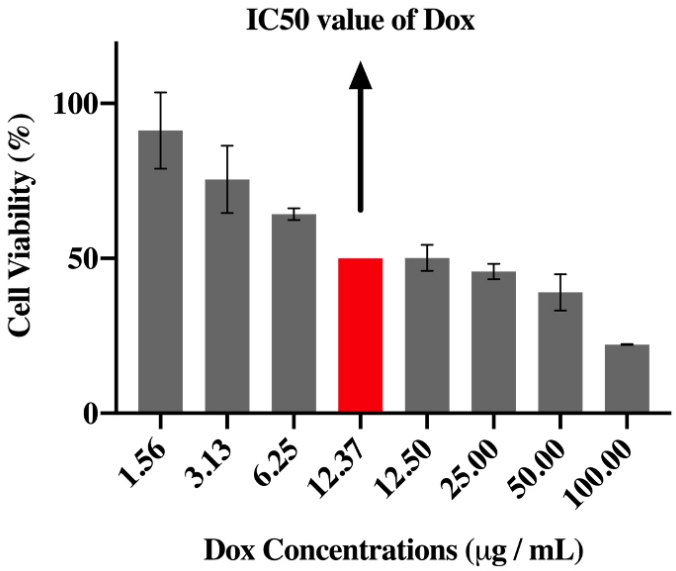

Figure 4.7 Calculated IC 50 value of DOX by MTT analysis for $2X10^4$ MCF-7 cells (n = 3).

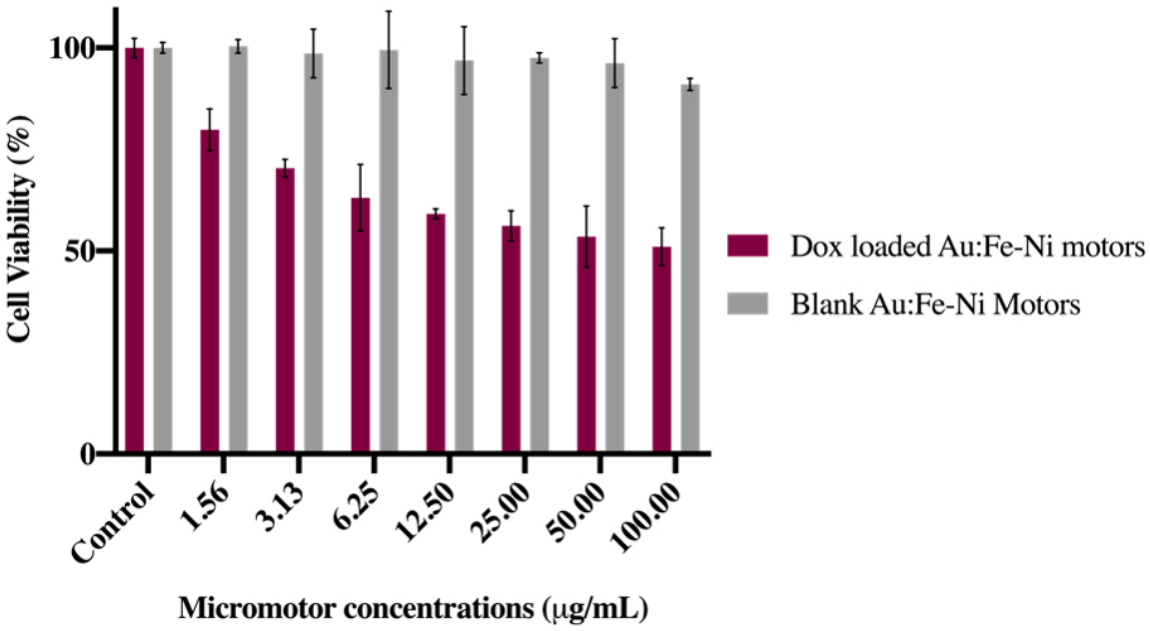

Figure 4.8 MTT analyses of Au:Fe-Ni micromotors and DOX loaded Au:Fe-Ni micromotors for 24h incubation with cells (n = 3).

Figure 4.8 compares the impact of micromotors, DOX-loaded micromotors and controlled drug released micromotors on cell viability. The MTT results revealed a significant decrease in cell viability percentages due to controlled drug release. Notably, the drug release demonstrated by 25 μg/mL DOX loaded micromotors loaded with DOX remained below the IC 50 value, indicating that controlled drug release had occurred, and thus Au:Fe-Ni micromotors are a promising candidate for drug delivery. Furthermore, the MTT results enable comparison of source of cytotoxicity of non-drug loaded micromotors versus released DOX from micromotors. The biocompatibility of non-drug loaded micromotors was also confirmed based on the results. Additionally, as previous mentioned in the drug release experiments conducted under pH 6.5, there was an increase in fluorescence absorbance change, suggesting that release, which depends on pH change. The drug release results obtained after incubation MCF-7 cells (which have an acidic environment around 6.5 to 6.9) for 24h.

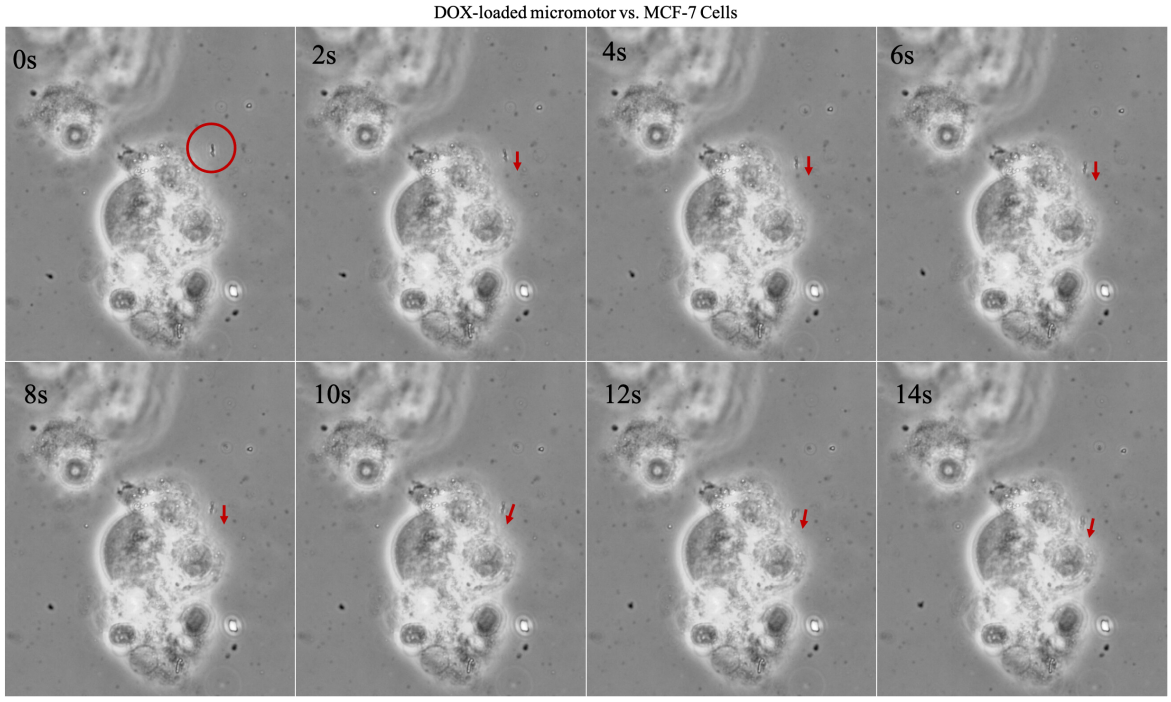

Figure 4.9 Visualized Video by splitting into frames every 2 seconds to show the propulsion of the DOX-loaded micromotor through MCF-7 cells and their interaction. (The images were captured under fluorescence microscope with 40 x magnification).

2D *in vitro* studies continued with video studies according to record micromotors and cell interactions. DOX loaded micromotors were observed during interaction with

MCF-7 cells. It is shown that, DOX loaded micromotors can be propelled towards the MCF-7 cells and interact controllably via external magnet (Figure 4.9). According to show diagnostic approach for anti-HER2 immobilized micromotors and cell interaction MCF-7 cells were also used, as a control SH-SY57 cells were chosen. Breast cancers has overexpressed HER2 receptors on the cell membrane. In the Figure 4.10, antiHER2 immobilized micromotor were guided towards the MCF-7 cells and interact with it. Then it was tried to move away but the micromotor continued to interact with the MCF-7 cells. The specific antibody-receptor interaction was also tested with SH-SY5Y neuroblastoma cells. This cell type is known that has no overexpressed HER2 receptor on the cell membrane [133]. In Figure 4.11, The antiHER2 immobilized were tried to interact with the SH-SY5Y cell, however the micromotor showed bouncing behavior and did not interact with the cell.

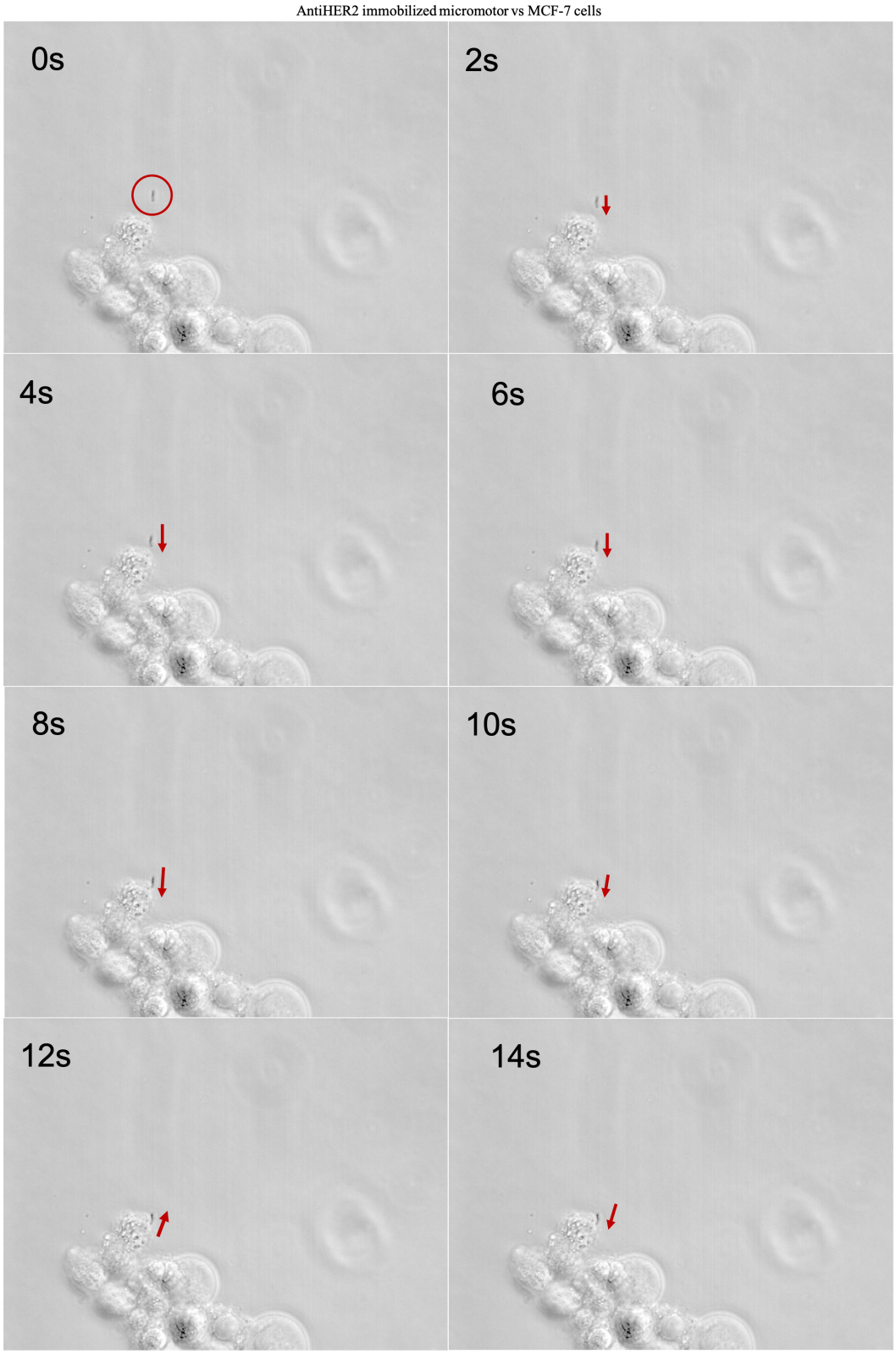

Figure 4.10 Visualized Video by splitting into frames every 2 seconds to show the propulsion of the AntiHER2 immobilized micromotor through MCF-7 cells. (The images were captured under fluorescence microscope with 40 x magnification).

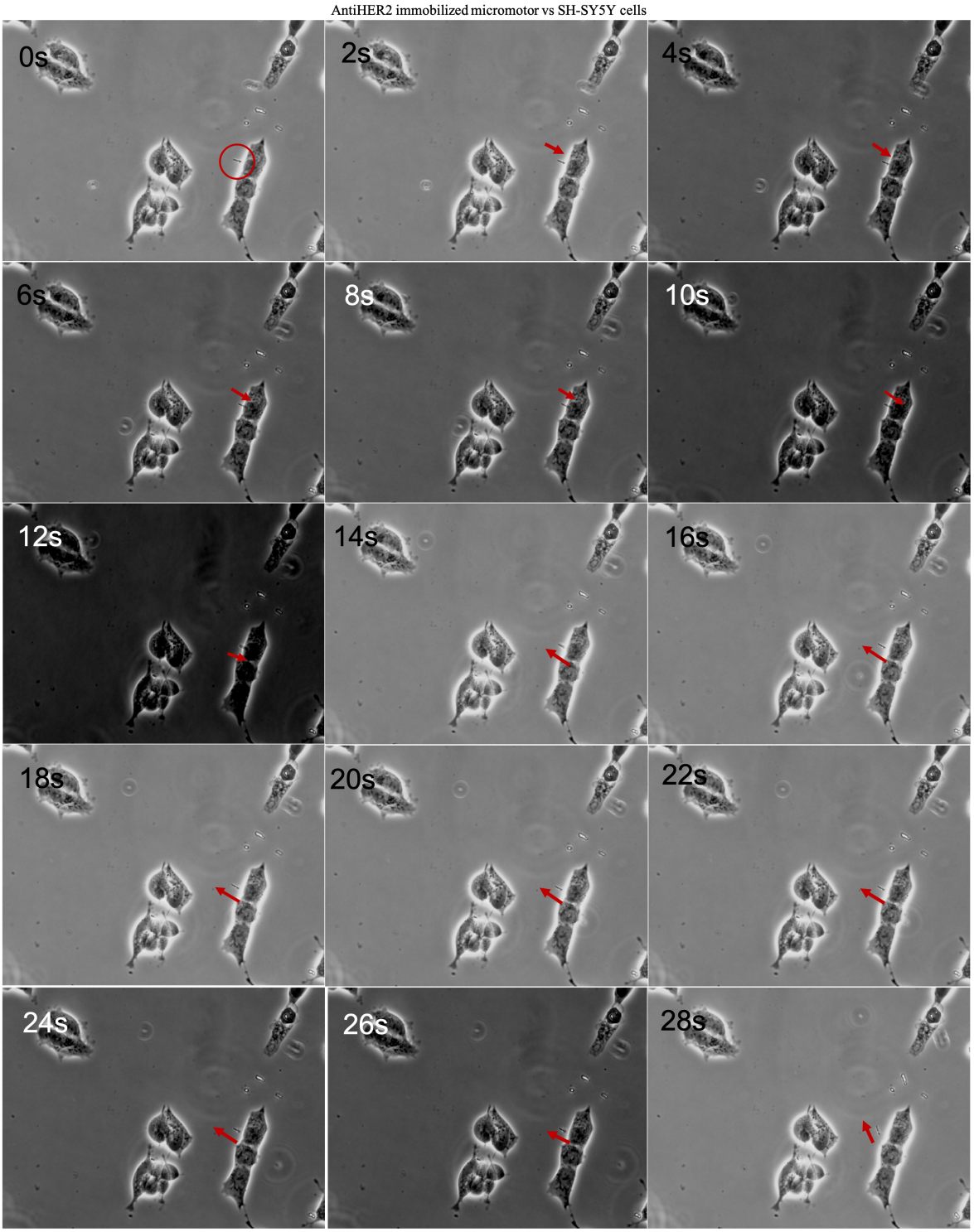

Figure 4.11 Visualized Video by splitting into frames every 2 seconds to show the propulsion of the AntiHER2 immobilized micromotor through SH-SY5Y cells according to show there is no interaction as control. (The images were captured under fluorescence microscope with 40 x magnification).

DOX release from metallic micromotors and micromotor interaction experiments with 3D cell culture were carried out to take the study to the next step. 3D cell culture, in other words spheroids can better mimic the *in vivo* environment and more accurate assessment of drug delivery system. Spheroids give opportunity to test the micromotors behavior with spheroids as 3D tissue like structure. It helps to understand the drug delivery system with nano/micromotors concept with all drawbacks and the advantages and create future perspective. Herein, the spheroids were cultured with 3000 cells via hanging drop method as described in experimental section. Considering video experiments, the number of cells had been decided as 3000 for easy observation while recording (Figure 4.2). Spheroids were harvested 3 days after hanged as cell suspension drops, and keep culturing for 7 days. The spheroids were fixed then stained with F-actin and DAPI to visualize the structures as cytoskeleton and nucleus of cells (Figure 4.12). Then, they were controlled with acridine orange/ propidium iodide staining which is used as live/dead assay before drug release experiment (Figure 4.15a). The green fluorescence show that spheroids had more alive cells than dead cells (red fluorescence).

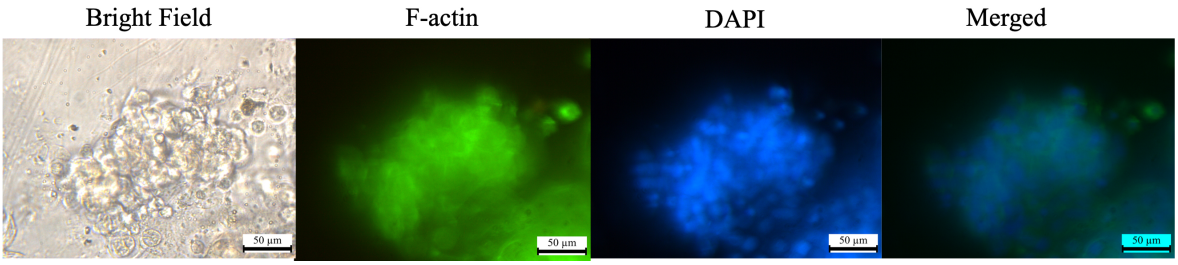

Figure 4.12 F-actin / DAPI stained spheroid to visualize 3D structures of spheroids (Scale bar = 50μm).

DOX loaded micromotors were incubated with MCF-7 spheroids for 24h as MTT analysis. Nevertheless, the cytotoxic effect of released DOX from micromotors were analyzed with Alamar Blue assay instead of MTT assay for spheroids. Since MTT solution cannot penetrate homogenously into the spheroids [131]. The release of the DOX from micromotors also showed cytotoxic effect on spheroids (Figure 4.15c) as cytotoxic effect on monolayer MCF-7 cells. The DOX uptake from spheroids also observed under microscope with florescence attachment (Figure 4.15b) which was belong

to drug release from 50 μg/mL DOX-loaded micromotors. In addition, the cell viability decrease was also shown in Figure 4.15c for 50μg/mL DOX-loaded micromotors after incubation with spheroids.

The interaction of the micromotors with spheroids and their maneuverability were also recording under microscope. Not only drug loaded micromotors, but also anti-HER2 modified micromotors were propelled by external magnet towards the spheroids. Anti-HER2 immobilized micromotors demonstrated similar behavior with 2D cell culture as clinging to the cells (Figure 4.14). DOX-loaded micromotor showed abilitiy to penetrate inside the spheroids, between the cells after magnetic propulsion through the spheroid (Figure 4.13).

According to compare the effect of drug release on MCF-7 monolayer and spheroids, cell viability was analyzed after incubation with DOX-loaded micromotors. Both experiment groups have shown decreased in cell viability because of the cytotoxic effect of released DOX. However, drug release from the same concentration (100μg/mL) DOX-loaded micromotors has shown different cell viability results for 2D and 3D *in vitro* systems statistically. The cell viability results were %14.1 $\pm$ 1.2 and %16.4 $\pm$ 0.71, respectively (Figure 4.15c).

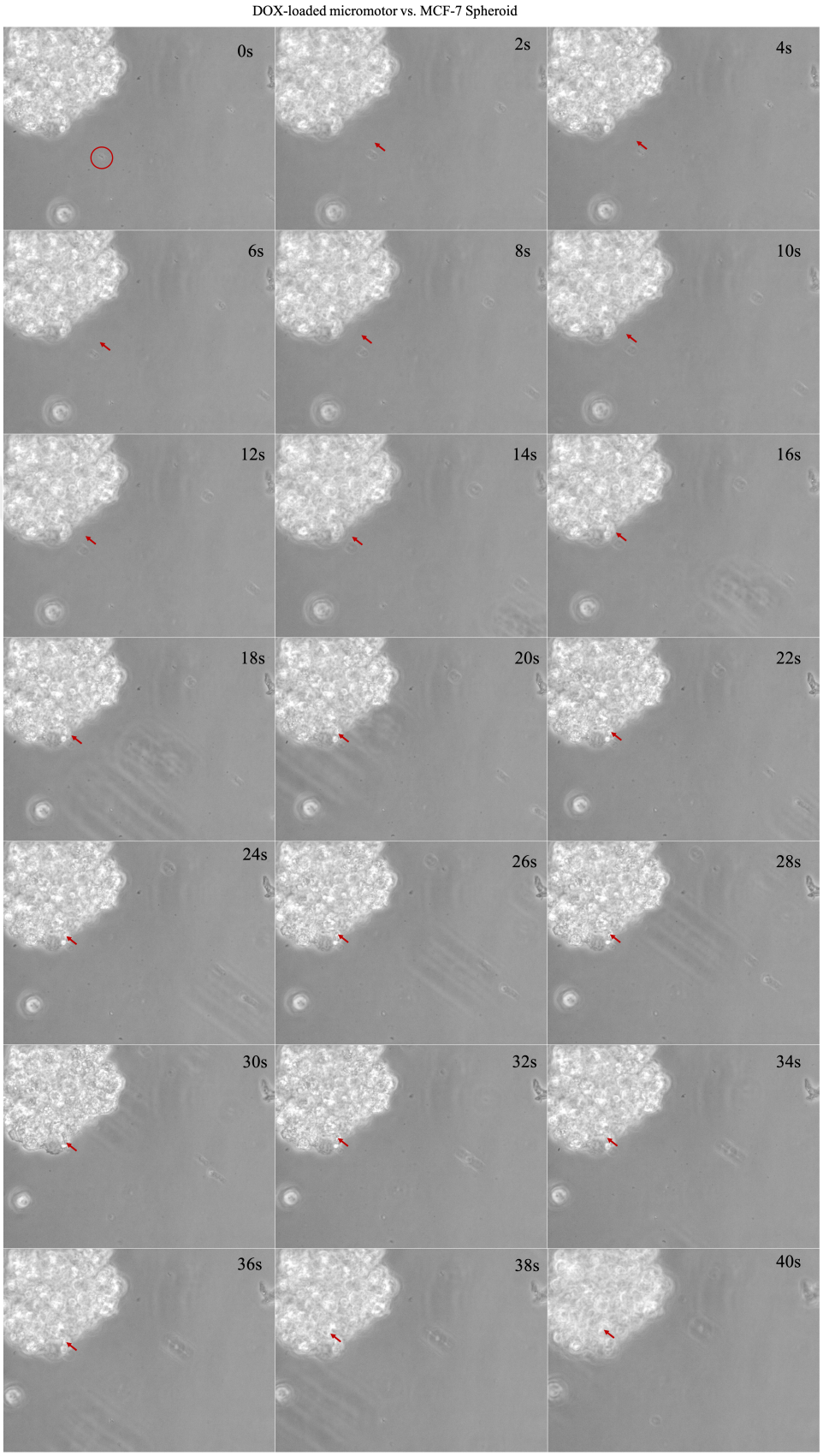

Figure 4.13 Visualized Video by splitting into frames every 2 seconds to show the propulsion of the DOX-loaded micromotor through MCF-7 spheroid and its penetration between the cells. (The images were captured under fluorescence microscope with 40 x magnification).

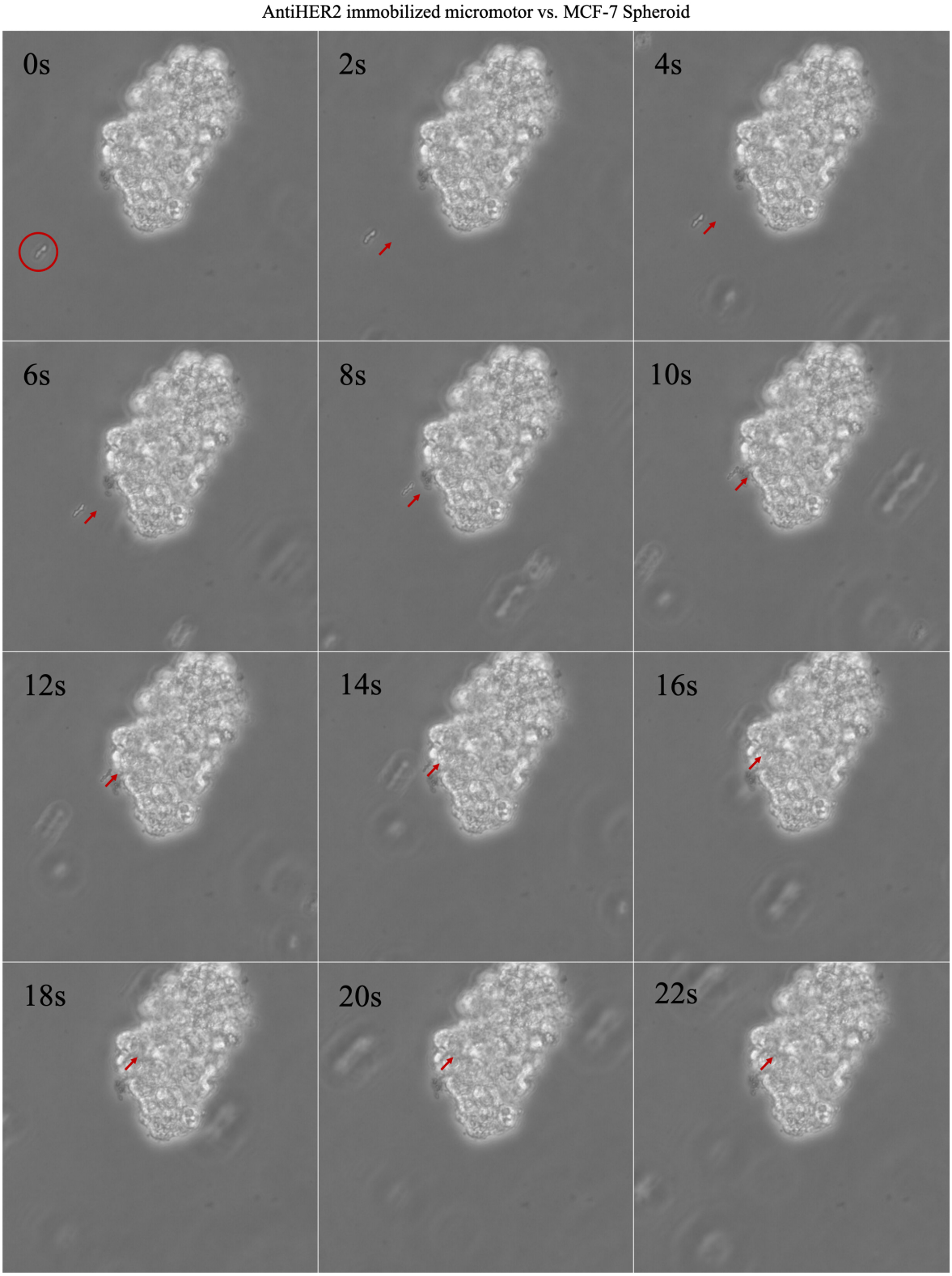

Figure 4.14 Visualized Video by splitting into frames every 2 seconds to show the propulsion of the AntiHER2 immobilized micromotor through MCF-7 spheroid and its interaction between the spheroid. (The images were captured under fluorescence microscope with 40 x magnification).

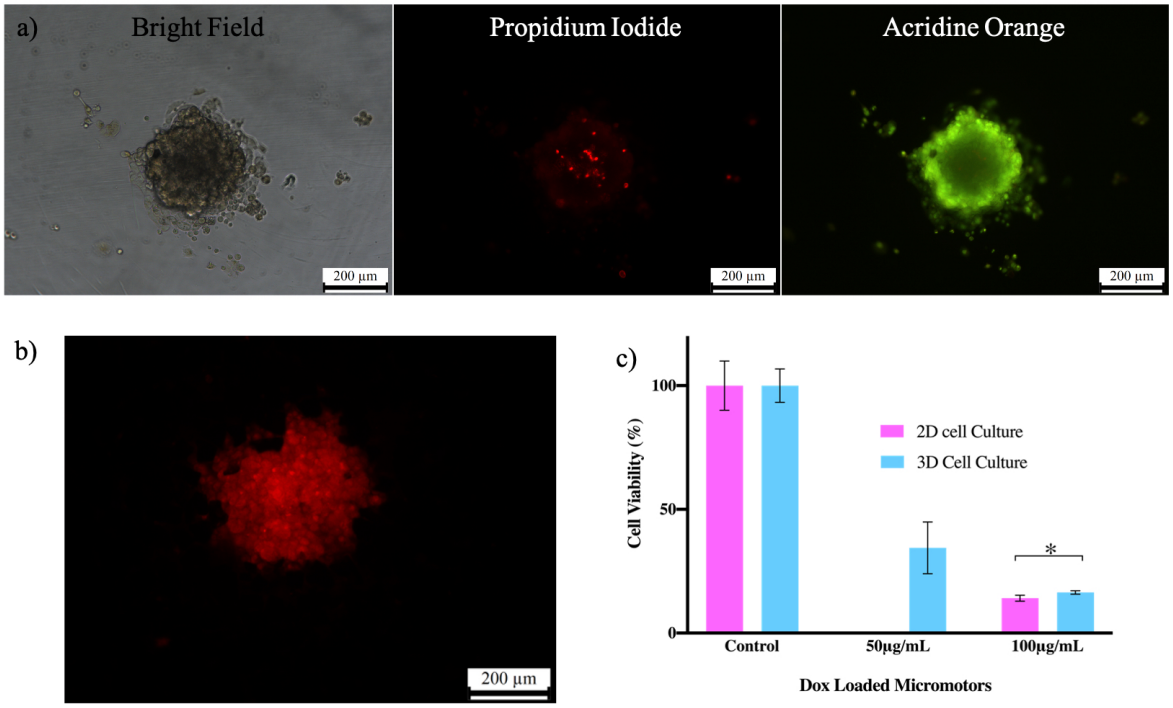

Figure 4.15 a) Live/Dead assay of spheroid before the drug release experiments with Acridine Orange/ Propidium Iodide, b) Cellular uptake of DOX by spheroid from 50 μg/mL DOX-loaded micromotors after incubation with DOX loaded micromotors for 24h, c) Comparison of the effect of drug release on 2D and 3D cell culture in terms of cell viability (n=3).

4.3 Discussion

In this section, metallic Au:Fe-Ni micromotors were synthesized successfully and the possessed ability of magnetic propulsion according to characterization results. SEM images and EDX color mapping demonstrate that rod-shaped 2-segmented micromotors synthesized and chemical composition was achieved as Au and Fe-Ni segments (Figure 4.3). The metallic motors were used to conduct drug loading and release studies of the chemotherapeutic agent Doxorubicin (DOX), which is a commonly used anti-cancer drug in breast cancer therapy. PSS modified Au segment of the micromotors and DOX have stable electrostatic interaction unless at low pH and high ionic strenght [149]. pH responsive drug release studies have been preferred for especially cancer studies due to acidic environment of cancer tissues (pH 6.5-6.9) [112].

After that, drug loading was evaluated by several analysis method. DOX has fluorescent feature itself. With the benefit of it, the drug-loaded micromotors were observed under light microscope with fluorescence attachments as red. Continuation, the drug loading was evaluated with the change of the velocity during magnetic propulsion, and it was observed that the velocity decreased after drug loading onto micromotors, which is expected result in nano/micromotors studies with drug loading [47]. In addition, Zeta Potential measurement values also support that loading of DOX and antiHER2 immobilization onto micromotors was achieved. DOX loading to Au:Fe-Ni made zeta potential more negative than unmodified micromotor which is expected results according to literature. For instance, while PSS modified gold nano rods have a zeta potential of -45.03 $\pm$ 0.2 mV, DOX loaded PSS modified nano rods continued to remain in the negative range with the observed increase in zeta potential with increasing DOX concentration, -43.05 $\pm$ 0.3, -42.90 $\pm$ 0.0, 41.30 $\pm$ 0.6, 40.60 $\pm$ 0.3, 39.50 $\pm$ 0.9, respectively. Causation of strong negative zeta potential of PSS, positively charged DOX was suppressed by PSS . After surface modification, total zeta potential become -22.67 $\pm$ 0.92 mV from -19.43 $\pm$ 0.23 mV after DOX loading via PSS, which is correlated with given literature example [134, 135].

According to carry out diagnostic approach with the micromotors, antiHER2

was immobilized on the Au segment of the micromotors. Immunocyto staining was chosen to show the immobilized antiHER2 antibodies on the micromotors in Figure 4.4b. The expected velocity decreased also observed for antiHER2 immobilized micromotors similar as DOX-loaded micromotors too (Figure 4.4c) [45]. Zeta Potential measurement of the antiHER2 immobilized micromotors also support that antibody immobilization was achieved. It was observed the zeta potential of antiHER2 immobilized micromotors become -4.50 ± 1.77 mV from -19.43 ± 0.23 mV, shifted positively after immobilization which is corrolated with literature (Figure 4.4d) [136].

Drug release studies show that, DOX-loaded micromotors could release the DOX under pH 6.5 condition which is expected behavior according to DOX-PSS interaction mechanism. Also this result [137]. This result was also supported with cell culture experiments as cellular uptake after 24h incubation of DOX-loaded micromotors and MCF-7 cells, it was visualized as fluorescent and measured as absorbance value. In addition, drug loading profile and drug entrapment efficiency (30.72%) results proved the DOX loading achievement.

Cell viability evaluation of the micromotors demonstrate the biocompatible behavior even increased micromotor concentration. DOX loaded micromotors show increased cytotoxic effect due to the drug release because of the acidic pH value of MCF-7 medium (pH 6.5-6.9) [112].

Magnetic propelled DOX loaded micromotors were observed under microscope during interaction with MCF-7 cells 2D cell culture. In figure 4.10, micromotors immobilized with antiHER2 were directed towards MCF-7 cells and interacted with them. Despite attempts to move away, the micromotors continued to interact with the MCF-7 cells. According to compare the specific antibody-receptor interaction using SH-SY5Y neuroblastoma cells, which are known to not have overexpressed HER2 receptors on their cell membranes [133]. In figure 4.11, the antiHER2 immobilized micromotors were attempted to interact with the SH-SY5Y cells, but the micromotors displayed bouncing behavior and did not interact with the cells.

The study was taken to the next level by conducting experiments with 3D cell culture, also known as spheroids. This approach is considered to be a more accurate way of assessing drug delivery systems as spheroids can better mimic the *in vivo* environment. By testing the micromotors' behavior with spheroids, which are 3D tissue-like structures, it was possible to gain a deeper understanding of the drug delivery system with nano/micromotors, including its drawbacks and advantages, and to create a future perspective. Drug release studies continued with spheroids, to analyze the cytotoxic effect of DOX released from micromotors on spheroids, the Alamar Blue assay was utilized instead of the MTT assay. The MTT solution was found to be inadequate for penetrating uniformly into the spheroids [131]. The release of DOX from the micromotors demonstrated decrease in cell viability due to cytotoxic effect of DOX (Figure 4.15c). Additionally, the uptake of DOX from spheroids was observed under microscope using fluorescence attachment (Figure 4.15b).

The comparison of the drug release effect on monolayer and spheroids were carried out in terms of cell viability because of the cytotoxic effect of released DOX. Both experiment groups have shown decreased manner in cell viability. However, drug release from the same concentration ($100\mu g$/mL) DOX-loaded micromotors has shown different cell viability results for 2D and 3D *in vitro* systems statistically, which were $\%14.1 \pm 1.2$ and $\%16.4 \pm 0.71$, respectively (Figure 4.15c). The structure and organization of cells in 3D cell culture show more similar to *in vivo* tumor microenvironment compared to 2D cell culture and these differences can affect cellular uptake of the drug and metabolism and potentially impacting drug efficacy. 3D cell cultures can contain regions of low oxygen and nutrient availability, similar to the hypoxic conditions for solid tumors. It should be considered that monolayer on a flat surface allows for easy access of the drug to the cells and the cytotoxic effect of drug may result more than spheroids (Figure 4.15c) [89]. Due to that reason, these designed micromotors could be effective to penetrate through multiple layers of cells and increase the drug release rate via pH sensitive modifications with 3D cell structures.

5. CONCLUSION

As a conclusion for the first part of the thesis, PAPBA catalytic nanomotors were successfully synthesized, loaded with anticancer drug PTX, and after drug conjugation they were directed toward the MCF-7 cell line under controllable motion. Drug loaded polymeric nanomotors released their payload in a controlled and efficient manner under NIR-induced environment. Their performance under pH dependent environment was also presented. By taking the advantage of functional polymeric surface, drug loading process and its efficiency were improved. PAPBA nanomotors, on the other hand, operated comfortably and with a long life in only 1% concentration of H_2O_2 fuel. At higher fuel concentrations, the synthesized nanomotors moved very fast. The tubular morphology and elemental distribution of nanomotors were clearly shown by using SEM and EDX characterization techniques. In addition, electroactive polymer/metallic tubular nanomotors coated surfaces showed good electrochemical features over unmodified surfaces to support the formation of nanomotors. Surface charge changes were successfully monitored to verify drug loading. According to the MTT analysis, no results were found that would adversely affect cell viability and showed the efficiency of drug release. Such motors can find broad interest in the biomedical applications.

In summary for the second part of the thesis, Au:Fe-Ni metallic micromotors were successfully synthesized, loaded with anticancer drug doxorubicin, and after drug loading they were propelled towards the MCF-7 cell line under controllable magnetic motion. Drug loaded metallic micromotors released their cargo in a controlled and efficient manner by pH respond. By taking the advantage of gold segment of micromotors, drug loading process, its efficiency and antibody immobilization were conducted. Rod-shaped two segmented structure and elemental distribution of micromotors were frankly demonstrated by using SEM and EDX characterization techniques. In addition, metallic rod-shaped micromotors surfaces were modified successfully according to drug release and diagnostic approach. According to the MTT analysis, no results were found that would adversely affect cell viability. And controlled drug released were ob-

tained as intended to 2D and 3D cell culture. The maneuverability of the drug loaded and antibody immobilized micromotors shown the promising results especially with spheroids. Such motors can find broad interest in the biomedical applications with 3D tissue like structures.

To sum up, nano/micromotors have great potential to develop for smart drug delivery systems. Their propulsion ability makes possible drug delivery to hard-to-reach areas such as inside the solid tumors. When these features are combined with surface engineering, they become very significant candidates for drug delivery systems. In addition, 3D cell cultures or spheroids are also one of the auxiliary elements of these studies to mimic tissue-like structures during drug delivery studies with nano/micromotors, especially they are illuminating in terms of reaching clinical applications.

REFERENCES

1. Bayda, S., M. Adeel, T. Tuccinardi, M. Cordani, and F. Rizzolio, "The history of nanoscience and nanotechnology: From chemical-physical applications to nanomedicine," *Molecules*, Vol. 25, p. 112, 2020.

2. TANIGUCHI, N., "On the basic concept of nanotechnology," *Proceeding of the ICPE*, 1974.

3. Medina-Sanchez, M., S. Miserere, and A. Merkoci, "Nanomaterials and lab-on-a-chip technologies," *Lab Chip*, Vol. 12, pp. 1932–1943, 2012.

4. Merkoci, A., M. Pumera, X. Llopis, B. Perez, M. del Valle, and S. Alegret, "New materials for electrochemical sensing vi: Carbon nanotubes," *TrAC Trends in Analytical Chemistry*, Vol. 24, no. 9, pp. 826–838, 2005.

5. Gao, W., and J. Wang, "Synthetic micro/nanomotors in drug delivery," *Nanoscale*, Vol. 6, pp. 10486–10494, 2014.

6. Tezel, G., S. S. Timur, F. Kuralay, R. N. Gürsoy, K. Ulubayram, L. Öner, and H. Eroğlu, "Current status of micro/nanomotors in drug delivery," *Journal of Drug Targeting*, 2020.

7. Mintmire, J. W., B. I. Dunlap, C. T. White, P. E. Nielsen, M. Engholm, R. H. Berg, O. . S. Buchardt, A. R. M. Verschueren, C. Dekker, V. Derycke, R. Martel, J. Appenzeller, P. Avouris, A. Bachtold, P. Hadley, T. Nakanishi, H. W. C. Postma, T. F. Teepen, Z. Yao, M. Grifoni, and J. Chen, "Carbon nanotubes with dna recognition," *Nature 2002 420:6917*, Vol. 420, pp. 761–761, 2002.

8. Phoenix, C., and E. Drexler, "Safe exponential manufacturing," *Nanotechnology*, Vol. 15, p. 869, 2004.

9. Valadares, L. F., Y. G. Tao, N. S. Zacharia, V. Kitaev, F. Galembeck, R. Kapral, and G. A. Ozin, "Catalytic nanomotors: Self-propelled sphere dimers," *Small*, Vol. 6, pp. 565–572, 2010.

10. Wang, J., and K. M. Manesh, "Motion control at the nanoscale," *Small*, Vol. 6, pp. 338–345, 2010.

11. Dreyfus, R., J. Baudry, M. L. Roper, M. Fermigier, H. A. Stone, and J. Bibette, "Microscopic artificial swimmers," *Nature 2005 437:7060*, Vol. 437, pp. 862–865, 2005.

12. Davis, A. P., "Synthetic molecular motors," *Nature 1999 401:6749*, Vol. 401, pp. 120–121, 1999.

13. Nevins, S., C. D. McLoughlin, A. Oliveros, J. B. Stein, M. A. Rashid, Y. Hou, M.-H. Jang, and K.-B. Lee, "Nanotechnology approaches for prevention and treatment of chemotherapy-induced neurotoxicity, neuropathy, and cardiomyopathy in breast and ovarian cancer survivors," *Small*, p. 2300744, 2023.

14. Li, H., F. Peng, X. Yan, C. Mao, X. Ma, D. A. Wilson, Q. He, and Y. Tu, "Medical micro- and nanomotors in the body," *Acta Pharmaceutica Sinica B*, Vol. 13, pp. 517–541, 2023.

15. Choi, H., J. Yi, S. H. Cho, and S. K. Hahn, "Multifunctional micro/nanomotors as an emerging platform for smart healthcare applications," *Biomaterials*, Vol. 279, p. 121201, 2021.

16. Xie, D., S. Fu, D. Fu, B. Chen, W. He, H. Liang, Y. Tu, D. A. Wilson, and F. Peng, "Adaptive particle patterning in the presence of active synthetic nanomotors," *Nanoscale*, Vol. 15, pp. 6619–6628, 2023.

17. Zheng, Y., H. Zhao, Y. Cai, B. Jurado-Sanchez, and R. Dong, "Recent advances in one-dimensional micro/nanomotors: Fabrication, propulsion and application," *Nano-Micro Letters*, Vol. 15, 2023.

18. Maria-Hormigos, R., B. Jurado-Sanchez, and A. Escarpa, "Biocompatible micromotors for biosensing," *Analytical and Bioanalytical Chemistry*, Vol. 414, pp. 7035–7049, 2022.

19. Pacheco, M., M. angel Lopez, B. Jurado-Sanchez, and A. Escarpa, "Self-propelled micromachines for analytical sensing: a critical review," *Analytical and Bioanalytical Chemistry*, Vol. 411, pp. 6561–6573, 2019.

20. Yue, H., X. Chang, J. Liu, D. Zhou, and L. Li, "Wheel-like magnetic-driven microswarm with a band-aid imitation for patching up microscale intestinal perforation," *ACS Applied Materials and Interfaces*, Vol. 14, pp. 8743–8752, 2022.

21. Wu, Y., S. Yakov, A. Fu, and G. Yossifon, "A magnetically and electrically powered hybrid micromotor in conductive solutions: Synergistic propulsion effects and label free cargo transport and sensing," *Advanced Science*, Vol. 10, 2023.

22. Liu, L., Q. Li, L. Chen, L. Song, X. Zhang, H. Huo, Z. You, Y. Wu, Z. Wu, J. Ye, Q. Fu, L. Su, X. Zhang, H. Yang, and J. Song, "Plasmon enhanced catalysis-driven nanomotors with autonomous navigation for deep cancer imaging and enhanced radiotherapy," *Chemical Science*, Vol. 13, pp. 12840–12850, 2022.

23. Liu, D., F. Yang, F. Xiong, and N. Gu, "The smart drug delivery system and its clinical potential," *Theranostics*, Vol. 6, 2016.

24. Sonzini, S., F. Caputo, D. Mehn, L. Calzolai, S. E. Borgos, A. Hyldbakk, K. Treacher, W. Li, M. Jackman, N. Mahmoudi, M. J. Lawrence, C. Patterson, D. Owen, M. Ashford, and N. Akhtar, "In depth characterization of physicochemical critical quality attributes of a clinical drug-dendrimer conjugate," *International Journal of Pharmaceutics*, Vol. 637, p. 122905, 2023.

25. Abdelgalil, R. M., S. N. Khattab, S. Ebrahim, K. A. Elkhodairy, M. Teleb, A. A. Bekhit, M. A. Sallam, and A. O. Elzoghby, "Engineered sericin-tagged layered double hydroxides for combined delivery of pemetrexed and zno quantum dots as biocompatible cancer nanotheranostics," *ACS Omega*, Vol. 8, pp. 5655–5671, 2023.

26. Musielak, M., A. Bos-Liedke, O. Piwocka, K. Kowalska, R. Markiewicz, B. Szymkowiak, P. Bakun, and W. M. Suchorska, "The role of functionalization and size of gold nanoparticles in the response of mcf-7 breast cancer cells to ionizing radiation comparing 2d and 3d in vitro models," *Pharmaceutics*, Vol. 15, p. 862, 2023.

27. Llopis-Lorente, A., A. Garcia-Fernandez, N. Murillo-Cremaes, A. C. Hortelao, T. Patino, R. Villalonga, F. Sancenon, R. Martinez-Manez, and S. Sanchez, "Enzyme-powered gated mesoporous silica nanomotors for on command intracellular payload delivery," *ACS Nano*, Vol. 13, pp. 12171–12183, 2019.

28. Chowdary, K. P., and A. S. Rao, "Nanoparticles as drug carriers," *Indian Drugs*, Vol. 34, pp. 549–556, 1997.

29. Li, J. J., and W. Tan, "A single dna molecule nanomotor," *Nano*, Vol. 2, pp. 315–318, 2002.

30. Ahmad, Z., and J. L. Cox, "Atp synthase: The right size base model for nanomotors in nanomedicine," *The Scientific World Journal*, Vol. 2014, 2014.

31. van den Heuvel, M. G. L., and C. Dekker, "Motor proteins at work for nanotechnology," *Science*, Vol. 317, pp. 333–336, 2007.

32. Guo, P., H. Noji, C. M. Yengo, Z. Zhao, and I. Grainge, "Biological nanomotors with a revolution, linear, or rotation motion mechanism," *Microbiology and Molecular Biology Reviews*, Vol. 80, pp. 161–186, 2016.

33. Khataee, H. R., M. Y. Ibrahim, and A. W. C. Liew, "Flexible autonomous behaviors of kinesin and muscle myosin bio-nanorobots," *IEEE Transactions on Industrial Electronics*, Vol. 60, pp. 5116–5123, 2013.

34. Schliwa, M., and G. Woehlke, "Molecular motors.," *Nature*, Vol. 422, pp. 759–65, 2003.

35. Ismagilov, R. F., A. Schwartz, N. Bowden, and G. M. Whitesides, "Autonomous movement and self-assembly," *Angewandte Chemie - International Edition*, Vol. 41, pp. 652–654, 2002.

36. Paxton, W. F., K. C. Kistler, C. C. Olmeda, A. Sen, S. K. S. Angelo, Y. Cao, T. E. Mallouk, P. E. Lammert, and V. H. Crespi, "Catalytic nanomotors: Autonomous movement of striped nanorods," *Journal of the American Chemical Society*, Vol. 126, pp. 13424–13431, 2004.

37. Vicario, J., R. Eelkema, W. R. Browne, A. Meetsma, R. M. L. Crois, and B. L. Feringa, "Catalytic molecular motors: fuelling autonomous movement by a surface bound synthetic manganese catalase.," *Chem. Comms.*, pp. 3936–8, 2005.

38. Thomas E Mallouk, A. S., "Powering nanorobots," pp. 74–79, 2009.

39. Wang, Y., R. M. Hernandez, D. J. Bartlett, J. M. Bingham, T. R. Kline, A. Sen, and T. E. Mallouk, "Bipolar electrochemical mechanism for the propulsion of catalytic nanomotors in hydrogen peroxide solutions," *Langmuir*, Vol. 22, pp. 10451–10456, 2006.

40. Paxton, W. F., S. Sundararajan, T. E. Mallouk, and A. Sen, "Chemical locomotion," *Angewandte Chemie - International Edition*, Vol. 45, pp. 5420–5429, 2006.

41. Paxton, W. F., A. Sen, and T. E. Mallouk, "Motility of catalytic nanoparticles through self-generated forces," *Chemistry - A European Journal*, Vol. 11, pp. 6462–6470, 2005.

42. Wilson, D., B. de Nijs, A. van Blaaderen, R. J. M. Nolte, and J. C. M. V. Hest, "Fuel concentration dependent movement of supramolecular catalytic nanomotors.," *Nanoscale*, Vol. 5, pp. 1315–8, 2013.

43. Kline, T. R., W. F. Paxton, T. E. Mallouk, and A. Sen, "Catalytic nanomotors: Remote-controlled autonomous movement of striped metallic nanorods**," pp. 744–746, 2005.

44. Kagan, D., R. Laocharoensuk, M. Zimmerman, C. Clawson, S. Balasubramanian, D. Kang, D. Bishop, S. Sattayasamitsathit, L. Zhang, and J. Wang, "Rapid delivery of drug carriers propelled and navigated by catalytic nanoshuttles," *Small*, Vol. 6, pp. 2741–2747, 2010.

45. Kuralay, F., S. Sattayasamitsathit, W. Gao, A. Uygun, A. Katzenberg, and J. Wang, "Self-propelled carbohydrate-sensitive microtransporters with built-in boronic acid recognition for isolating sugars and cells," *Journal of the American Chemical Society*, Vol. 134, pp. 15217–15220, 2012.

46. L., G., "The hydrogen peroxide paradox," *Orv Hetil*, Vol. 147, pp. 887–893, 2006.

47. Mirkovic, T., N. S. Zacharia, G. D. Scholes, and G. A. Ozin, "Fuel for thought: Chemically powered nanomotors out-swim nature's flagellated bacteria," *ACS Nano*, Vol. 4, pp. 1782–1789, 2010.

48. Campuzano, S., J. Orozco, D. Kagan, M. Guix, W. Gao, S. Sattayasamitsathit, J. C. Claussen, A. Merkoci, and J. Wang, "Bacterial isolation by lectin-modified microengines," *Nano Letters*, Vol. 12, pp. 396–401, 2012.

49. Peng, F., Y. Tu, J. C. M. V. Hest, D. A. Wilson, J. C. M. V. Hest, and D. A. Wilson, "Self-guided supramolecular cargo-loaded nanomotors with chemotactic behavior towards cells," *Angewandte Chemie - International Edition*, Vol. 54, pp. 11662–11665, 2015.

50. Demirbuken, S. E., G. Y. Karaca, H. K. Kaya, L. Oksuz, B. Garipcan, A. U. Oksuz, and F. Kuralay, "Paclitaxel-conjugated phenylboronic acid-enriched catalytic robots as smart drug delivery systems," *Materials Today Chemistry*, Vol. 26, p. 101172, 2022.

51. Gao, W., R. Dong, S. Thamphiwatana, J. Li, W. Gao, L. Zhang, and J. Wang, "Artificial micromotors in the mouse's stomach: A step toward in vivo use of synthetic motors," *ACS Nano*, Vol. 9, pp. 117–123, 2015.

52. Gao, W., S. Sattayasamitsathit, and J. Wang, "Catalytically propelled micro-/nanomotors: How fast can they move?," *Chemical Record*, Vol. 12, pp. 224–231, 2012.

53. Sun, J., M. Mathesh, W. Li, and D. A. Wilson, "Enzyme-powered nanomotors with controlled size for biomedical applications," *ACS Nano*, Vol. 13, pp. 10191–10200, 2019.

54. Wang, L., M. Marciello, M. Estevez-Gay, P. E. S. Rodriguez, Y. L. Morato, J. Iglesias-Fernandez, X. Huang, S. Osuna, M. Filice, and S. Sanchez, "Enzyme conformation influences the performance of lipase-powered nanomotors," *Angewandte Chemie International Edition*, Vol. 59, pp. 21080–21087, 2020.

55. Hortelao, A. C., C. Simo, M. Guix, S. Guallar-Garrido, E. Julian, D. Vilela, L. Rejc, P. Ramos-Cabrer, U. Cossio, V. Gomez-Vallejo, T. Patino, J. Llop, and S. Sanchez, "Swarming behavior and in vivo monitoring of enzymatic nanomotors within the bladder," *Science Robotics*, Vol. 6, 2021.

56. Ahmed, S., W. Wang, L. Bai, D. T. Gentekos, M. Hoyos, and T. E. Mallouk, "Density and shape effects in the acoustic propulsion of bimetallic nanorod motors," *ACS Nano*, Vol. 10, pp. 4763–4769, 2016.

57. Garcia-Gradilla, V., J. Orozco, S. Sattayasamitsathit, F. Soto, F. Kuralay, A. Pourazary, A. Katzenberg, W. Gao, Y. Shen, and J. Wang, "Functionalized ultrasound-propelled magnetically guided nanomotors: Toward practical biomedical applications," *ACS Nano*, Vol. 7, pp. 9232–9240, 2013.

58. Choi, H., G.-H. Lee, K. S. Kim, and S. K. Hahn, "Light-guided nanomotor systems for autonomous photothermal cancer therapy," *ACS Applied Materials & Interfaces*, Vol. 10, no. 3, pp. 2338–2346, 2018. PMID: 29280612.

59. Guo, J., J. J. Gallegos, A. R. Tom, and D. Fan, "Electric-field-guided precision manipulation of catalytic nanomotors for cargo delivery and powering nanoelectromechanical devices," 2018.

60. Karaca, G. Y., F. Kuralay, E. Uygun, K. Ozaltin, S. E. Demirbuken, B. Garipcan, L. Oksuz, and A. U. Oksuz, "Gold-nickel nanowires as nanomotors for cancer marker biodetection and chemotherapeutic drug delivery," *ACS Appl. Nano Mater*, Vol. 2021, p. 3388, 2021.

61. Balasubramanian, S., D. Kagan, K. M. Manesh, P. Calvo-Marzal, G. U. Flechsig, and J. Wang, "Thermal modulation of nanomotor movement," *Small*, Vol. 5, pp. 1569–1574, 2009.

62. Abdelmohsen, L. K. E. A., F. Peng, Y. Tu, and D. A. Wilson, "Micro-and nano-motors for biomedical applications," pp. 2395–2408, 2014.

63. Kadiri, V. M., C. Bussi, A. W. Holle, K. Son, H. Kwon, G. Schütz, M. G. Gutierrez, P. Fischer, V. M. Kadiri, K. Son, H. Kwon, G. Schütz, P. Fischer, C. Bussi, M. G. Gutierrez, and A. W. Holle, "Biocompatible magnetic micro- and nanodevices: Fabrication of fept nanopropellers and cell transfection," *Advanced Materials*, Vol. 32, p. 2001114, 2020.

64. Bayramlı, Y., and F. Kuralay, *Nanomotors: Their Synthesis and Applications, Advanced Electrochemistry*, Ankara: Advanced Electrochemistry, Editör: Abacı, S. 50th Year of Hacettepe University Series, 2018.

65. Chang, X., Y. Feng, B. Guo, D. Zhou, and L. Li, "Nature inspired micro/nanomotors," *Nanoscale*, 2022.

66. Chen, Y., B. Xu, and Y. Mei, "Design and fabrication of tubular micro/nanomotors via 3d laser lithography," *Chemistry - An Asian Journal*, Vol. 14, pp. 2472–2478, 2019.

67. Peng, F., Y. Tu, and D. A. Wilson, "Micro/nanomotors towards in vivo application: cell, tissue and biofluid," *Chemical Society Reviews*, Vol. 46, pp. 5289–5310, 2017.

68. Ou, J., K. Liu, J. Jiang, D. A. Wilson, L. Liu, F. Wang, S. Wang, Y. Tu, and F. Peng, "Micro-/nanomotors toward biomedical applications: The recent progress in biocompatibility," *Small*, Vol. 16, 2020.

69. Molinero-Fernandez, L. Arruza, M. angel Lopez, and A. Escarpa, "On-the-fly rapid immunoassay for neonatal sepsis diagnosis: C-reactive protein accurate determination using magnetic graphene-based micromotors," *Biosensors and Bioelectronics*, Vol. 158, p. 112156, 2020.

70. Zhang, Y., L. Zhang, L. Yang, C. I. Vong, K. F. Chan, W. K. Wu, T. N. Kwong, N. W. Lo, M. Ip, S. H. Wong, J. J. Sung, P. W. Chiu, and L. Zhang, "Real-time tracking of fluorescent magnetic spore-based microrobots for remote detection of c. diff toxins," *Science Advances*, Vol. 5, pp. 9650–9661, 2019.

71. Mayorga-Martinez, C. C., J. Vyskocil, F. Novotny, P. Bednar, D. Ruzek, O. Alduhaishe, and M. Pumera, "Collective behavior of magnetic microrobots through immuno-sandwich assay: On-the-fly covid-19 sensing," *Applied Materials Today*, Vol. 26, p. 101337, 2022.

72. Gao, C., Y. Wang, Z. Ye, Z. Lin, X. Ma, Q. He, C. Y. Gao, Z. H. Lin, Q. He, Y. Wang, Z. H. Ye, and X. Ma, "Biomedical micro-/nanomotors: From overcoming biological barriers to in vivo imaging," *Advanced Materials*, Vol. 33, p. 2000512, 2021.

73. Zheng, S., Y. Wang, S. Pan, E. Ma, S. Jin, M. Jiao, W. Wang, J. Li, K. Xu, and H. Wang, "Biocompatible nanomotors as active diagnostic imaging agents for enhanced magnetic resonance imaging of tumor tissues in vivo," *Advanced Functional Materials*, Vol. 31, p. 2100936, 2021.

74. Li, J., B. E. F. D. avila, W. Gao, L. Zhang, and J. Wang, "Micro/nanorobots for biomedicine: Delivery, surgery, sensing, and detoxification," *Science Robotics*, Vol. 2, 2017.

75. Ning, H., Y. Zhang, H. Zhu, A. Ingham, G. Huang, Y. Mei, and A. A. Solovev, "Geometry design, principles and assembly of micromotors," *Micromachines 2018, Vol. 9, Page 75*, Vol. 9, p. 75, 2018.

76. Falahati, M., M. Sharifi, and T. L. Hagen, "Explaining chemical clues of metal organic framework-nanozyme nano-/micro-motors in targeted treatment of cancers: benchmarks and challenges," *Journal of Nanobiotechnology 2022 20:1*, Vol. 20, pp. 1–26, 2022.

77. Meisami, A. H., M. Abbasi, S. Mosleh-Shirazi, A. Azari, A. M. Amani, A. Vaez, and A. Golchin, "Self-propelled micro/nanobots: A new insight into precisely targeting cancerous cells through intelligent and deep cancer penetration," *European Journal of Pharmacology*, Vol. 926, p. 175011, 2022.

78. Chen, S., Y. Chen, M. Fu, Q. Cao, B. Wang, W. Chen, and X. Ma, "Active nanomotors surpass passive nanomedicines: current progress and challenges," *J. Mater. Chem. B*, Vol. 10, p. 7099, 2022.

79. Jeong, J., D. Jang, D. Kim, D. Lee, and S. K. Chung, "Acoustic bubble-based drug manipulation: carrying, releasing and penetrating for targeted drug delivery using an electromagnetically actuated microrobot," *Sensors and Actuators A: Physical*, 2020.

80. Garcia-Gradilla, V., S. Sattayasamitsathit, F. Soto, F. Kuralay, C. Yardimci, D. Wiitala, M. Galarnyk, and J. Wang, "Ultrasound-propelled nanoporous gold wire for efficient drug loading and release," *Small*, Vol. 10, pp. 4154–4159, 2014.

81. Andhari, S. S., R. D. Wavhale, K. D. Dhobale, B. V. Tawade, G. P. Chate, Y. N. Patil, J. J. Khandare, and S. S. Banerjee, "Self-propelling targeted magneto-nanobots for deep tumor penetration and ph-responsive intracellular drug delivery," *Scientific Reports 2020 10:1*, Vol. 10, pp. 1–16, 2020.

82. Weaver, B. A., "How taxol/paclitaxel kills cancer cells," *Molecular Biology of the Cell*, Vol. 25, pp. 2677–2681, 2014.

83. Thorn, C. F., C. Oshiro, S. Marsh, T. Hernandez-Boussard, H. McLeod, T. E. Klein, and R. B. Altman, "Doxorubicin pathways: pharmacodynamics and adverse effects," *Pharmacogenetics and Genomics*, Vol. 21, p. 440, 2011.

84. Zasadil, L. M., K. A. Andersen, D. Yeum, G. B. Rocque, L. G. Wilke, A. J. Tevaarwerk, R. T. Raines, M. E. Burkard, and B. A. Weaver, "Cytotoxicity of paclitaxel in breast cancer is due to chromosome missegregation on multipolar spindles," *Science Translational Medicine*, Vol. 6, 2014.

85. Chen, M., C. Chen, Z. Shen, X. Zhang, Y. Chen, F. Lin, X. Ma, C. Zhuang, Y. Mao, H. Gan, P. Chen, X. Zong, and R. Wu, "Extracellular ph is a biomarker enabling detection of breast cancer and liver cancer using cest mri," *Oncotarget*, Vol. 8, pp. 45759–45767, 2017.

86. Feng, Z. Q., K. Yan, J. Li, X. Xu, T. Yuan, T. Wang, and J. Zheng, "Magnetic janus particles as a multifunctional drug delivery system for paclitaxel in efficient cancer treatment," *Materials Science and Engineering: C*, Vol. 104, p. 110001, 2019.

87. Mohan, P., and N. Rapoport, "Doxorubicin as a molecular nanotheranostic agent: effect of doxorubicin encapsulation in micelles or nanoemulsions on the ultrasound-mediated intracellular delivery and nuclear trafficking," *Mol Pharm*, Vol. 7, pp. 1959–1973, 2010.

88. Tu, Y., F. Peng, A. A. Andre, Y. Men, M. Srinivas, and D. A. Wilson, "Biodegradable hybrid stomatocyte nanomotors for drug delivery," *ACS Nano*, Vol. 11, pp. 1957–1963, 2017.

89. Abdullah, C. S., P. Ray, S. Alam, N. Kale, R. Aishwarya, M. Morshed, D. Dutta, C. Hudziak, S. K. Banerjee, S. Mallik, S. Banerjee, M. S. Bhuiyan, and M. Quadir, "Chemical architecture of block copolymers differentially abrogate cardiotoxicity and maintain the anticancer efficacy of doxorubicin," *Molecular Pharmaceutics*, Vol. 17, pp. 4676–4690, 2020.

90. Roy, S. M., V. Garg, S. Barman, C. Ghosh, A. R. Maity, and S. K. Ghosh, "Kinetics of nanomedicine in tumor spheroid as an in vitro model system for efficient tumor-targeted drug delivery with insights from mathematical models," *Frontiers in Bioengineering and Biotechnology*, Vol. 9, 2021.

91. Wang, L., . X. Hao, Z. Gao, Z. Yang, Y. Long, M. Luo, and J. Guan, "Artificial nanomotors: Fabrication, locomotion characterization, motion manipulation, and biomedical applications," *Interdisciplinary Materials*, Vol. 1, pp. 256–280, 2022.

92. Hortelao, A. C., T. Patino, A. Perez-Jimenez, A. Blanco, and S. Sanchez, "Enzyme powered nanobots enhance anticancer drug delivery," *Advanced Functional Materials*, Vol. 28, p. 1705086, 2018.

93. Xu, L., K. Zhang, X. Ma, Y. Li, Y. Jin, C. Liang, Y. Wang, W. Duan, H. Zhang, Z. Zhang, J. Shi, J. Liu, Y. Wang, and W. Li, "Boosting cisplatin chemotherapy by nanomotor enhanced tumor penetration and dna adducts formation," *Journal of Nanobiotechnology*, Vol. 20, pp. 1–17, 2022.

94. Xu, D., Y. Wang, C. Liang, Y. You, S. Sanchez, and X. Ma, "Self propelled micro/nanomotors for on-demand biomedical cargo transportation," *Small*, Vol. 1902464, p. 1902464, 2019.

95. Solovev, A. A., W. Xi, D. H. Gracias, S. M. Harazim, C. Deneke, S. Sanchez, and O. G. Schmidt, "Self-propelled nanotools," pp. 1751–1756, 2012.

96. Xi, W., A. A. Solovev, A. N. Ananth, D. H. Gracias, S. Sanchez, and O. G. Schmidt, "Rolled-up magnetic microdrillers: towards remotely controlled minimally invasive surgery," *Nanoscale*, Vol. 5, pp. 1294–1297, 2013.

97. Kagan, D., M. J. Benchimol, J. C. Claussen, E. Chuluun-Erdene, S. Esener, and J. Wang, "Acoustic droplet vaporization and propulsion of perfluorocarbon-loaded microbullets for targeted tissue penetration and deformation," *Angewandte Chemie International Edition*, Vol. 51, pp. 7519–7522, 2012.

98. Öksüz, L., G. Y. Karaca, F. Kuralay, E. Uygun, İsmihan Ümran Koc, and A. U. öksüz, "Preparation of self-propelled cu-pt micromotors and their application in mirna monitoring," *Turkish Journal of Chemistry*, 2018.

99. Falah, M., M. Rayan, and A. Rayan, "A novel paclitaxel conjugate with higher efficiency and lower toxicity: A new drug candidate for cancer treatment," *International Journal of Molecular Sciences*, Vol. 20, 2019.

100. Kim, S. G., B. Ryplida, P. T. M. Phuong, H. J. Won, G. Lee, S. H. Bhang, and S. Y. Park, "Reduction-triggered paclitaxel release nano-hybrid system based on core-crosslinked polymer dots with a ph-responsive shell-cleavable colorimetric biosensor," *International Journal of Molecular Sciences 2019, Vol. 20, Page 5368*, Vol. 20, p. 5368, 2019.

101. Gowda, J. I., and S. T. Nandibewoor, "Electrochemical behavior of paclitaxel and its determination at glassy carbon electrode," *Asian Journal of Pharmaceutical Sciences*, Vol. 9, pp. 42–49, 2014.

102. Zhang, Y.-M., N.-Y. Zhang, K. Xiao, Q. Yu, and Y. Liu, "Photo-controlled reversible microtubule assembly mediated by paclitaxel-modified cyclodextrin," *Angewandte Chemie*, Vol. 130, pp. 8785–8789, 2018.

103. Lothian, G. F., "Beer's law and its use in analysis. a review," *The Analyst*, Vol. 88, pp. 678–685, 1963.

104. Sugo, K., and M. Ebara, "A simple spectrophotometric evaluation method for the hydrophobic anticancer drug paclitaxel," *PeerJ Analytical Chemistry*, Vol. 2, p. e3, 2020.

105. Chen, W., S. Zhou, L. Ge, W. Wu, and X. Jiang, "Translatable high drug loading drug delivery systems based on biocompatible polymer nanocarriers," *Biomacromolecules*, Vol. 19, pp. 1732–1745, 2018.

106. Khezri, B., S. M. B. Mousavi, L. Krejcova, Z. Heger, Z. Sofer, and M. Pumera, "Ultrafast electrochemical trigger drug delivery mechanism for nanographene micromachines," *Advanced Functional Materials*, Vol. 29, p. 1806696, 2019.

107. Karaca, G. Y., H. K. Kaya, F. Kuralay, and A. U. Oksuz, "Chitosan functionalized gold-nickel bimetallic magnetic nanomachines for motion-based deoxyribonucleic acid recognition," *International Journal of Biological Macromolecules*, Vol. 193, pp. 370–377, 2021.

108. Cogal, G. C., G. Y. Karaca, E. Uygun, F. Kuralay, L. Oksuz, M. Remskar, and A. U. Oksuz, "Rf plasma-enhanced conducting polymer/w_5o_{14} based self-propelled micromotors for mirna detection," *Analytica Chimica Acta*, Vol. 1138, pp. 69–78, 2020.

109. Shi, D., M. Ran, L. Zhang, H. Huang, X. Li, M. Chen, and M. Akashi, "Fabrication of biobased polyelectrolyte capsules and their application for glucose-triggered insulin delivery," *ACS Applied Materials and Interfaces*, Vol. 8, pp. 13688–13697, 2016.

110. Kook, J. K., V. D. Phung, D. Y. Koh, and S. W. Lee, "Facile synthesis of boronic acid-functionalized magnetic nanoparticles for efficient dopamine extraction," *Nano Convergence*, Vol. 6, pp. 1–8, 2019.

111. Jayeoye, T. J., and T. Rujiralai, "Sensitive and selective colorimetric probe for fluoride detection based on the interaction between 3-aminophenylboronic acid and dithiobis(succinimidylpropionate) modified gold nanoparticles," *New Journal of Chemistry*, Vol. 44, pp. 5711–5719, 2020.

112. Chen, M., C. Chen, Z. Shen, X. Zhang, Y. Chen, F. Lin, X. Ma, C. Zhuang, Y. Mao, H. Gan, P. Chen, X. Zong, and R. Wu, "Extracellular ph is a biomarker enabling detection of breast cancer and liver cancer using cest mri.," *Oncotarget*, Vol. 8, pp. 45759–45767, 2017.

113. Abazari, R., A. R. Mahjoub, F. Ataei, A. Morsali, C. L. Carpenter-Warren, K. Mehdizadeh, and A. M. Slawin, "Chitosan immobilization on bio-mof nanostructures: A biocompatible ph-responsive nanocarrier for doxorubicin release on mcf-7 cell lines of human breast cancer," *Inorganic Chemistry*, Vol. 57, pp. 13364–13379, 2018.

114. Daniel, J., M. Montaleytang, S. Nagarajan, S. Picard, G. Clermont, A. N. Lazar, N. Dumas, F. Correard, D. Braguer, M. Blanchard-Desce, M. A. EstÃ¨ve, and M. Vaultier, "Hydrophilic fluorescent nanoprodrug of paclitaxel for glioblastoma chemotherapy," *ACS Omega*, Vol. 4, pp. 18342–18354, 2019.

115. Rosli, N. F., C. C. Mayorga-Martinez, A. C. Fisher, O. Alduhaish, R. D. Webster, and M. Pumera, "Arsenene nanomotors as anticancer drug carrier," *Applied Materials Today*, Vol. 21, p. 100819, 2020.

116. Gao, S., J. Hou, J. Zeng, J. J. Richardson, Z. Gu, X. Gao, D. Li, M. Gao, D. W. Wang, P. Chen, V. Chen, K. Liang, D. Zhao, and B. Kong, "Superassembled biocatalytic porous framework micromotors with reversible and sensitive ph-speed regulation at ultralow physiological h2o2 concentration," *Advanced Functional Materials*, Vol. 29, p. 1808900, 2019.

117. Huang, Y., T. Li, W. Gao, Q. Wang, X. Li, C. Mao, M. Zhou, M. Wan, and J. Shen, "Platelet-derived nanomotor coated balloon for atherosclerosis combination therapy," *Journal of Materials Chemistry B*, Vol. 8, pp. 5765–5775, 2020.

118. Chng, E. L. K., G. Zhao, and M. Pumera, "Towards biocompatible nano/microscale machines: Self-propelled catalytic nanomotors not exhibiting acute toxicity," *Nanoscale*, Vol. 6, pp. 2119–2124, 2014.

119. Xiao, Q., J. Li, J. Han, K. X. Xu, Z. X. Huang, J. Hu, and J. J. Sun, "The role of hydrazine in mixed fuels for au-fe/ni nanomotors," *RSC Advances*, Vol. 5, pp. 71139–71143, 2015.

120. Mirza, A. Z., and H. Shamshad, "Fabrication and characterization of doxorubicin functionalized pss coated gold nanorod," *Arabian Journal of Chemistry*, Vol. 12, pp. 146–150, 2019.

121. Yang, H., L. Deng, T. Li, X. Shen, J. Yan, L. Zuo, C. Wu, and Y. Liu, "Multifunctional plga nanobubbles as theranostic agents: Combining doxorubicin and p-gp sirna co-delivery into human breast cancer cells and ultrasound cellular imaging," *Journal of Biomedical Nanotechnology*, Vol. 11, pp. 2124–2136, 2015.

122. Huang, Y., L. He, W. Liu, C. Fan, W. Zheng, Y. S. Wong, and T. Chen, "Selective cellular uptake and induction of apoptosis of cancer-targeted selenium nanoparticles," *Biomaterials*, Vol. 34, pp. 7106–7116, 2013.

123. Crowley, E., F. D. Nicolantonio, F. Loupakis, and A. Bardelli, "Liquid biopsy: monitoring cancer-genetics in the blood," *Nature Reviews Clinical Oncology 2013 10:8*, Vol. 10, pp. 472–484, 2013.

124. Codognoto, L., E. Winter, J. A. Paschoal, H. B. Suffredini, M. F. Cabral, S. A. Machado, and S. Rath, "Electrochemical behavior of dopamine at a 3, 3' -dithiodipropionic acid self-assembled monolayers," *Talanta*, Vol. 72, pp. 427–433, 2007.

125. Campuzano, S., D. Kagan, J. Orozco, and J. Wang, "Motion-driven sensing and biosensing using electrochemically propelled nanomotors," *The Analyst*, Vol. 136, p. 4621, 2011.

126. Shankar Balasubramanian, Daniel Kagan, C. M. J. H. S. C. M. J. L.-C., N. Lim, D. Y. Kang, M. Zimmerman, and J. W. Liangfang Zhang, "Micromachine-enabled capture and isolation of cancer cells in complex media," *Angewandte Chemie - International Edition*, Vol. 50, pp. 4161–4164, 2011.

127. Iso, "Biological evaluation of medical devices," *International Standard*, Vol. 10993, pp. 1–26, 2007.

128. Zhang, W., C. Li, B. C. Baguley, F. Zhou, W. Zhou, J. P. Shaw, Z. Wang, Z. Wu, and J. Liu, "Optimization of the formation of embedded multicellular spheroids of mcf-7 cells: How to reliably produce a biomimetic 3d model," *Analytical Biochemistry*, Vol. 515, pp. 47–54, 2016.

129. Shen, H., S. Cai, C. Wu, W. Yang, H. Yu, and L. Liu, "Recent advances in three-dimensional multicellular spheroid culture and future development," *Micromachines 2021, Vol. 12, Page 96*, Vol. 12, p. 96, 2021.

130. Timmins, N. E., and L. K. Nielsen, "Generation of multicellular tumor spheroids by the hanging-drop method," *Methods in molecular medicine*, Vol. 140, pp. 141–151, 2007.

131. Gong, X., C. Lin, J. Cheng, J. Su, H. Zhao, T. Liu, X. Wen, and P. Zhao, "Generation of multicellular tumor spheroids with microwell-based agarose scaffolds for drug testing," *PLoS ONE*, Vol. 10, pp. 1–18, 2015.

132. Nguyen, T. N., T. T. Nguyen, T. H. L. Nghiem, D. T. Nguyen, T. T. H. Tran, D. Vu, T. B. N. Nguyen, T. M. H. Nguyen, V. T. Nguyen, and M. H. Nguyen, "Optical properties of doxorubicin hydrochloride load and release on silica nanoparticle platform," *Molecules*, Vol. 26, 2021.

133. Orlova, A., M. Magnusson, T. L. Eriksson, M. Nilsson, B. Larsson, I. Höiden-Guthenberg, C. Widström, J. Carlsson, V. Tolmachev, S. Stahl, and F. Y. Nilsson, "Tumor imaging using a picomolar affinity her2 binding affibody molecule," *Cancer Research*, Vol. 66, pp. 4339–4348, 2006.

134. Venkatesan, R., A. Pichaimani, K. Hari, P. K. Balasubramanian, J. Kulandaivel, and K. Premkumar, "Doxorubicin conjugated gold nanorods: a sustained drug delivery carrier for improved anticancer therapy," *Journal of Materials Chemistry B*, Vol. 1, pp. 1010–1018, 2013.

135. Chakraborty, D., S. Tripathi, K. R. Ethiraj, N. Chandrasekaran, and A. Mukherjee, "Human serum albumin corona on functionalized gold nanorods modulates doxorubicin loading and release," *New Journal of Chemistry*, Vol. 42, pp. 16555–16563, 2018.

136. Luo, J., D. Liang, X. Li, S. Liu, L. Deng, F. Ma, Z. Wang, M. Yang, and X. Chen, "Photoelectrochemical detection of human epidermal growth factor receptor 2 (her2) based on co3o4-ascorbic acid oxidase as multiple signal amplifier," *Microchimica Acta*, Vol. 188, pp. 1–9, 2021.

137. Margaritis, A., and B. Manocha, "Controlled release of doxorubicin from doxorubicin/ γ polyglutamic acid ionic complex," *Journal of Nanomaterials*, Vol. 2010, 2010.